EXPERIMENTAL AND THEORETICAL STUDY OF CARBON DIOXIDE ABSORPTION INTO POTASSIUM CARBONATE SOLUTION PROMOTED WITH ENZYME

BY

AREZOO KHODAYARI

THESIS

Submitted in partial fulfillment of the requirements
for the degree of Master of Science in Environmental Engineering in Civil Engineering
in the Graduate College of the
University of Illinois at Urbana-Champaign, 2010

Urbana, Illinois

Advisors:
Professor Mark J. Rood
Yongqi Lu, Ph.D.

ABSTRACT

According to the Intergovernmental Panel on Climate Change (IPCC), carbon dioxide (CO_2) concentration in the atmosphere has increased from its pre-industrial value of 280 parts per million by volume (ppmv) to 384 ppmv. IPCC predicts that CO_2 concentration in the atmosphere will rise to 550 ppmv by the year 2100, if anthropogenic emissions continue to increase. The average temperature at the Earth's surface could increase 1.8-4.0K above the 1990 levels by the end of this century. Such warming is anticipated to cause sea level rise, increased intensity and frequency of extreme weather events, ice shelf disruption, and changes in rainfall patterns. As a result, reducing CO_2 emissions from anthropogenic sources is a high priority.

Combustion of fossil fuels for power generation is the major contributors of CO_2 emission into the environment. Currently, CO_2 chemical absorption using monoethanolamine (MEA) as a solvent is the best available option for CO_2 capture from flue gas streams. The issue with this technology is the high capture cost which ranges from $50/metric ton to $70/metric ton CO_2 avoided. Energy consumption by the process contributes to 60% of the cost. Thus, use of solvents with lower heats of absorption is preferable. A novel process called Integrated Vacuum Carbonate Absorption Process (IVCAP), which employs potassium carbonate (PC) as a solvent, has been proposed. Since chemical affinity of CO_2 to K_2CO_3 is weak compared to MEA, the regeneration of CO_2-rich solution can be operated under vacuum at a lower temperature. Hence, a low quality steam from the power plant steam cycle can be used as the heat source for the regeneration. IVCAP process is expected to have 25-30% lower energy requirements as compared to an MEA-based process.

However, compared with the MEA solution, PC solutions with low heats of absorption generally exhibit much slower CO_2 absorption rates. Hence, a biological catalyst, *carbonic anhydrase* (CA) was investigated to promote the rate of CO_2 absorption into select PC solutions. Experiments were performed in a stirred-tank reactor to evaluate the activity of the CA enzyme under IVCAP conditions. Results revealed that addition of up to 300 mg/l CA enzyme to the PC solutions at 25^{o}C increases the absorption rate by a factor of 6-20 when compared with the same solution without the CA. It was also observed that, the CO_2 absorption rates into the aqueous PC

solutions with different initial conversion levels of PC to potassium bicarbonate are similar, with differences no larger than 20%, when the concentration of CA enzyme is 300 mg/l. It was also observed that, at the 300 mg/l CA concentration, increasing the temperature from 25^{o}C to 50^{o}C reduces the rate of CO_2 absorption, by up to 20%.

A mathematical model based on Higbie's penetration theory was developed to simulate the absorption of CO_2 into the PC solutions. A comparison of modeled to experimental absorption rates of CO_2 provided agreement within 30%. The modeling results revealed that at CA concentrations > 3,000 mg/l, the absorption rate of CO_2 is independent of CA concentration. Compared to the enzyme concentration (300 mg/l) used in this study, a further increase of enzyme concentration to a level not larger than 3,000 mg/l could further increase the absorption rate of CO_2.

Based on the experimental and modeling results obtained in this research, it is recommended that the CO_2 absorption rate into PC-CA be further enhanced by improving other parameters such as the activity of CA enzyme and design optimization of the absorption column including the type of packing material. Further work is required to investigate the stability of the CA enzyme at longer test duration and use of immobilized CA enzyme. Effectiveness of the regeneration cycle also needs to be investigated. Further work should also include the test of an integrated absorption/ regeneration system for CO_2 capture at a real flue gas condition.

To my parents and my brother, Omid

whose love and support have sustained me throughout.

ACKNOWLEDGMENTS

It is a pleasure to thank many people who made this thesis possible.

I owe my deepest gratitude to Professor Massoud Rostam-Abadi, Professor Mark J. Rood and Dr. Yongqi Lu for providing me the opportunity to work on this research topic.

I would like to thank my advisor, Professor Mark J. Rood, and my co-advisor, Dr. Yongqi Lu, whose guidance from the beginning of this research project to its completion that enabled me to develop deep and unique understanding of CO_2 separation from gas streams.

I am indebted to David Ruhter and Hamidreza Emamipour for their help with the experimental apparatus. I am also grateful to the members of the Air Quality Engineering and Science group at the University of Illinois for their support and encouragement.

I am grateful for the financial support in part by the U.S. Department of Energy/ National Energy Technology Laboratory, through Cooperative Agreement No. DE-FC26-08NT0005498, and by the Illinois Department of Commerce and Economic Opportunity, through the Office of Coal Development and the Illinois Clean Coal Institute under Contract No.08-1/1.1B-3. I am also grateful to Dr. Sotiria Koloutsou-Vakakis and Professor Albert J. Valocchi, the Associate Head of the Department of Civil and Environmental Engineering for providing me a teaching assistantship during spring semester 2010.

I wish to thank my parents and brother for their never-ending love and support which helped me to get through difficult times during my graduate studies.

Finally, I would like to extend my heart-felt appreciation to Professor Donald J. Wuebbles for being a powerful source of inspiration and his willingness to support me in all my endeavors, which made it possible for me to continue my Ph.D. studies.

TABLE OF CONTENTS

LIST OF TABLES

LIST OF FIGURES

1 INTRODUCTION

1.1 Anthropogenic CO_2 emissions and their sources

The rise in anthropogenic carbon dioxide (CO_2) emissions is a growing concern during the 21th century. Scientists believe that anthropogenic CO_2 emissions are the main cause for global warming. IPCC predictions, with an assumed 100-year time horizon and 1990 emissions, indicates that relative contribution of CO_2 to global warming is 61%. Methane is second (at 15%), CFC-12 is third (at 7%), and nitrous oxide is fourth (at 4%) [IPCC, 1990]. IPCC also predicts that the CO_2 concentration in the atmosphere will rise to 550 ppmv by the year 2100, if anthropogenic emissions continue to increase [IPCC, 2007]. Based on such an increase in the CO_2 concentration, leading climate models predict that the average temperature at the Earth's surface could increase 1.8-4.0K above the 1990 levels by the end of this century [IPCC, 2007]. Figure 1-1 shows the averaged measured warming temperature and linear regression warming temperature trends for the Earth's surface. Such warming is anticipated to cause a rise in sea level, increase the intensity and frequency of extreme weather events, disrupt ice shelves, and change rainfall patterns [IPCC, 2001].

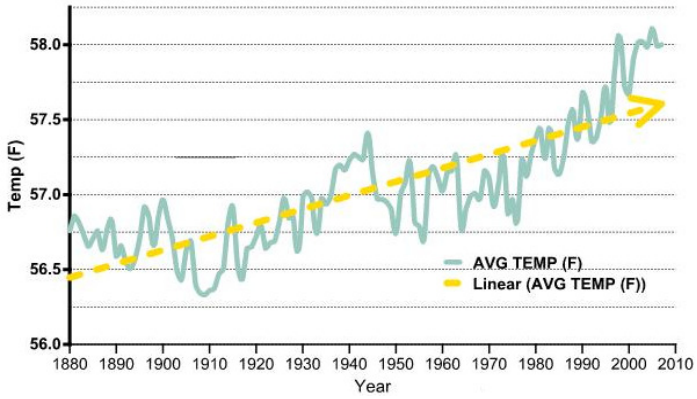

Figure 1-1 Global mean temperature over land and ocean (Jan-Dec) [Yuwei, 2008]

The CO_2 emissions from the ocean and vegetation are 770 giga metric tons (GMT) per year as compared to 29 GMT per year of anthropogenic CO_2 emissions [IPCC, 2007]. However, The CO_2 that nature emits is balanced by natural processes. Land plants and the ocean absorb 450 and 338 GMT of CO_2 per year, respectively [IPCC, 2007]. Anthropogenic CO_2 emissions

perturb the natural balance and cause rising CO_2 concentration to levels not seen in at least 800,000 years [IPCC, 2007].

Combustion of fossil fuels has the largest contribution to the total anthropogenic CO_2 emissions to the atmosphere as compared to other anthropogenic sources such as the chemical, steel or cement industries for USA. During 2008, 5,920 million metric tonne (MMT) of CO_2 was emitted to the atmosphere from anthropogenic sources in the USA [USEPA, 2010a]. Fossil-fuel combustion contributed 5,570 MMT or 94% of USA's anthropogenic CO_2 emissions [USEPA, 2010a]. Anthropogenic CO_2 emissions from fossil-fuel combustion come from a wide range of sectors, with the electricity and transportation sectors contributing the most CO_2 (Figure 1.2).

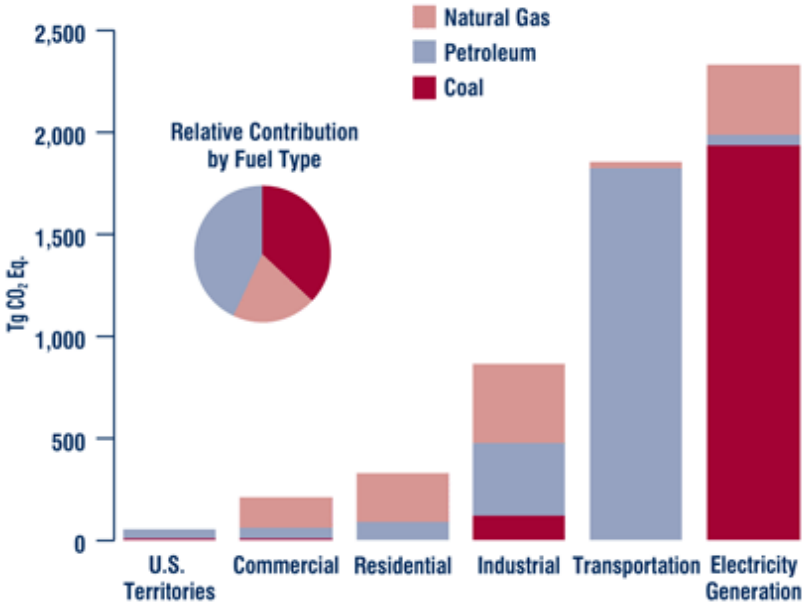

Figure 1-2 CO_2 emissions from fossil fuel combustion by sector and fuel type for 2006 [USEPA, 2010b]

There are primarily three alternatives to lowering CO_2 emissions to the atmosphere: 1) use alternative energy sources to meet energy demands while lowering CO_2 emissions; 2) lower the consumption of energy that produces CO_2; and 3) capture and sequester CO_2 before it is emitted to the atmosphere. To implement the first alternative it is required to switch to fossil fuels that produce more energy per unit mass carbon and/or switch to non-fossil fuels such as hydro-energy, wind and solar energy, bio-energy, geothermal and ocean energy. The second alternative

calls for the efficient use of energy and the third alternative is possible through the development of CO_2 capture and sequestration technologies. This research focuses on the first part of the third alternative: development of CO_2 capture technologies for coal-fired electric utilities due to their large relative contribution of CO_2 emissions to the atmosphere.

1.2 CO_2 Capture technologies for stationary coal-fired power plants

There are three different configurations for CO_2 capture from coal-based power plants: pre-combustion, oxygen-enriched combustion (oxy-combustion), and post-combustion processes. Pre-combustion processes are applicable to coal gasification plants, where coal is converted into CO, CO_2 and H_2 before combustion. Oxy-combustion processes uses concentrated O_2 instead of air in coal combustion, producing a flue gas, which is mostly composed of H_2O vapor and CO_2 with smaller amounts of sulfur oxides (SO_x) and nitrogen oxides (NO_x). This characteristic reduces the cost of separation systems due to the reduction in size of the equipment used to burn the coal. Post-combustion processes capture CO_2 from flue gases after coal is burned with air. For the electric utility generation sector, the choice of CO_2 capture option mainly depends on the power generation process used [Chen et al., 2004]. However, post-combustion capture is the most important option for the existing electric utility generation sector if CO_2 emission control is mandated in the near future. This is true because existing technologies can be retrofitted to existing power plants without the need for redesigning the plants [DOE, 2008]. The choice of new power generation technologies in the future will depend on the growth in demand for electricity, trends in fuel prices, the costs and efficiencies of new technologies, and the availability of federal tax credits for some technologies. The Annual Energy Outlook 2009 report predicts that by 2030 only 3% of the existing power generation capacity will be phased out with the new plants [DOE/EIA, 2009]. Thus, it is important to retrofit existing coal-fired power plants to meet energy demands while reducing CO_2 emissions.

1.2.1 Post-combustion CO_2 capture

Removal of CO_2 with a post-combustion process when burning fossil fuels with O_2 in air is described schematically in Figure 1-3. The CO_2 concentration in the flue gas stream that is generated by combustion of coal with air usually ranges from 10 to 15% by volume because the combustion flue gas is diluted with the N_2 in the air. The resulting partial pressure of CO_2 in the

flue gas is less than 15kPa because the total pressure of the flue gas stream from conventional coal-fired boilers (i.e., pulverized, cyclonic, or stoker boilers) is near atmospheric pressure. Such a low partial pressure implies a low thermodynamic driving force for CO_2 capture and thus makes it challenging to develop a cost-effective post-combustion capture process.

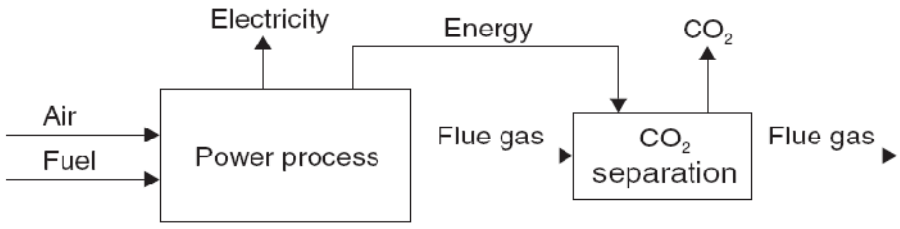

Figure 1-3 Post-combustion CO_2 capture

Important factors that need to be considered to select a CO_2 capture process include technical feasibility, economic feasibility, scalability of the capture process to the power plant, separation factor and equipment capacity, product value, and technology maturity [Chen et al., 2004].

Many of the commercially available capture technologies are not practical or economical for separating and capturing CO_2 from coal combustion flue gases because of the large-scale CO_2 emissions, and relatively low-value of CO_2 [Chen et al., 2004]. For example, adsorption-based processes are not realistic for CO_2 capture from flue gases, because they require large quantities of adsorbents [Chen et al., 2004]. Technologies that have a potential for CO_2 capture from coal-power plant flue gases are: cryogenic, membrane, and absorption processes. Disadvantages of cryogenic processes are intense energy consumption and possibility of blockages if some components such as water freeze before they are not removed before the gas stream is cooled [Aaron, 2005]. Membrane separation processes have disadvantages of lower CO_2 purity at a higher CO_2 recovery rate [Aaron and Tsouris, 2005]. Currently, absorption is the best available technology for CO_2 capture from flue gases, in terms of cost and reliability. Chemical absorption is preferable for CO_2 capture from coal combustion flue gases with typical CO_2 content ranging from 3% to 15% by volume at atmospheric pressure [Chen et al., 2004]. That is because, as it will be discussed in the following section, chemically absorbing solvents have more capacity than physically absorbing solvents at low pressures.

1.2.2 Absorption processes

In an absorption process a solvent is used as a reagent to capture CO_2 in the flue gas. In this process, the flue gas enters an absorption column and is mixed with the solvent. The solvent selectively absorbs CO_2 through a physical and/or chemical absorption. The resulting CO_2-rich solvent then exits the bottom of the absorber and is passed into a stripping (desorption) column where it is heated with steam or evacuated with vacuum to release a concentrated CO_2 from the solvent. The resulting CO_2-concentrated gas stream that is released in the stripper is recovered, while the resulting CO_2-lean solvent is circulated back to the absorption tower. Usually, when a chemically absorbing solvent such as monoethanolamine (MEA) is used, the CO_2 recovery rate is high (> 98%) and the resulting CO_2 product purity is also high (> 99%) [Rao et al., 2004; Yang et al., 2008]. However, since chemically absorbing solvents such as MEA have a greater affinity to some other contaminates present in the flue gas such as SO_x and NO_x than CO_2, there should be some pretreatment requirement to remove SO_x and NO_x from the flue gas before the CO_2 is separated from the flue gas stream.

CO_2 absorption capacity depends on the operating conditions of the process such as temperature, CO_2 partial pressure in the flue gas, and the physical/chemical properties of the solvent. For chemically absorbing solvents, absorption is based on chemical interaction between CO_2 and solvent molecules. Chemically absorbing solvents thus have a limited capacity of CO_2 and absorption capacity levels off after the CO_2 partial pressure increases to a certain degree. However, for physically absorbing solvents, absorption occurs through physical interaction between CO_2 and solvent molecules, and the absorption capacity is proportional to the CO_2 partial pressure. Figure 1-4 shows the relation between CO_2 partial pressure and absorption capacity for chemically and physically absorbing solvents. At low partial pressure, the absorption capacity of the physically absorbing solvent is much smaller than that of the chemically absorbing solvent. As previously mentioned, the CO_2 partial pressure in flue gas is low (< 15kPa) and such a condition makes chemical absorption more appropriate technique than physical absorption to remove the CO_2 from the gas stream [Chen et al., 2004].

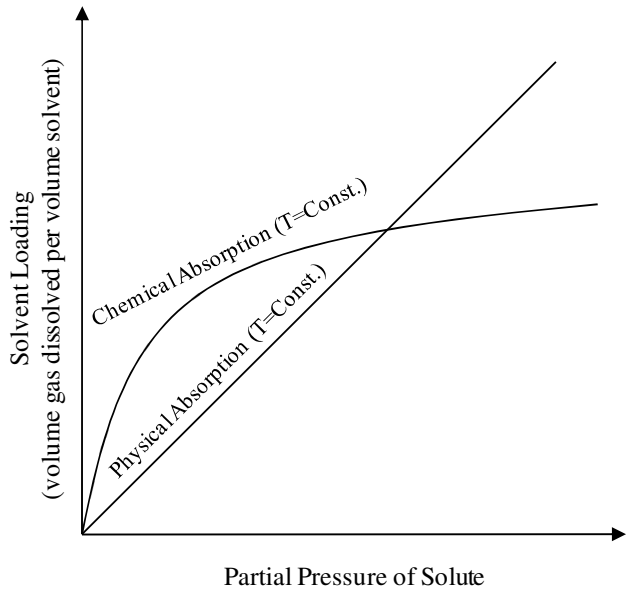

Figure 1-4 Relationship between CO_2 partial pressure and absorption capacity in the solvent [Gottlicher, 2004]

Amine-based chemical absorption processes have been studied for CO_2 capture and have been used for more than 60 yr in the chemical and oil industries [Herzog, 1999]. The major reactions contributing to the CO_2 absorption into the MEA solution are [Greer, 2008]:

$$CO_2 + Am \underset{k_{72}}{\overset{k_{71}}{\Leftrightarrow}} AmH^+COO^- \qquad \text{Eq 1-1}$$

$$Am + AmH^+COO^- \underset{k_{82}}{\overset{k_{81}}{\Leftrightarrow}} AmH^+ + AmCOO^- \qquad \text{Eq 1-2}$$

Where Am stands for amine.

Reaction (8) (Equation 1-2) happens very quickly so that it can be considered instantaneous [Greer, 2008].

The main advantage of this technology is the relatively high purity (> 99%) of produced CO_2 stream [Rao et al., 2004]. However, chemical absorption systems using MEA as a chemical solvent have some obstacles. The main one is the degradation of MEA due to its reaction with SO_x and NO_x present in the flue gas stream and self polymerization at high temperatures. Also, the corrosion of equipment in the presence of O_2 in the MEA or other amine-based CO_2 absorption units is another concern [Yang et al., 2008]. Also, regeneration of MEA requires an extensive amount of energy due to the high heat of absorption of CO_2 in MEA which contributes to 60% of the cost. Because of these drawbacks it is necessary to develop new solvents with higher CO_2 capacity, lower potential for corrosion, lower potential for solvent degradation and lower energy requirements.

Extensive studies have occurred to optimize MEA absorption process operations and development of new solvents to lower the process costs [Abanades et al., 2004; Goff and Rochelle, 2006; Derks, 2006; Dugas and Rochelle, 2009]. These process improvements include the development of high-efficiency packing materials, integrated heat use, development of additives to reduce the corrosion of equipment, and optimization of the regeneration process. However, there are other technologies such as mixed amines absorption, ammonia absorption process, the dual-alkali absorption process, and the integrated vacuum carbonate absorption process (IVCAP), which can be used as alternatives to the use of MEA. These technologies are summarized below.

1.2.2.1 Mixed amines absorption

Amines are classified into three categories as primary, secondary and tertiary amines, with the general formula of RNH_2, R-NH-R', and R'-NR-R", respectively, where R, R', and R" are the alkyl groups. The primary and secondary amines have a high reactivity rate with CO_2 which leads to a high absorption rate when compared to the tertiary amines. However, the tertiary amines have a low heat of reaction with CO_2, which could lead to lower energy and cost requirements to regenerate the solvent. The most commonly used amines in CO_2 capture plants are MEA (primary amine), di-glycol-amine (DGA, primary amine), di-ethanol-amine (DEA, secondary amine), di-iso-propanol-amine (DIPA, secondary amine), and methyl-di-ethanol-

amine (MDEA, tertiary amine). Typical concentrations, CO_2 loadings, heats of absorption, and reaction rates at 25°C, for these amines, are provided in Table 1.1 (Bailey and Feron, 2005).

Table 1-1 Overview of characteristics of selected primary, secondary and tertiary amines [Bailey and Feron, 2005]

Solvent in Water	MEA	DGA	DEA	DIPA	MDEA
Concentration (% mass)	< 30	< 60	< 40	< 40	< 50
Typical CO_2 loading (mol/mol)	0.3	0.35	0.30-0.70	0.45	0.45
Heat of absorption (MJ/kg of CO_2)	2.0	2.0	1.5	1.5	1.3
Reaction rate at 25°C (m^3 / kmole·s)	7,600	4,000	1,500	400	5

A mixture of primary and tertiary amines or secondary and tertiary amines could offer a lower cost option for solvent regeneration. The CO_2 capture performance of aqueous solutions containing MEA (5 M) and then an aqueous mixture containing MEA/MDEA (4/1 molar ratio at 5 M) were compared and a reduction in the heat of absorption up to 13% was observed for the aqueous-amine mixture compared to the aqueous MEA solvent [Idem et al., 2006]. However, the absorption rate into such mixtures was still lower than the MEA solution. A low absorption rate increases the capital cost since a larger absorber is required to achieve the same level of CO_2 removal.

1.2.2.2 Ammonia absorption process

In the ammonia absorption process, aqueous ammonia solution is used as the absorbent solution in an absorption column to chemically absorb CO_2. The regeneration of the CO_2-rich solution is carried out in a stripping column using steam heating. The CO_2 gas stream exits the stripper and then passes through a condenser. The regenerated solution is then cooled and pumped back to the absorption column. The major by-products are ammonium sulfate and ammonium nitrate when SO_x and NO_x are presented in the flue gas, which have the potential to be used as fertilizers for certain crops [Yeh et al., 2005].

CO_2 removal efficiency by aqueous based NH_3 and MEA solvents have achieved 99% and 94%, respectively, in a semi-continuous flow reactor (continuous flow with respect to gas phase and batch flow with respect to liquid phase) [Yeh and Bai, 1999]. The CO_2 loading capacity by NH_3 and MEA absorbents can approach 1.20 kg CO_2/kg NH_3 and 0.40 kg CO_2/kg MEA, respectively, under the same test conditions. Hence, ammonia's CO_2 loading is three times that of MEA's loading at these conditions. Furthermore, it was observed that industrial grade NH_3 is 1/6 the cost of MEA on the same weight basis [Yeh and Bai, 1999]. It was also observed that the maximum temperature to achieve a reasonable amount of absorption of CO_2 into 35% wt MEA was 50°C, while it was less than 40°C when using 35% wt NH_3 solutions. They also concluded that the energy consumption for the regeneration of NH_3 solution should be less than that for the regeneration of MEA solution. Unlike the MEA process, most of the acid producing gases such as SO_x, NO_x and CO_2 are removed with the NH_3 process in a single process which lowers the capital cost of the capture process. Another advantage of the NH_3 process over the MEA process is the absence of corrosion in the equipment and less solvent degradation in the presence of SO_x or O_2 in the flue gas [Yeh and Bai, 1999].

The main drawback of the NH_3 process is the volatility of NH_3 above 25°C, which required an additional column to remove the NH_3 from flue gas [Derks, 2009]. Another disadvantage of this absorption process is the possibility of formation of CO_2-containing ammonium salts such as ammonium bicarbonate and ammonium carbonate, which can plug the pipes or produce scales on the walls. As such, regeneration of the NH_3 must be started before the formation of crystals [Yeh et al., 2005].

1.2.2.3 Dual-alkali absorption process

In the dual-alkali absorption process CO_2 reacts with a primary alkali such as methyl-amino-ethanol (MAE, $HOCH_2CH_2(CH_3)NH$) in the presence of sodium chloride (NaCl) to produce sodium bicarbonate salt ($NaHCO_3$) according to following reactions [Huang et al., 2001]:

carbamate formation:

$$CO_2 + 2HOCH_2CH_2(CH_3)NH \longleftrightarrow HOCH_2CH_2(CH_3)NCO_2HHN(CH_3)CH_2CH_2OH \quad \text{Eq 1-3}$$

bicarbonate formation:

$$\begin{aligned} &H\,OCH_2CH_2(CH_3)NCO_2HHN(CH_3)CH_2CH_2OH + H_2O \longleftrightarrow \\ &\quad HOCH_2CH_2(CH_3)NHH^+ \cdot HCO_3^- + \\ &\qquad\qquad HOCH_2CH_2(CH_3)NH \end{aligned} \qquad \text{Eq 1-4}$$

sodium bicarbonate formation:

$$\begin{aligned} &HOCH_2CH_2(CH_3)NHH^+ \cdot HCO_3^- + NaCl \longleftrightarrow NaHCO_3 \downarrow + \\ &\qquad\qquad H\,OCH_2CH_2(CH_3)NH.H^+ \cdot Cl^- \end{aligned} \qquad \text{Eq 1-5}$$

Following the formation of $NaHCO_3$, it is separated by filtration, and is then heated to convert it to sodium carbonate (Na_2CO_3) that can be safely returned to the environment.

In the second step of the dual alkali process, a secondary alkali is used to regenerate the first alkali. This step was not investigated for MAE by Huang et al. (2001) but they studied the use of activated carbon (AC) as a secondary alkaline to regenerate ammonia from ammonium chloride solution in the Solvay process:

$$NH_4Cl + AC \longleftrightarrow NH_3 + AC \cdot HCl \qquad \text{Eq 1-6}$$

The saturated activated carbon can be regenerate with water extraction of the adsorbed HCl. [Huang et al., 2001].

The CO_2 absorption capacities of MAE (1.2 M), and MAE/NaCl (1.2 M/ 3.4 M) were estimated to be 0.75, and 0.92 mol of CO_2 per mol of amine, respectively [Huang et al., 2001]. The increase in the CO_2 absorption capacity of MAE in the presence of NaCl is due to the precipitation of $NaHCO_3$ which breaks the equilibrium between carbamate and bicarbonate (Eq 1-5). Consequently, the carbamate is converted to bicarbonate which produces free MAE and increases the pH of the solution and as a result of that, more CO_2 is absorbed.

However, the presence of NaCl has an inhibitory effect on the rate of reaction by increasing the ionic strength of the solution and consequently decreasing the solubility and diffusion rate of CO_2. In order to prevent this inhibitory effect, the use of a two-step process was suggested

[Huang et al., 2001]. In this process, CO_2 absorption is initially carried out in 30% MAE, the solution is then transferred into a separate vessel and sodium chloride salt is added to precipitate $NaHCO_3$.

1.2.2.4 Integrated vacuum carbonate absorption process (IVCAP)

IVCAP is being developed at the University of Illinois as an absorption-based process in which PC aqueous solution is used as the absorption solution (Figure 1-5) [Lu et al., 2007]. CO_2 is absorbed into the PC solution in the absorption column, and the CO_2-rich solution is transferred to a stripping column, where it is regenerated by heating with steam under vacuum. The CO_2 gas stream exits the stripper and then passes through a condenser, and the CO_2-lean solution is recycled to the absorption column in a closed-loop.

The advantages of a PC solution compared to an MEA solution is its lower heat of absorption for CO_2, 609 kJ/kg, compared to 1,918 kJ/kg for the MEA solution. Because of the lower affinity between CO_2 and K_2CO_3, the stripper can be operated under a lower temperature than that of the MEA process. A typical MEA absorption process operates between 93 to 121^oC and at 101 to 202kPa for CO_2 stripping. In order to maintain the required temperature difference which is the driving force for heat transfer, the steam used in the reboiler of an MEA process must be extracted from the power plant steam cycle at a gauge pressure of 415kPa (saturation temperature of 145^oC) [Nsakala, 2001]. The need to use high temperature steam increases the electricity loss for CO_2 capture. In the IVCAP process, the stripper can be operated at a lower temperature than for the MEA process because of the lower affinity between CO_2 and K_2CO_3. At a lower temperature, the CO_2-rich solution boils at a lower pressure. This allows regeneration of the CO_2-rich solution to be conducted under vacuum (total pressure < 101kPa), so that a low quality or a waste steam from the power plant can be used as a heat source and a stripping gas. As a result, the associated electricity loss due to the steam demand is less for the IVCAP process when compared to the MEA process. For example, if the stripper operates at total absolute pressure of 20.3kPa, the total electricity loss (including CO_2 compression) is 24% less than the MEA process [Lu et al., 2007]. The low heat of absorption and desorption requirements under vacuum conditions are close to the exhaust steam condition which make IVCAP an attractive technology when compared to other existing technologies.

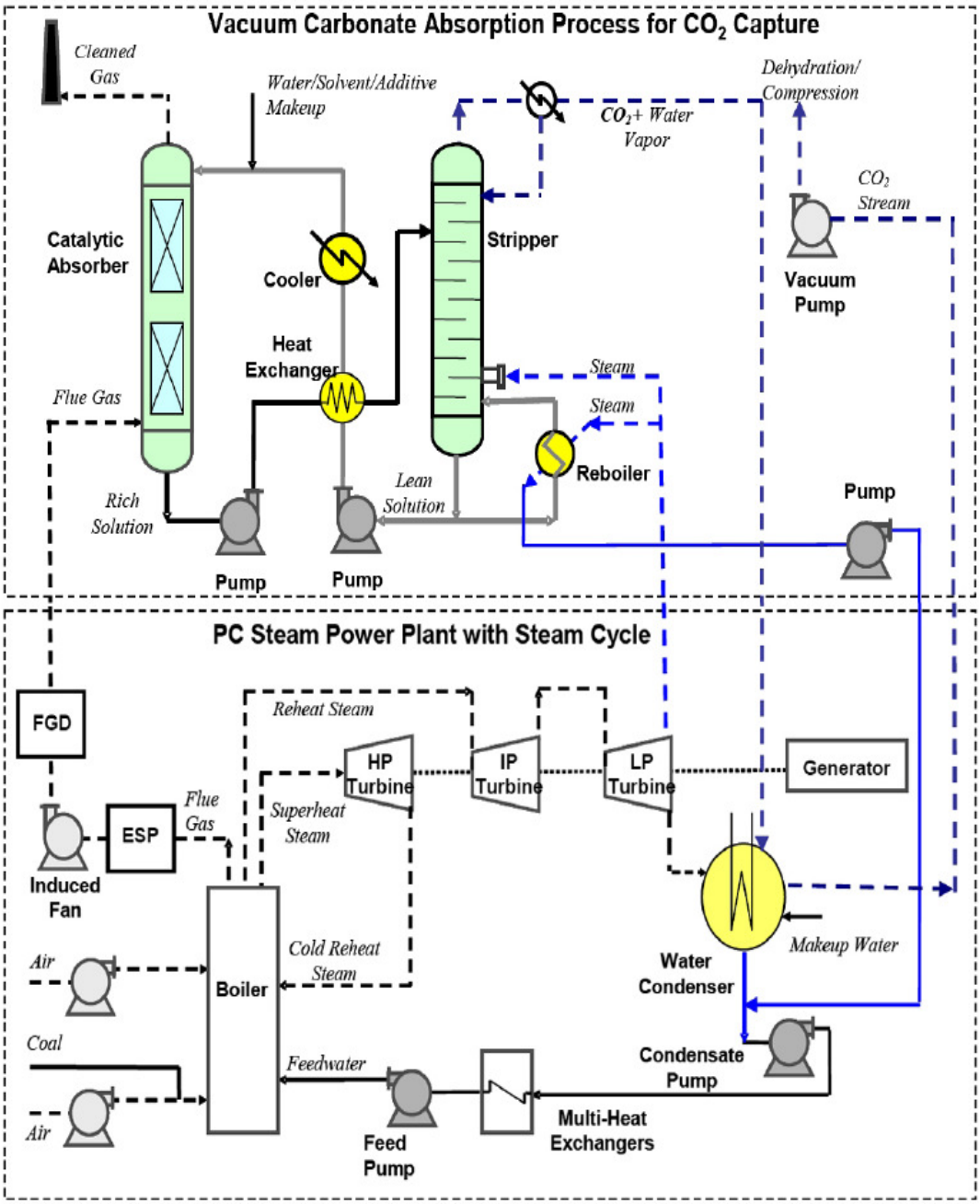

Figure 1-5 Schematic diagram of proposed IVCAP [Lu et al., 2007]

However, there is a technical issue with IVCAP technology that needs to be addressed. The issue is the lower rate of absorption of CO_2 into the PC solution when compared to rate of absorption of CO_2 into the MEA solution, which results in a larger absorber column. However, this issue can be resolved by using a promoter/activator to enhance the rate of chemical reaction between CO_2 and K_2CO_3, which is the limiting step in the absorption process. Different

promoters have been studied for this purpose and some of them are commercialized. Recently, Cullinane and Rochelle (2004, 2006) demonstrated that a 20% wt% K_2CO_3 solution promoted with 0.6 M piperazine (PZ) could achieve absorption rates comparable to those in 5M MEA at 313.15K to 353.15K. However, the heat of absorption in the PC-PZ mixture is much higher than the aqueous K_2CO_3 solution alone, indicating more energy is required during desorption. In addition, piperazine is solid at ambient temperature and pressure and has limited solubility in water. Therefore, a need exists to develop a better promoter/activator to make the CO_2 capture process more economically feasible. In this research the role of *carbonic anhydrase* (CA) as a biocatalyst promoter for the absorption of CO_2 into the PC solution under the IVCAP condition was studied.

1.3 Biocatalysts for promoting CO_2 absorption

A few catalysts such as arsenite, sulfide, hypochlorite, and formaldehyde have been studied for catalyzing CO_2 absorption into various aqueous solutions [Augugliaro and Rizzuti, 1987; Kohl and Riesenfeld, 1985; Sharma and Danckwerts, 1963; Pohorecki, 1968]. These catalysts can accelerate the CO_2-water hydration reaction by 2-4 orders of magnitude. However, the most effective CO_2 hydration catalyst known to date is the CA family of enzymes. It has been reported that the turnover number of the CA enzyme could reach more than one million per second [Davy, 2009]. The *carbonic anhydrases* are a broad group of zinc metallo-proteins (enzymes) that was first identified in 1933 in the red blood cell of cows [Dutta and Goodsell, 2004]. *Carbonic anhydrases* are ubiquitous in all animals, photosynthesizing plants, and some non-photosynthetic bacteria which catalyze both the CO_2 hydration and bicarbonate dehydration reactions [Dodgson et al., 1991]. *Carbonic anhydrases* facilitate CO_2 transport in the human body and accelerates CO_2 desorption into the lungs (the reverse reaction of CO_2 hydration). It also plays a main role in plant photosynthesis carbon fixation [Riebesell, 2000]. It has some pharmaceutical applications as well. For example, it has been used in synthesizing drugs such as acetazolamide, methazolamide, and dichlorphenamide for the treatment of glaucoma [Lindskog, 1997].

1.3.1 Carbonic anhydrase structure

Figure 1-6 illustrates the structure of *carbonic anhydrase*. The active site is a zinc prosthetic group, shown as a black sphere, which has tetrahedral coordination with three histidine side chains and one water molecule. This geometry enhances the Lewis acidity of the zinc atom and also Bronsted acidity of the coordinated water [Davy, 2009]. Nitrogen atoms of the three histidines [His 96, His 94, His 119], shown with a pink color, directly synchronize the zinc. Atoms from threonine 199 and glutamate 106 colored in blue interact through coordination with water (colored in red). It should be noted that the difference between *carbonic anhydrase* isozymes is in these attached amino acid groups and other residues which impact the activity of the isozymes. All these three histidine groups and His 64 help the zinc active site to stimulate the bound water molecule to generate a hydroxide ion (OH^-) which can cause CO_2 to form bicarbonate. Although, His 64 is not directly coordinated with the zinc atom, it can help to charge the zinc ion by swaying towards and away from it and recharge zinc with a new OH^- [Pohorecki, 1968]. The zinc active site reduces the bound water's pKa value to 7 and therefore the OH^- can be released at pH > 7. After the OH^- converts CO_2 to HCO_3^-, the enzyme is ready to react with another CO_2 molecule. The catalysis of CO_2 hydration can thus be initiated with the nucleophilic reaction with the carbon atom of CO_2 by zinc-bound OH^- to produce HCO_3^-.

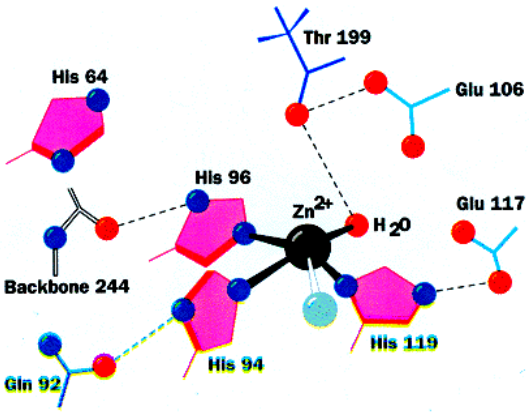

Figure 1-6 *Carbonic anhydrase* structure [Voet, 1990]

1.3.1.1 Carbonic anhydrase gene family

Carbonic anhydrase is categorized into three different classes: alpha, beta and gamma. Although three different classes have only small sequence or structure in common, they still perform the same function with a zinc ion as the active site. All known CA enzymes from the animal empire are in the alpha class. The CA enzymes from the plant kingdom are in the beta class and those from methane-producing bacteria are in the gamma class. There are also seven mammalian isozymes (CA I-VII) that distinguish from each other by their tissue and intracellular locations [Voet, 1990].

The evolution of the CA gene family happened by the protein sequence data and also sequences inferred from cDNA and genomic DNA sequences [Augugliaro and Rizzuti, 1987]. The isozyme with the highest concentration of erythrocyte has the highest turnover number and vice versa. Therefore CA II as the isozyme with the highest erythrocyte concentration is known as the one with the highest turnover number of any kind [Lindskog, 1997]. Table 1-2 shows the maximum values of the CO_2 hydration reaction rate constants [Michaelis-Menten parameters] for different CA types at 298K. At pH = 9 and 298K, the turnover number of a human CA II molecule was reported as 1.4×10^6 s^{-1} [Khalifah, 1971]. Note that all nomenclature is defined in section 7. This means that each CA II molecule can produce 1.4 million molecules of bicarbonate per second. In comparison, the turnover number for the bovine CA II is 1×10^6 s^{-1} [Kernohan, 1965]. Therefore, the catalyzed CO_2 hydration reaction happens as fast as CO_2 can diffuse to the enzyme active site. The exceptional performance of the CA enzyme can be better revealed by comparing the rate constant of the catalyzed reaction (k_{cat}/K_M) to the non-catalytic rate constant of CO_2 reaction with OH^- which is 8.5×10^3 $M^{-1}s^{-1}$ [Dodgson et al., 1991].

Table 1-2 Michaelis-Menten kinetic parameters for CO_2 hydration catalyzed by three CA isozymes[a] [Dodgson et al., 1991]

Isozyme	k_{cat} (s^{-1})	k_{cat}/K_M ($M^{-1}s^{-1}$)
CA I (human)	2×10^5	5×10^7
CA II (human)	1.4×10^6	1.5×10^8
CA III (feline)	1×10^4	3×10^5

[a]Data were obtained at 298K and absolute pressure of 100kPa.

1.3.2 Catalytic mechanism

The rate of the CO_2 hydration reaction catalyzed with CA strongly depends on the pH of the solution. Both k_{cat} and k_{cat}/K_M depend on pH, indicating that the ionizing group with a pK_a of 7 for CA I and CA II controls the hydration reaction [Davy, 2009; Smith et al., 2000; Ghannam et al., 1986]. This ionizing group is indeed the liganded water molecule that is attached to the zinc active site. The pK_a of unbound water is 15.5 [Davy, 2009]. However, zinc can lower that pK_a value to 7 because of its high catalytic effect. For a monoprotic acid the pK_a is the pH at which 50% of that acid is in the deprotonated form. For an acid with a pH above the pK_a, the conjugate base will predominate and with a pH below the pK_a the conjugate acid will predominate. Therefore, at pH > 7, the predominant form of CA is $(His)_3Zn\text{-}OH^-$ which catalyzes the CO_2 hydration reaction to form the bicarbonate ion. At pH < 7, the predominant form of CA is $(His)_3Zn\text{-}OH_2$ which catalyzes the reverse reaction to dehydrate the bicarbonate ion to form CO_2. Figure 1-7 illustrates the mechanism of the CO_2 hydration reaction catalyzed with CA.

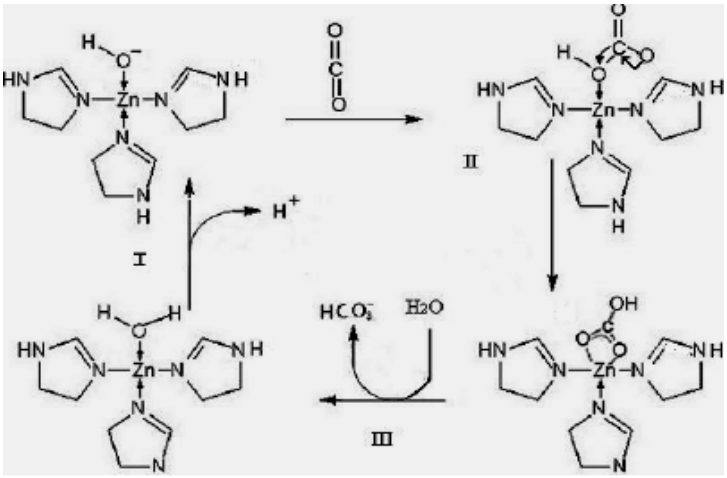

Figure 1-7 Mechanism of CA catalyzed CO_2 hydration [Davy, 2009]

Therefore the chemical reaction takes place in the CA-catalyzed CO_2 hydration reaction can be summarized as below:

$$E\ Zn\ H_2O = E\ Zn\ OH^- + H^+ \qquad \text{Eq 1-7}$$

$$E\ Zn\ OH^- + CO_2 = E\ Zn\ HCO_3^- \quad \text{Eq 1-8}$$

$$E\ Zn\ HCO_3^- + H_2O = E\ Zn\ H_2O + HCO_3^- \quad \text{Eq 1-9}$$

Based on the above mechanism, the overall reaction is: $H_2O+CO_2 = HCO_3^- +H^+$. Therefore, the CO_2 hydration reaction $CO_2+ H_2O = H_2CO_3$, which is the slowest, is eliminated and the overall reaction can be accelerated.

1.3.3 CA biocatalyst-promoted absorption processes

A CA catalyst-based absorption concept using hollow fiber contained liquid membrane (HFCLM) was investigated by Carbozyme, Inc. [Bao and Trachtenberg, 2005, 2006]. In this process the CA enzyme is immobilized in a liquid membrane which is located on the shell side between the two sets of microporous hollow fibers. The feed gas is passed through the hollow space of one set of fibers while the sweep gas is passed through the hollow space of the other set of fibers. Simulation results demonstrated that the overall absorption rate of 15% vol CO_2 with the CA + buffer (3.0 g/L CA and 1.0 M Na_2CO_3-$NaHCO_3$) system is 109% greater than with 20% wt DEA, and 52% greater than with 30% wt DEA [Bao and Trachtenberg, 2006]. Experimental results revealed that at 10.0% by volume CO_2 feed, the measured CO_2 permeance facilitated by 20.0% wt DEA is only 33.5% of that by CA + buffer [Bao and Trachtenberg, 2006].

Operating temperature is an important issue concerning the activity of CA enzyme. However, a study performed by Carbozyme Inc. with three different CA isozymes concluded that these isozymes worked well between 293K and 358K [Trachtenberg et al., 2007]. Despite the successful demonstration of maintaining CA activity, there are concerns about the low permeance of CO_2 through HFCLM, and high energy consumption of the CO_2 stripping at the retentate side of membrane. The permeance of CO_2 through HFCLM is less than 10^{-7} mol/Pa·m^{2}·s [Bao et al., 2005], which results in a large membrane surface area to be effective.

Researchers at New Mexico Institute of Mining and Technology developed a bench-scale and a laboratory-scale experimental setup in which *bovine carbonate anhydrase* (BCA) enzyme was

used to catalyze the rate of CO_2 hydration for subsequent formation of stable mineral carbonates [Liu et al., 2005]. In the bench-scale tests, pH value and precipitation time were measured in solutions with and without BCA. They observed that the precipitation time decreased from 86 s in a control solution for the synthetic San Juan Basin produced water, to 15 s in the presence of BCA in the synthetic San Juan Basin produced water. However, for West Pearl Queen Reservoir produced water, the precipitation time was 254 s in the BCA-control solution mixture and 326 s in the control solution. They attributed this to the higher magnesium-to-calcium ratio in West Pearl Queen Reservoir produced water but this can be overcome by modest heating (from 298K to 318K - 328K). For the laboratory-scale experiment, they used immobilized BCA in chitosan-alginate beads. The results showed that the precipitation times with/without BCA were 252 s/303 s and 7 s/122 s for West Pearl Queen Reservoir and San Juan Basin, respectively.

Another technology which is using aqueous amine solutions and immobilized CA enzyme in a packed-bed to capture CO_2 from gas streams is being developed by CO_2 Solution Inc. [Se´vigny, 2005; CO_2 Solution, 2007]. In this process, regeneration of the CO_2-rich solution is performed by heating the solution with the facility steam in an enzyme-immobilized packed column. The concentrated CO_2 can then be conditioned and compressed for underground storage, enhanced oil recovery or other industrial uses. The lean solution is recycled to the absorption column in a closed loop.

A regenerable amine-bearing polyacrylamide buffering beads (PABB) and CA-bearing carrier water were tested for the capture of CO_2 from mixed industrial gas streams [Dilmore et al., 2009]. In this process, the saturated PABB is thermally regenerated after being separated from the CA-bearing carrier water which is recycled to the absorption stage. They reported that increasing the acrylamide buffer concentration in PABB increases the CO_2-bearing capacity per unit dry weight of PABB at CO_2 partial pressure of 0.5 bar, 301.5K and a relative humidity of 96%. Based on their preliminary results, the complete regeneration of PABB occurred at 373K and total pressure of 100kPa.

1.4 Objectives, significance, and scope of the research

1.4.1 Objectives and significance

The objectives and significance of this study are as follows:

- Develop experimental apparatus to be used for obtaining kinetic data for CO_2 absorption into select solutions. The apparatus will be a continuously stirred tank reactor (CSTR) reactor equipped with gas and liquid analysis instruments.

- Evaluation of the activity of the CA enzyme in the PC solution. This part of the research will quantify the effectiveness of the CA enzyme to promote the absorption rate of CO_2 into the PC solution and compare the promoted rate with the un-promoted rate and with the MEA system. The activity (kinetic) data obtained from this study are significant because they will provide the basic information required to evaluate the effectiveness of the CA enzyme and for design calculations, process optimization and cost analysis for the scale-up of the IVCAP.

- Development of a mathematical model to simulate the absorption of CO_2 into the PC-CA solution in a stirred tank reactor. This model will be evaluated against experimental data. The significance of the evaluated model is that it will be used to predict the absorption flux at operating conditions beyond that of experimental tests (e.g. high temperatures, high enzyme concentrations). The model can also guide the future experimental design and the design calculations of the resulting absorption column.

1.4.2 Overall scope of this research

The overall scope of this research is described in Figure 1-8**.** A laboratory-scale CSTR system was designed and built for the activity testing of the catalyst.

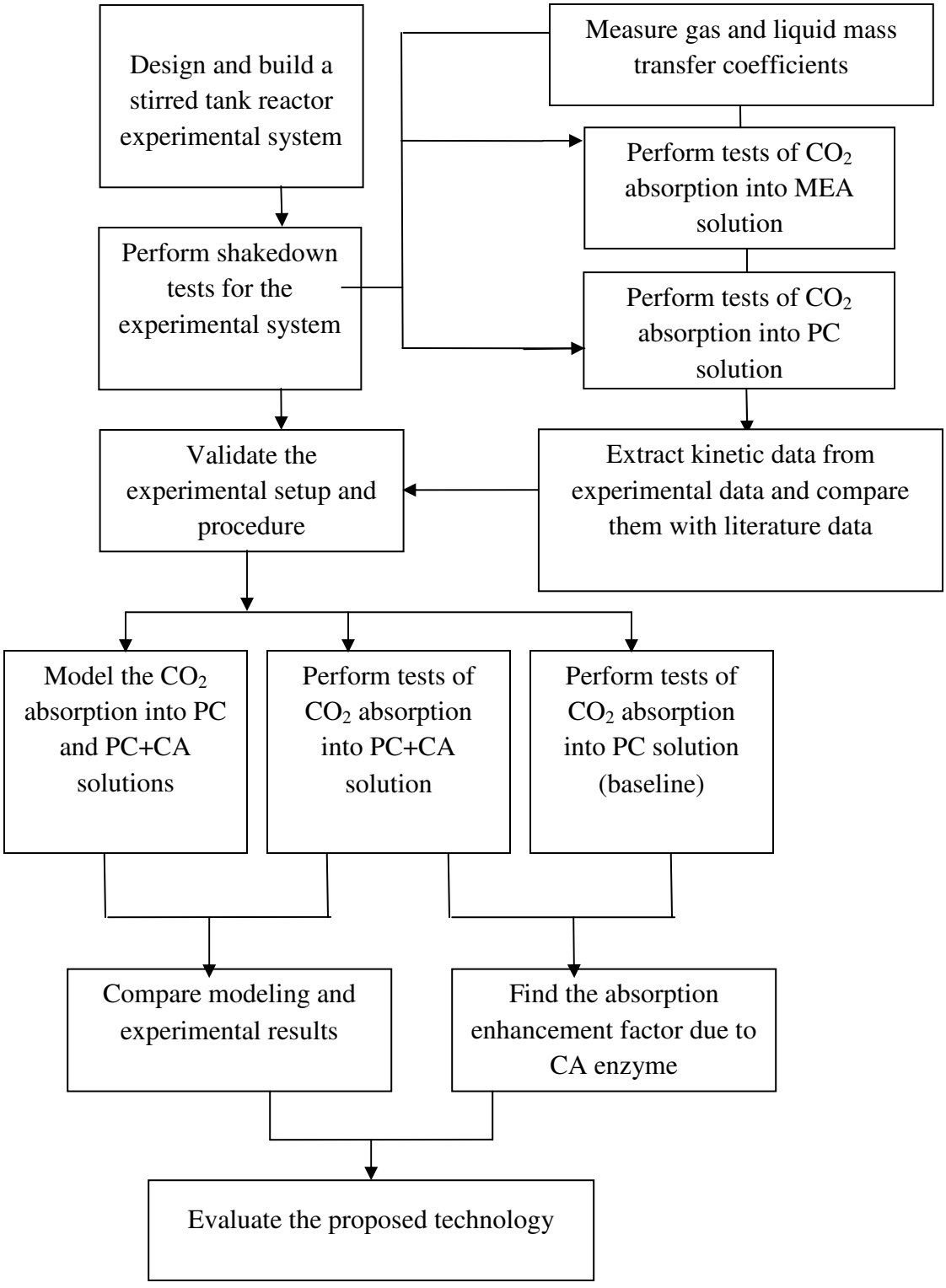

Figure 1-8 Schematic of research scope

Pre-tests were then performed to determine the performances of the liquid-phase mass transfer coefficients in this system. Absorption tests then occurred with the PC and MEA solutions at select operating conditions (e.g. PC concentration, CO_2 loading, temperature, partial pressure of CO_2).These results provided a baseline for the comparison and can also be used to validate the experimental setup with comparisons to data reported in the literature. Next, the catalytic activity of the CA enzyme was measured by performing the absorption tests using the PC-CA solution. A mathematical model was developed to simulate the CO_2 absorption into the PC and PC-CA solutions in the CSTR and these results were compared with experimental results. Finally, the feasibility of the CA enzyme used for promoting CO_2 absorption into the PC solution was evaluated.

1.4.3 Scope of work

The research focus is placed on the experimental and theoretical evaluations of the activity of the CA enzyme for promoting the absorption of CO_2 into the PC solution at select process conditions. The parameters to be tested include the PC concentration, CO_2 loading, enzyme dosage level, temperature, and partial pressure of CO_2. Based on experimental and modeling data, the optimal process conditions are to be identified for the CO_2 absorption.

2 EXPERIMENTAL SET-UP AND METHODOLOGY

2.1 Experimental set-up

Figure 2-1 presents a schematic of the experimental set-up. It consists of a gas supply unit, a stirred-tank reactor, and instrumentation for gas and liquid detection. The reactor is a Plexiglas vessel, 10.2 cm in internal diameter and 17.8 cm in height which is not insulated from the surrondings. Heating or cooling of the solution inside the reactor is achieved by circulating water through a stainless steel coil (0.6 cm O.D., 0.08 cm wall thickness) which is located inside the reactor. The water is circulated through a temperature controlled thermostatic water bath (Neslab, model RTE-110). Four symmetrical baffles, each, 10.2 cm tall and 1.3 cm width, are attached inside the vessel to prevent the formation of a vortex in the liquid phase. A magnetic stirrer (Corning stirrer/hotplate, model PC 320) with a 5.1 cm Telfon stir bar provides mixing at 60-1,100 rpm in the liquid-phase. A stirrer driven by an external motor (Caframo, model BCD2002) via a magnetic coupling provides mixing at 0-3,000 rpm in the gas-phase (1 cm above the liquid-phase in the reactor). The mixing rates are controlled to sustain a flat gas-liquid interface during the absorption rate measurements. The reactor is equipped with a pH meter (Denver Instrument, model 220) that is located 1 cm from the vessel wall and 4.5 cm from the bottom of the vessel. The pH meter measures the pH and also the temperature of the liquid-phase. A thermocouple (0.3 cm X 30 cm, Omega, Type K, model KMQSS-125-G-6) is located 2 cm from the vessel wall and 4.5 cm from the top of the vessel to measure the temperature of the gas-phase. A small amount of liquid can be sampled during the experiment for chemical analysis.

The gas supply system consists of a gas cylinder to supply CO_2 (Coleman grade, 99.99% purity, S. J. Smith). The gauge pressure of outlet gas from the gas cylinder is regulate at 135kPa by a pressure regulator which is connected to the cylinder.The inlet gas flow rate is measured using a mass flow meter (Alicat Scientific, model M-200SCCM-D/5M). The pressure of the reactor is controlled and measured by a vacuum controller (Alicat Scientific, model PC-30PSIA-D/5P). Downstream of the reactor, a vacuum pump (Dekker, model RVL002H-01) is equipped to provide the initial vacuum required in the system. Temperature, pressure, mass flow rate data are monitored and recorded with LabView and Hyperterminal software and a data acquisition system (National Instrument Digital Data Acquisition (DAQ) Systems, model NI USB 6009).

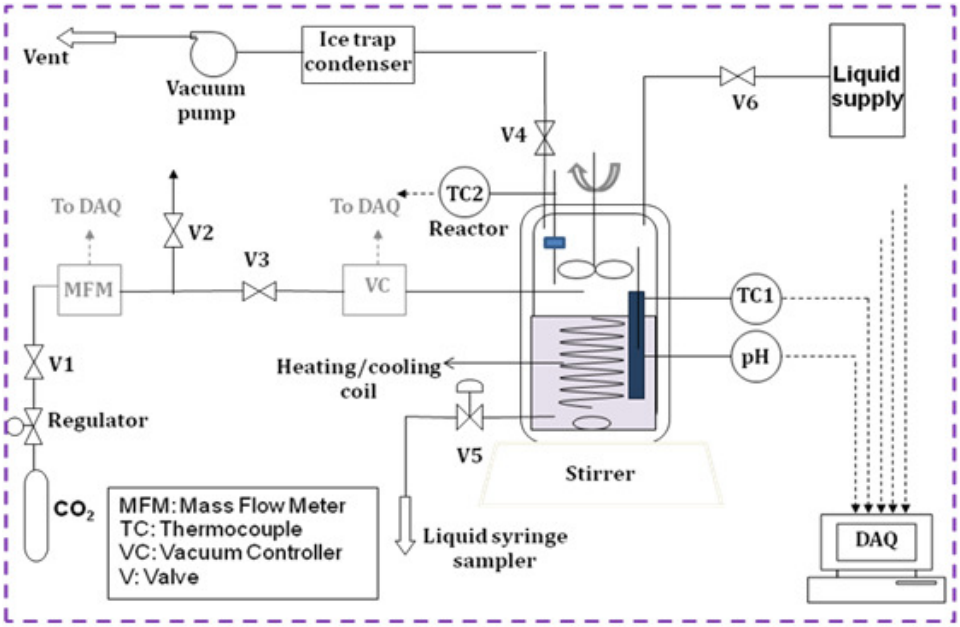

Figure 2-1 Experimental setup

2.1.1 Experimental methodology

The absorption rates of CO_2 in two types of solutions are measured: a baseline CO_2-PC system with no catalyst, and a CO_2-PC-CA system promoted with catalysts, or a CO_2-MEA based system. The CO_2 absorption is expected to be slow in the baseline solution and relatively fast in the promoted PC or MEA solutions. The MEA solution is tested both for the validation of the experimental set-up and for comparison with the promoted PC solution. The experimental system is operated under two different modes, either a gas-phase batch mode for a slow absorption system or a gas-phase semi-continuous mode for a fast absorption system. A similar experimental set up was successfully demonstrated for measuring the kinetics of CO_2 absorption in apiperazine solution [Derks, 2006].

2.1.1.1 Measurement of CO_2 absorption rate

Batch operation

All kinetic measurements for the CO_2-PC, CO_2-PC-CA, and select CO_2-MEA systems were performed in the batch mode with respect to both the liquid-phase and the gas-phase. In a typical experiment, 800 ml volume of the solution is used. The PC solution is prepared by dissolving K_2CO_3 (Sigma-Aldrich, purity > 99%) and $KHCO_3$ (Sigma-Aldrich, purity > 99.5%) granules in

deionized (DI) water to obtain the required concentrations of each compound in the solution. Before the start of an experiment, the valves V1, V2, and V3 are closed, valve V4 is opened, and the vacuum pump and the magnetic stirrer are turned on to degas the system. The time dedicated to degas the system was 30 minutes for experiments conducted at 25^{o}C and 5 min for the experiments conducted at 50^{o}C, respectively. The system was degased under 2.7kPa. The gas outlet V4 is then closed, the vacuum pump is turned off, and the solution is allowed to equilibrate at a reaction temperature. The water-vapor pressure of the solution, after being stabilized, is recorded and the magnetic stirrer is turned off. Before filling the reactor with CO_2, the valves V1 and V2 are opened to allow the CO_2 from the gas cylinder to purge the inlet tubes for 5-10 minutes. Valve V2 is then closed and valve V3 is opened to allow the CO_2 to flow into the reactor. Once the pressure inside the reactor reaches a desired value, the valve V3 is closed, the gas stirrer and the magnetic stirrer are turned on, and the total pressure, temperatures of the liquid and gas, and pH are continuously monitored and recorded by the data acquisition system. The CO_2 partial pressure is obtained by subtracting the solution's water vapor pressure, determined at the beginning of the experiment, from the total pressure measured during the experiment.

Semi-continuous operation

The reactor system was operated in a semi-continuous mode for select CO_2-MEA-based systems because the rates of CO_2 absorption into the MEA solutions are fast and when measured under the batch-mode, a rapid decrease in CO_2 partial pressure in the reactor will occur which make data collection difficult and less accurate. Under the semi-continuous mode, the absorption experiment is conducted at a constant total pressure as pure CO_2 gas continuously flows into the reactor to compensate for the amount of gas absorbed while the reactor outlet is closed.

In a typical experiment, the valves V1, V2, and V3 are closed, the valve V4 is opened, and the vacuum pump and the magnetic stirrer are turned on to degas the system for 30 minutes for the experiments conducted at 25^{o}C and 5 minutes for the experiments conducted at 50^{o}C. Gas outlet V4 is then closed, the vacuum pump is turned off, and the solution is then allowed to equilibrate with the gas phase at a specified reaction temperature. After the vapor pressure of water above the solution is stabilized, the total pressure of the gas in the vessel is recorded, the magnetic

stirrer is turned off, and the pressure controller is set to a desired pressure. Before filling the reactor with CO_2, the valves V1 and V2 are opened to purge the inlet tubes with the CO_2 from the gas cylinder for 5-10 minutes. The valve V2 is then closed and the valve V3 is opened to allow pure CO_2 to flow from the compressed gas cylinder to the reactor. Once the set pressure is reached, the gas stirrer and magnetic stirrer are turned on, and the gas flow rate, total pressure, temperatures of the liquid and gas, and pH are continuously monitored and recorded by the computer.

2.2 Matrix of tests

Two sets of the tests were performed. One set of tests were completed for the two reference solutions (i.e., the PC aqueous solution with no catalyst and the MEA aqueous solution, Table 2-1A-B, respectively). Another set of tests were completed for the CA-promoted PC aqueous solution. Note: The initial conversion as referenced in the following table is defined as percentage of the reactant (i.e., PC or MEA) which has reacted with CO_2 and indicates the capacity of the solution for the CO_2 absorption (higher the conversion, lower the capacity). It should be noted that 1 mol of CO_2 reacts with 1 mol of PC or 2 mols of MEA.

Table 2-1 Test matrix for CO_2 absorption into aqueous PC, MEA, and PC-CA solutions*

A - Absorption of CO_2 into PC solution (Reference tests)	Temperature (^oC)		CO_2 partial pressure (kPa)
	25	50	1-20
K_2CO_3, 20% wt, 0% initial conversion	Test 1	Test 2	
$K_2CO_3/KHCO_3$, 20% wt, 20% initial conversion	Test 3	Test 4	
$K_2CO_3/KHCO_3$, 20% wt, 40% initial conversion	Test 5	Test 6	
$K_2CO_3/KHCO_3$, 20% wt, 60% initial conversion	Test 7	Test 8	
$K_2CO_3/KHCO_3$, 30% wt, 40% initial conversion	Test 9	Test 10	

Table 2-1 continued from page 25

B - Absorption of CO_2 into 3M MEA solution	Temperature (^oC)		CO_2 partial pressure (kPa)
	25	50	1-20
MEA, 0% initial conversion	Test 11	Test 12	
MEA/carbamate, 40% initial conversion	Test 13	Test 14	
MEA/carbamate, 80% initial conversion	Test 15	Test 16	

C - Absorption of CO_2 into PC solution with CA enzyme	CA enzyme concentration (mg/l)	Temperature (^oC)		CO_2 partial pressure (kPa)
		25	50	1-20
K_2CO_3 20% wt, 0% initial conversion	30	Test 17	Test 18	
	300	Test 19	Test 20	
$K_2CO_3/KHCO_3$ 20% wt, 20% initial conversion	30	Test 21	Test 22	
	300	Test 23	Test 24	
$K_2CO_3/KHCO_3$ 20% wt, 40% initial conversion	30	Test 25	Test 26	
	300	Test 27	Test 28	
$K_2CO_3/KHCO_3$ 20% wt, 60% initial conversion	30	Test 29	Test 30	
	300	Test 31	Test 32	
$K_2CO_3/KHCO_3$ 30% wt, 40% initial conversion	30	Test 33	Test 34	
	300	Test 35	Test 36	

* the concentration of $K_2CO_3/KHCO_3$ solution is based on the K_2CO_3-equivalent concentration calculated as if all $KHCO_3$ is converted to K_2CO_3.

The reference tests for the PC (witout CA) and MEA solutions were aimed to verify the experimental setup, operating procedures, and the data analysis. It also serves as the baseline for the comparison with the CO_2 absorption into the CA-promoted PC solution tests. As previously mentioned, batch mode was used for the CO_2 absorption into the PC solution tests, while both

the batch and semi-continuous modes were employed for the MEA solution tests. The 20% wt PC aqueous solution with no initial conversion corresponds to an aqueous solution with 20% wt K_2CO_3 and no initial additon of $KHCO_3$. The 20% wt PC aqueous solution with 20%/40%/60% initial PC conversion corresponds to an aqueous solution starting with 20% wt K_2CO_3but has 20%/40%/60% of that K_2CO_3 initially converted to $KHCO_3$. Since each mol of CO_2 reacts with one mol of K_2CO_3 and produces two moles of $KHCO_3$, 20%/40%/60% initial conversion corresponds to initial molar ratio of K_2CO_3 to $KHCO_3$ of 2:1/3:4/1:3, respectively. The 30% wt PC aqueous solution with 40% initial PC conversion corresponds to an aqueous solution starting with 30% wt K_2CO_3 but has 40% of that K_2CO_3 initially converted to $KHCO_3$ resulting in an initial molar ratio of K_2CO_3 to $KHCO_3$ of 3:4. The reference MEA test used a 3M MEA aqueous solution with 0%/40%/80%initial conversion. The 3M MEA aqueous solution with no initial conversion corresponds to an aqueous solution with 3M MEA and no initial carbamate. The 3M MEA aqueous solution with 40%/80% initial conversion corresponds to an aqueous solution starting with 3M MEA but has 40%/80% of that MEA initially converted to carbamate. Since each mol of CO_2 reacts with two mol of MEA and produces one mol of carbamate, 40%/80% initial conversion corresponds to initial molar ratio of MEA to carbamate of 3:1/1:2. Two temperatures, i.e., 25^{o}C and 50^{o}C, were selected for all of the absorption tests since the former is a temperature mostly used in literature and the latter is close to the practical temperature of flue gas streams.

As previously mentioned, batch mode was used for all of the CO_2 absorption tests with the CA-PC solutions. Two CA enzymes, one from the Sigma-Aldrich (C3934 $\geq$ 2,500 Wilbur-Anderson units/mg protein) and another from undisclosed Company A were used in the tests. The Sigma-Aldrich enzyme is a commercialy available bovine CA product that is received in the form of a powder. The enzyme from Company A was fermented for this study and was concentrated in the liquid as received.

Prior to the enzyme tests, two different options of enzyme mixing were investigated. The first was to dissolve the enzyme in the PC solution beforehand. The second was to initially fill the PC solution in the reactor, and then right before the start of the test, the required amount of concentrated enzyme liquid sample from Company A was poured into the solution. Both

methods were tested under the same conditions. No difference (average difference in absorption fluxes < 3%) of the absorption rate was observed between these two runs. Therefore, the PC-CA solution was prepared before it was added to the reactor.

2.3 Data analysis

The data from the absortpton tests described above are further processed to obtain the absorption fluxes, enhancement factors, reaction rate constants, and mass transfer coefficients as described below. Data from the data acquisition system were converted into a spreadsheet format to facilitate data analysis.

2.3.1 Absorption flux

Under the batch mode, the reactor is closed during the experiment, and the total pressure change is recorded over time (Figure 2-2a). Based on the pressure profile, the instant flux of CO_2 absorption into the liquid phase is determined by :

$$J_{CO_2} = \frac{dP_{CO_2}}{dt} . \frac{V_g}{R_g T A_{gl}} \qquad \text{Eq 2-1}$$

Variables are defined in the Nomenclature Section.

As previously mentioned, under the semi-continuous mode, the absorption measurement is performed at a constant pressure as pure CO_2 gas continuously flows into the reactor system to compensate for the amount of gas absorbed during the test while the reactor outlet is closed. The recorded gas flow rate profile (Figure 2-2b) is used to calculate the instant CO_2 absorption flux according to the following expression:

$$J_{CO_2} = \frac{P_{CO_2} Q_{CO_2}}{R_g T A_{gl}} \qquad \text{Eq 2-2}$$

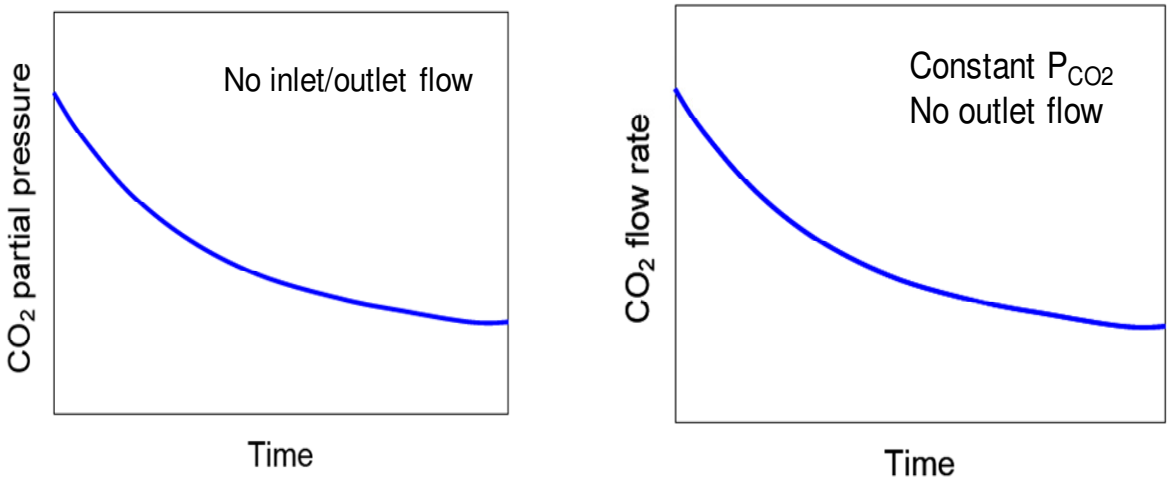

(a) Data obtained for the batch test

(b) Data obtained for the semi-continuous test

Figure 2-2 Data recording in the batch and semi-continuous tests

2.3.2 Enzyme enhancement factor

Enzyme enhancement factor (E_{enzyme}) is the ratio of the absorption flux of CO_2 into the PC solution in the presence of enzyme to the absorption flux in the absence of enzyme and is calculated as follows:

$$E_{enzyme} = \frac{J_{CO_2,PC-enzyme}}{J_{CO_2,PC}} \qquad \text{Eq 2-3}$$

The enhancement factor indicates the ability of the enzyme to improve the absorption flux at the specific conditions such as temperature and concentration of different species in the solution.

2.3.3 Reaction rate constant

According to Danckwert's surface renewal theory (Danckwerts,1970), the enhancement factor for gas absorption with a chemical reaction between components A and B (i.e., A is CO_2, and B is PC or MEA) is calculated as follows:

$$E = \sqrt{(1+Ha^2)} \qquad \text{Eq 2-4}$$

Hatta number (Ha) is defined as:

$$Ha = \sqrt{D_A k_1 C_B^b} / k_L \qquad \text{Eq 2-5}$$

k_1 can be the rate constant of one of the following major reactions:

$$CO_2 + OH^- \xrightarrow{k_1} HCO_3^- \text{ (PC solution)} \qquad \text{Eq 2-6}$$

$$CO_2 + H_2O + CA \xrightarrow{k_1} HCO_3^- + H^+ + CA \text{ (PC-CA solution)} \qquad \text{Eq 2-7}$$

$$CO_2 + RNH_2 \xrightarrow{k_1} RNHCOO^- + H^+ \text{ (MEA solution)} \qquad \text{Eq 2-8}$$

C_B^b is the bulk concentration of component B (B = OH^- in PC solution, CA in PC-CA solution, RNH_2 in MEA solution). In the absence of CA or amine (RNH_2), the reaction with OH^- is much faster than the CO_2 hydrolysis reaction and it is considered as the major reaction. However in the presence of CA the hydrolysis reaction is much faster than reaction with OH^- and hence it is the major reaction in the system.

If the absorption conditions satisfy the criteria below (Danckwerts, 1970),

$$Ha >> 2 \qquad \text{and} \qquad Ha << E_{inf} \qquad \text{Eq 2-9}$$

where E_{inf} is the enhancement factor in the infinite diluted solution and decreases with the CO_2 partial pressure, then $E \approx Ha$ and the reaction of CO_2 with the solution can be assumed as a pseudo first order reaction. In accordance, the absorption rate can be determined using the following equation:

$$J_{CO_2} = k_L E H_{CO_2} P_{CO_2} = \sqrt{(D_A k_1 C_B^b)}\ H_{CO_2} P_{CO_2} \qquad \text{Eq 2-10}$$

Therefore, the value of k_1 can be determined from the slope of a linear plot of J_{CO_2} as a function of P_{CO_2} ($\sqrt{(D_A k_1 C_B^b)}$ H_{CO_2}) within the pseudo first order region.

2.3.4 Mass transfer coefficients

CO_2 absorption in the PC, PC-CA and MEA solutions is a process combined with physical mass transfers and chemical reactions. Therefore to determine the absorption kinetics from the overall absorption rate mearsured, it is necessary to know the physical mass transfer performance of CO_2 in the liquid phase.

The liquid phase-based overall mass transfer coefficient K_L is related to the individual gas-phase and liquid-phase coefficients according to the following equation:

$$\frac{1}{K_L} = \frac{1}{k_L} + \frac{H}{k_G} \qquad \text{Eq 2-11}$$

When the liquid phase dominates in the mass transfer, i.e., $\frac{1}{k_L} >> \frac{H}{k_G}$, then

$$K_L = k_L \qquad \text{Eq 2-12}$$

The mass transfer resistance in the gas phase can be eliminated by studying the absorption of pure CO_2 gas into a liquid. In this case, the absorption rate is completely limited by the transport of CO_2 in the liquid and the absorption flux can be expressed as follows:

$$J_{CO_2} = k_L \left(C^*_{CO_2} - C_{CO_2}\right) \qquad \text{Eq 2-13}$$

Therefore, the value of k_L can be obtained from the slope of J_{CO_2} versus $\left(C^*_{CO_2} - C_{CO_2}\right)$ plot. J_{CO_2} into the previously boiled DI water was measured at 25°C under the batch mode as described in the section 2.1.1.1. Bulk concentration of CO_2 in the liquid phase was calculated from a mass balance assuming negligible dissociation of dissolved CO_2.

3 MODELING APPROACH

A mathematical model was developed to predict the performance of the CO_2 absorption into the PC-CA solution. The model is based on Higbie's penetration theory and includes the major reactions involved in the absorption of CO_2 into the PC-CA solution under variable and constant CO_2 pressures. A detailed description of the model is described in this chapter.

3.1 Reactions in carbonate solution

There are four dissolved CO_2 species considered in the pure carbonate-aqueous solution (i.e., CO_2, H_2CO_3, HCO_3^- and CO_3^{2-}). The existence of H_2CO_3 is negligible because of its strong tendency of dissociation. The relative importance of other species is highly related to the pH of the solution since it determines the speciation. Figure 3-1 demonstrates the relative proportions of different species as a function of pH at 25°C for this carbonate system. Since the absorption of CO_2 into the aqueous PC solution is usually maintained at a weak basic to basic condition, both HCO_3^- and CO_3^{2-} ions exist while the concentration of dissolved CO_2 is negligible.

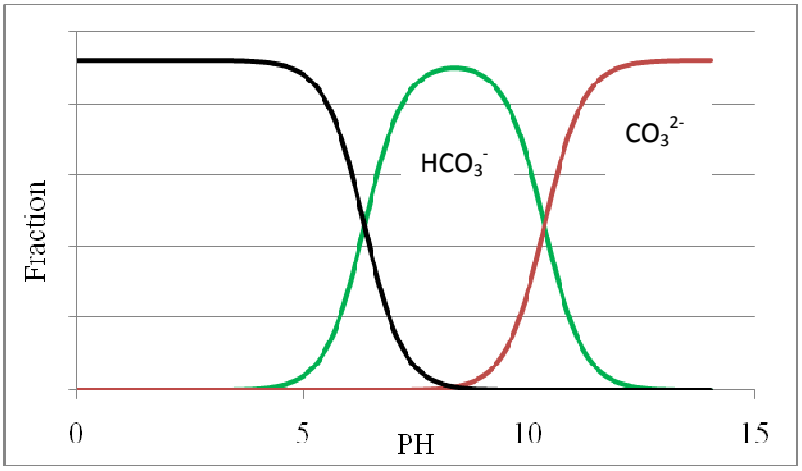

Figure 3-1 Relative proportions of carbonic species with varying pH conditions at 25°C . Fraction is defined as the concentration of each carbonic species over their total concentration.

During the absorption of CO_2, the following reactions occur:

$$CO_2 + OH^- \underset{k_{12}}{\overset{k_{11}}{\Leftrightarrow}} HCO_3^- \qquad \text{Eq 3-1}$$

$$HCO_3^- + OH^- \underset{k_{22}}{\overset{k_{21}}{\Leftrightarrow}} CO_3^{2-} + H_2O \quad \text{Eq 3-2}$$

$$OH^- + H^+ \underset{k_{32}}{\overset{k_{31}}{\Leftrightarrow}} H_2O \quad \text{Eq 3-3}$$

$$CO_2 + H_2O \underset{k_{42}}{\overset{k_{41}}{\Leftrightarrow}} HCO_3^- + H^+ \quad \text{Eq 3-4}$$

$$HCO_3^- \underset{k_{52}}{\overset{k_{51}}{\Leftrightarrow}} CO_3^{2-} + H^+ \quad \text{Eq 3-5}$$

The solution containing HCO_3^- and CO_3^{2-} has buffer capacity based on the equations 3-4 and 3-5 [Snoeyink and Jenkins, 1980].

The rate constants for the above mentioned reactions are dependent on the temperature and ionic strength of the PC solution and are discussed in section 3.4.

In the presence of the CA enzyme, the CO_2 hydration reaction is catalyzed:

$$CO_2 + H_2O + CA \underset{k_{62}}{\overset{k_{61}}{\Leftrightarrow}} HCO_3^- + H^+ + CA \quad \text{Eq 3-6}$$

Assuming the Michaelis–Menten kinetic mechanism [Buchholz et al., 2005] applicable for the reaction (6) (Eq 3-6), the reaction rate can be expressed as:

$$r_{CO_2} = -\frac{k_{cat} C_{CA}}{K_M + C_{CO_2}} C_{CO_2} \quad \text{Eq 3-7}$$

The rate constant k_{cat} is directly correlated to the CA enzyme activity, and varies with varying CA sources. In the preliminary calculations, the values of k_{cat} and K_M were adopted as those reported in the literature [Dilmore et al., 2009 and Bao et al., 2004] (i.e., $k_{cat} = 2\times10^6$ s^{-1} and K_M =20 mol/m^3). These two variables can be changed in the sensitivity analysis to investigate their impacts on the CO_2 absorption rate. For a specific CA enzyme, they can be obtained by fitting model predictions with experimental data. For the maximum partial pressure of CO_2 in the

absorption column which is 15kPa the concentration of dissolved CO_2 estimated using Henry's constant (H_{CO_2} = 11.53 mol/atm·m^3) at 25°C is 1.7 mol/m^3. Therefore the highest CO_2 concentration in the solution is still one order of magnitude lower than K_M. Except at the gas-liquid interface, the concentration of CO_2 is expected to be much lower than this value, because it is consumed in the chemical reactions, thus:

$$K_M \succ\succ C_{CO_2} \qquad \text{Eq 3-8}$$

Therefore the reaction rate described in Eq 3-7 can be reduced to:

$$r_{CO_2} = -\frac{k_{cat} C_{CA}}{K_M} C_{CO_2} \qquad \text{Eq 3-9}$$

Considering the fact that the concentration of the CA enzyme is constant, K_{61} can be expressed as a constant:

$$k_{61} = \frac{k_{cat} C_{CA}}{K_M} \qquad \text{Eq 3-10}$$

There are several different theories that can be used for modeling the absorption process with chemical reaction. The film theory [Whitman, 1923], the surface renewal theory [Danckwerts, 1955], and the penetration theory [Higbie, 1935] have been most widely used to predict the absorption rates in various systems. However it has been shown that these theories give almost same quantitative predictions [Danckwerts and Gillham, 1966]. Penetration theory is particularly applicable to the systems with fluid mixing and short contact time (in order of seconds) between the elements of two phases, such as stirred cell reactors. Hence, in this study, the penetration theory has been employed to predict the absorption rate of CO_2 into PC solutions with and without CA enzyme.

3.2 Penetration theory

The Higbie's penetration model is based on the concept that interfacial transfer occurs by turbulent eddies moving from the liquid bulk to the interface where unsteady-state molecular diffusion happens until the eddy is displaced from the surface after some time, called the

exposure time (Figure 3-2). The Higbie's penetration model gives the following relationship for the exposure time, t_e:

$$t_e = \frac{4D_A}{\pi k_L^2} \qquad \text{Eq 3-11}$$

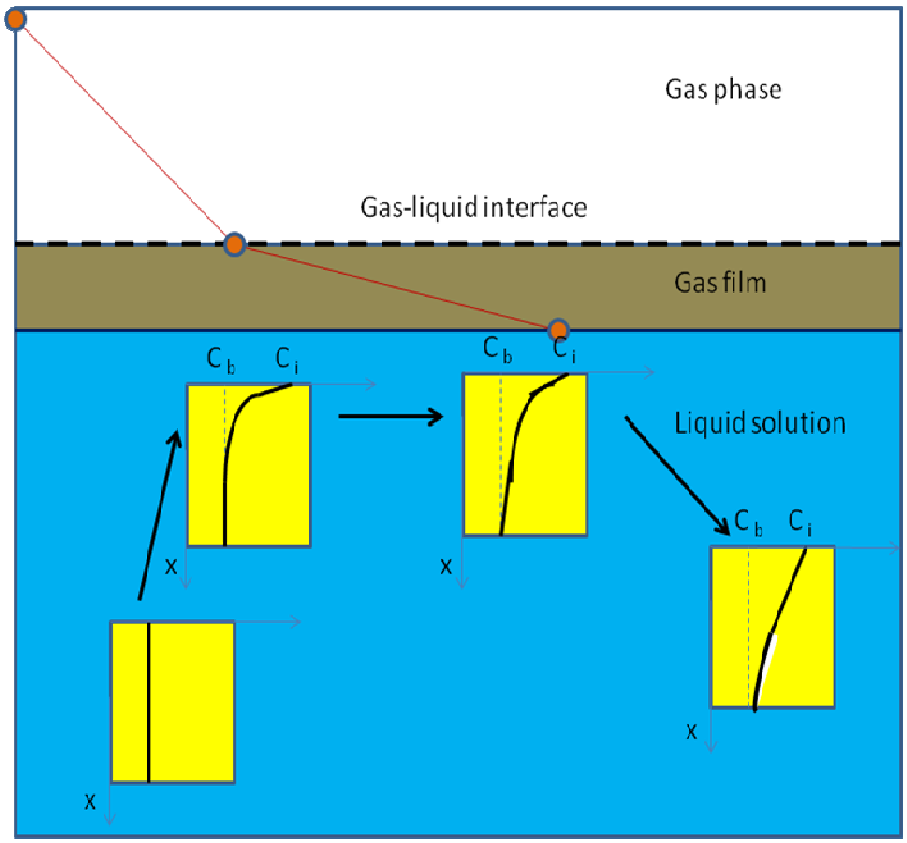

Figure 3-2 Schematic describing Higbie's penetration theory: A fluid element (eddy) moving toward then away from the gas liquid interface with a commensurate change in its concentration gradient

The concentration profiles of all the species in the liquid eddies can be calculated as a function of exposure time of eddies, by solving the conservation of mass equation for each of the species:

$$\frac{\partial C_A(x,t)}{\partial t} = D_A \frac{\partial^2 C_A(x,t)}{\partial x^2} + r_A(x,t) \qquad \text{Eq 3-12}$$

A in the case of CO_2 absorption into the PC-CA solution can be CO_2, HCO_3^-, CO_3^{2-}, H^+ or OH.

The reaction rate for each of these species can be expressed as:

$$r_{co_2} = k_{12}C_{HCO_3^-} - k_{11}C_{CO_2}C_{OH^-} + k_{62}C_{HCO_3^-}C_{H^+} - k_{61}C_{CO_2} + k_{42}C_{HCO_3^-}C_{H^+} - k_{41}C_{CO_2} \qquad \text{Eq 3-13}$$

$$r_{OH^-} = k_{12}C_{HCO_3^-} - k_{11}C_{CO_2}C_{OH^-} + k_{22}C_{CO_3^{2-}} - k_{21}C_{HCO_3^-}C_{OH^-} + k_{32} - k_{31}C_{OH^-}C_{H^+} \qquad \text{Eq 3-14}$$

$$r_{HCO_3^-} = k_{11}C_{CO_2}C_{OH^-} - k_{12}C_{HCO_3^-} + k_{22}C_{CO_3^{2-}} - k_{21}C_{HCO_3-}C_{OH^-} + k_{61}C_{CO_2} - k_{62}C_{HCO_3^-}C_{H^+} \qquad \text{Eq 3-15}$$

$$r_{CO_3^{2-}} = k_{21}C_{HCO_3^-}C_{OH^-} - k_{22}C_{CO_3^{2-}} + k_{51}C_{HCO_3^-} - k_{52}C_{CO_3^{2-}}C_{H^+} \qquad \text{Eq 3-16}$$

$$r_{H^+} = k_{32} - k_{31}C_{OH^-}C_{H^+} + k_{61}C_{CO_2} - k_{62}C_{HCO_3^-}C_{H^+} + k_{51}C_{HCO_3^-} - k_{52}C_{CO_3^{2-}}C_{H^+} \qquad \text{Eq 3-17}$$

To solve the set of equations described above, two boundary conditions and one initial condition are necessary for each species. The initial condition is obvious as the concentration of each species is equal to its initial value before absorption occurs, which can be calculated from the equilibrium relationships. The liquid eddies have two boundaries, one at the gas-liquid interface ($x = 0$) and another at the depth ($x = \delta$) of the eddies. At $x = 0$, the concentration of CO_2 in the liquid eddies is determined by assuming that it is in equilibrium with the CO_2 in the gas phase according to the Henry's law. For other species, there is no mass transfer between the liquid and the gas phase, and their fluxes at the interface are therefore equal to zero. Eddy depth is mathematically considered infinity. Hence, at $x = \infty$, the concentration of each species is assumed to approach the concentration in the bulk of liquid. The initial and boundary conditions are given in Eq 3-18 through Eq 3-20:

$$x = \infty \quad t > 0 \quad C_i = C_i^b \qquad i = CO_2, HCO_3^-, CO_3^{2-}, H^+, OH^- \qquad \text{Eq 3-18}$$

$$x = 0 \quad t > 0 \quad \begin{cases} C_{CO_2} = H_{CO_2} P_{CO_2} \\ \dfrac{\partial C_i}{dx} = 0 \quad i = CO_2, HCO_3^-, CO_3^{2-}, H^+, OH^- \end{cases} \qquad \text{Eq 3-19}$$

$$x = \infty \quad t > 0 \quad C_i = C_i^b \qquad i = CO_2, HCO_3^-, CO_3^{2-}, H^+, OH^- \qquad \text{Eq 3-20}$$

The concentrations of all species in the bulk of liquid are calculated using the equilibrium constraints, the overall carbon balance, and the electro-neutrality constraint.

Partial pressure of CO_2 also changes over time and its value can be determined by solving the following equation:

$$\frac{dP_{CO_2}}{dt} = \frac{R_g T A_{gl} D_{CO_2}}{V_g t_e} \int_0^{t_e} \left. \frac{\partial C_{CO_2}}{\partial x} \right|_{x=0} dt \qquad \text{Eq 3-21}$$

with the initial condition:

$$t = 0 \qquad P_{CO_2} = P_{CO_2}^0 \qquad \text{Eq 3-22}$$

By solving the above conservation of mass equations and the rate equations, the flux of CO_2 through the gas-liquid interface (J_{CO_2}) can be calculated using the following equation:

$$J_{CO_2} = -\frac{1}{t_e}\int_0^{t_e} D_{CO_2} \left.\frac{\partial C_{CO_2}}{\partial x}\right|_{x=0} dt \qquad \text{Eq 3-23}$$

The exposure time of the eddies was determined according to the following expression:

$$t_e = \frac{4D_{CO_2}}{\pi k_{L,CO_2}^2} \qquad \text{Eq 3-24}$$

The value of k_{L,CO_2} was estimated based on the liquid-phase mass transfer coefficient of CO_2 in water (k_{L,CO_2}^0) by assuming:

$$\frac{k_{L,CO_2}}{k_{L,CO_2}^0} = \frac{\sqrt{D_{CO_2}}}{\sqrt{D_{CO_2}^0}} \qquad \text{Eq 3-25}$$

D_{CO_2} and $D_{CO_2}^0$ can be estimated by the following correlation with the viscosity [Joosten, 1972]:

$$D_{CO_2}\mu^{0.82} = \text{constant} \qquad \text{Eq 3-26}$$

3.3 Numerical method

The finite difference method was used for the spatial discretization (Figure 3-3) of the differential equations.

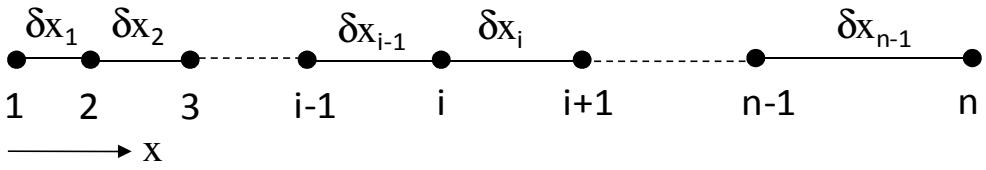

Figure 3-3 Finite difference mesh

In order to increase the accuracy of the numerical calculations, smaller mesh intervals were used near the gas-liquid interfacial area where the concentration profiles change more with displacement. Specifically, at high concentration of CA enzyme, the penetration depth for CO_2

(δ_1) is very small in comparison to the depth δ of the eddy and uniform grid may cause significant numerical error. Hence, it is better to increase the mesh size with increasing distance from the gas-liquid interface. The mesh growth rate, η, is defined as:

$$\eta = \frac{\delta x_i}{\delta x_{i-1}} \qquad \text{Eq 3-27}$$

The number of finite difference points for CO_2 penetration zone (n_1) was determined from:

$$\frac{n_1 - 1}{n - 1} = \xi \frac{\delta_1}{\delta} \qquad \text{Eq 3-28}$$

ξ is a factor which is 1 for a uniform mesh, and greater than 1 for a mesh which is growing from the gas-liquid interface. The sum of all finite difference intervals must be equal to δ:

$$\delta = \delta x_1 + \delta x_2 + \delta x_3 + ... + \delta x_{n-1} = \delta x_1 + \eta \delta x_1 + \eta^2 \delta x_1 .... + \eta^{n-2} \delta x_1 = \delta x_1 \left(1 + \eta + \eta^2 + ... + \eta^{n-2}\right) \qquad \text{Eq 3-29}$$

Similarly, the sum of finite difference intervals in the CO_2 penetration zone must be equal to δ_1:

$$\delta_1 = \delta x_1 + \delta x_2 + \delta x_3 + ... + \delta x_{n_1-1} = \delta x_1 + \eta \delta x_1 + \eta^2 \delta x_1 .... + \eta^{n_1-2} \delta x_1 = \delta x_1 \left(1 + \eta + \eta^2 + ... + \eta^{n_1-2}\right) \qquad \text{Eq 3-30}$$

δx_1 and η were then determined by solving Eq 3-29 and 3-30, simultaneously.

Second derivatives were approximated as:

$$\frac{\partial^2 C_{A,i}}{\partial x^2} = \frac{\dfrac{\dfrac{C_{A,i+1}-C_{A,i}}{\delta x_i} - \dfrac{C_{A,i}-C_{A,i-1}}{\delta x_{i-1}}}{\dfrac{\delta x_i + \delta x_{i-1}}{2}}}{} = 2\frac{\delta x_{i-1}C_{A,i+1} - (\delta x_i + \delta x_{i-1})C_{A,i} + \delta x_i C_{A,i-1}}{(\delta x_i \delta x_{i-1})(\delta x_i + \delta x_{i-1})};\ i = 2, n-1 \qquad \text{Eq 3-31}$$

where $C_{A,i}$ is concentration of species A at i^{th} node.

Substituting Eq 3-31 into Eq 3-12 yields:

$$\frac{dC_{A,i}}{dt} = 2D_A \frac{\delta x_{i-1}C_{A,i+1} - (\delta x_i + \delta x_{i-1})C_{A,i} + \delta x_i C_{A,i-1}}{(\delta x_i \delta x_{i-1})(\delta x_i + \delta x_{i-1})} + r_{A,i};\quad i = 2, n-1 \qquad \text{Eq 3-32}$$

where $r_{A,i}$ is the rate of reaction for species A at the i^{th} node.

Eq 3-16 can be discretized using the following forward differentiation formula:

$$\frac{dP_{CO_2}}{dt} = \frac{R_g T A_{gl} D_{CO_2}}{V_g t_e} \int_0^{t_e} \frac{C_{CO_2,2} - C_{CO_2,1}}{\delta x_1} dt \qquad \text{Eq 3-33}$$

initial and boundary conditions can be written as:

t=0:

$$C_{A,i} = C_A^0;\quad i = 2, n-1 \qquad \text{Eq 3-34}$$

$$P_{CO_2} = P_{CO_2}^0 \qquad \text{Eq 3-35}$$

t > 0:

$$C_{A,1} = H_{CO_2} P_A; \qquad A = CO_2 \qquad \text{Eq 3-36}$$

$$C_{A,1} = C_{A,2}; \qquad A = HCO_3^-, CO_3^{2-}, H^+, OH^- \qquad \text{Eq 3-37}$$

$$C_{A,n} = C_A^b; \qquad A = CO_2, HCO_3^-, CO_3^{2-}, H^+, OH^- \qquad \text{Eq 3-38}$$

The resulting equations are ordinary differential equations (ODEs) with time as the independent variable, which are solved efficiently using MATLAB ODE solver, ode15s.

Since penetration theory assumes that the diffusing components don't reach the bulk fluid, a value must be chosen for the penetration depth which is big enough that penetrating components wouldn't reach the bulk liquid during the eddy's exposure time. A guess value for δ is chosen and discretized equations are solved on a uniform mesh ($\xi = 1$) for the duration of the eddy's exposure to interface ($t = 0$ to t_e). Spatial concentration profiles of penetrating species are checked visually to make sure that penetrating components don't reach the bulk liquid. If not, the calculations are repeated for larger values of δ until concentration profiles are flat at $x = \delta$. From the concentration profile of CO_2, a value of δ_1 is determined which is where the CO_2 profile starts flattening. Calculations are repeated for finer and non-uniform mesh by increasing the number of grid points and selecting a value of ξ greater than 1. A value of ξ between 2-3 is good in the most cases, but if the area of a sharp CO_2 concentration profile is very small (that may happen at high enzyme concentrations), a larger value must be chosen for ξ to make sure that there are enough grid points in that area. The last step is repeated until calculated initial absorption flux (time averaged from $t = 0$ to t_e) is independent of the mesh resolution.

3.4 Evaluation and selection of model parameters

The correlations available in the literature were evaluated and selected to predict the related reaction rate constants, gas and liquid physical properties, and Henry's constants for CO_2 dissolution in the PC solutions. These correlations or parameters are required as data inputs for the mathematical model. A detailed description is provided as follows.

3.4.1 Kinetic parameters

Two major reactions that are important for the CO_2 absorption into PC-CA solution are the reactions of dissolved CO_2 with OH^- ion and the hydration reaction of CO_2 with H_2O catalyzed by the CA enzyme [Alper and Deckwer, 1980]. In order to accurately calculate the rates of individual reactions, it is important to input the correct reaction rate constants. These constants generally vary with the concentrations of ions present in the solution and the temperature.

Reaction rate constants for reaction (1):

The reaction rate constant for the forward reaction in the presence of co-electrolytes can be obtained using the following correlations [Pohorecki and Moniuk, 1988]:

$$\log \frac{k_{11}}{k_{11}^{\infty}} = 0.11\times10^{-3} C_{K^+} + 0.17\times10^{-3} C_{CO_3^{2-}} \qquad \text{Eq 3-39}$$

$$\log k_{11}^{\infty} = 8.916 - \frac{2383}{T} \quad (\text{Cents et al., 2005})$$

Eq 3-40 The rate constant for the reverse reaction is calculated based on the known k_{11} and equilibrium constants K_1 [Edwards, 1978] and K_w [Tsonopoulos, 1976]:

$$k_{12} = \frac{k_{11} K_w}{K_4} \qquad \text{Eq 3-41}$$

$$K_4 = \frac{C_{H^+} C_{HCO_3^-}}{C_{CO_2}} \qquad \text{Eq 3-42}$$

$$K_w = C_{H^+} C_{OH^-} \qquad \text{Eq 3-43}$$

$$K_4 = \exp\left(-\frac{12092.1}{T} - 36.786\ln(T) + 235.482\right)\rho_W \qquad \text{Eq 3-44}$$

$$\log\left(\frac{K_W}{\rho_W^2}\right) = -\frac{5839.5}{T} - 22.4773\log(T) + 61.2062 \qquad \text{Eq 3-45}$$

Reaction rate constants for reaction (6):

Assuming the Michaelis–Menten kinetic mechanism is applicable for the reaction (6) the rate constant, k_{61} can be written as Eq 3-10.

The rate constant for the reverse reaction can be calculated if k_{61} and equilibrium constant K_4 are known:

$$k_{62} = \frac{k_{61}}{K_4} \qquad \text{Eq 3-46}$$

Reaction rate constants for reaction (2), (3), (4) and (5):

The contributions of Reactions (2), (3) and (4) to the overall absorption rate is not as significant as reactions (1) and (5) [Augugliaro and Rizzuti, 1987; Dindore et al., 2005]. Therefore, constant values for k_{21} [Eigen, 1963], k_{31} [Cents et al., 2005], and k_{41} [Danckwerts and Sharma, 1966] at 25^{o}C were used without correcting their dependence on the temperature and species concentrations of the solution:

$$k_{21} = 6.0\times10^{6}\ \frac{m^3}{mol\cdot s} \qquad \text{Eq 3-47}$$

$$k_{31} = 1.4\times10^{8}\ \frac{m^3}{mol\cdot s} \qquad \text{Eq 3-48}$$

$$k_{41} = 0.24\times10^{-1}\ \frac{1}{s} \qquad \text{Eq 3-49}$$

The values of the rate constants for the individual backward reactions can be calculated based on the equilibrium constants of these reactions:

$$k_{22} = \frac{k_{21}}{K_2} \qquad \text{Eq3-50}$$

$$k_{32} = k_{31} * K_W \qquad \text{Eq 3-51}$$

$$k_{42} = \frac{k_{41}}{K_4} \qquad \text{Eq 3-52}$$

$$K_2 = \frac{C_{CO_3^{2-}}}{C_{HCO_3^-} C_{OH^-}} \qquad \text{Eq 3-53}$$

Where K_2 can be calculated from the following correlation [Hikita et al., 1976]:

$$\log(K_2) = \frac{1568.9}{T} - 2.5866 - 6.737 \times 10^{-3} T \qquad \text{Eq 3-54}$$

3.4.2 Physical properties

Accurate values of CO_2 diffusivities and Henry's constants in PC solutions are important for precise predictions of absorption rates. The correlations used to predict these parameters are described below:

3.4.2.1 Diffusivity of CO_2 in PC solution

CO_2 diffusivity, D_{CO_2}, at 25 °C was calculated from the following expression [Park et al., 1997]:

$$\frac{D_{CO_2}}{D^0_{CO_2}} = 1 - (C_1 C_{CO_3^{2-}} + C_2 C_{HCO_3^-} + C_3 C_{OH^-}) \qquad \text{Eq 3-55}$$

where C_1, C_2 and C_3 are the correlation constants having the values of 2.61×10^{-4}, 1.40×10^{-4}, and 1.29×10^{-4} m^3/mol, respectively.

$D^0_{CO_2}$ is the diffusivity of CO_2 into water at 25°C, which is 1.88×10^{-9} m^2/s [Versteeg 1987]. CO_2 diffusivity into PC solution was corrected for temperature based on the change in viscosity using the following expression [Joosten and Danckwerts 1972]:

$$\frac{D_{CO_2}}{D^0_{CO_2}} = \left(\frac{\mu^0}{\mu}\right)^{0.82} \quad \text{Eq 3-56}$$

Viscosity of solution at 20°C was calculated from the following equation:

$$\mu^0 = \mu^0_w + \left(\mu^0_{K_2CO_3} - \mu^0_w\right) + \left(\mu^0_{KHCO_3} - \mu^0_w\right) = \mu^0_{K_2CO_3} + \mu^0_{KHCO_3} - \mu^0_w \quad \text{Eq 3-57}$$

It was assumed that impact of temperature on the viscosity of solution is the same as that on the viscosity of water:

$$\frac{\mu}{\mu^0} = \frac{\mu_w}{\mu^0_w} \quad \text{Eq 3-58}$$

3.4.2.2 Henry's constant for CO_2 dissolution in PC solution:

To estimate the gas-liquid mass transfer rate, it is required to know the concentration of CO_2 at the gas-liquid interface which is assumed at equilibrium between gas- and liquid phase CO_2. The liquid-phase equilibrium concentration can be calculated based on the Henry's constant of CO_2 in solution. The following correlation suggested by Schumpe (1993) is used to determine the solubility of CO_2 in the PC solution.

$$\log\left(\frac{C_{G,0}}{C_G}\right) = \sum\left(h_i + h_G\right)C_i \quad \text{Eq 3-59}$$

Assuming Henry's law applies:

$$\frac{H_0}{H} = \frac{C_{G,0}}{C_G} \quad \text{Eq 3-60}$$

Where H_0 and H are Henry's constants in pure water and salt solution, respectively. It is assumed that h_G has a linear correlation with temperature:

$$h_G = h_{G,o} + h_T(T - 298.15) \qquad \text{Eq 3-61}$$

Henry's constant for CO_2 in water $(\text{mol/m}^3 \cdot \text{atm})$ was determined using a correlation proposed by Versteeg and van Swaaij (1988):

$$H_{CO_2,0} = 3.59 \times 10^{-2} \exp\left(\frac{2044}{T}\right) \qquad \text{Eq 3-62}$$

Parameters needed for calculating the CO_2 solubility in the PC solution are listed in Tables 3-1 and 3-2:

Table 3-1 CO_2 specific parameters $h_{G,0}$ and h_T

Gas	$10^3 \times h_{G,o}$ $[m^3 \cdot mol^{-1}]$	$10^6 \times h_T$ $[m^3 \cdot mol^{-1} \cdot K^{-1}]$
CO_2	-0.0172	-0.338

Table 3-2 Ion-specific parameters for parameter h_i

Ion	$10^3 \times h_i$ $[m^3 \cdot mol^{-1}]$
H^+	0
K^+	0.0922
HCO_3^-	0.0967
CO_3^{2-}	0.1423
OH^-	0.0839

Initial equilibrium concentration of each ion was used in the calculation of Henry's constant. These initial concentrations can be calculated by simultaneously solving the equilibrium equations (Equations 3-42, 3-43, 3-53), carbonic species balance, and electric charge balance:

$$C_{CO_2} + C_{HCO_3^-} + C_{CO_3^{2-}} = C_{T,CO_2} \quad \text{Eq 3-63}$$

$$C_{HCO_3^-} + 2C_{CO_3^{2-}} + C_{OH^-} = C_{K^+} + C_{H^+} \quad \text{Eq 3-64}$$

Where C_{T,CO_2} is the total concentration of carbonic species in the solution.

4 RESULTS AND DISCUSSION

4.1 Experimental section

4.1.1 CO_2 absorption into water

The mass transfer coefficient for the absorption of pure CO_2 into DI water was determined from the plot of absorption flux against the equilibrium concentration of CO_2 in the liquid phase (Figure 4-1) at 25°C by using the batch experimental setup described in Section 2.1. The value of the slope of the line is the liquid-phase mass transfer coefficient k_L which is equal to 5.09×10^{-5} $m{\cdot}s^{-1}$. It can be shown from equilibrium equations, carbonic species balance, and electric charge balance that the pH of water after absorption of a very small amount of CO_2 would reduce to less than 5.5 and at this pH dissociation of dissolved CO_2 is negligible. Hence, the measured k_L can be considered as pure physical liquid-phase mass transfer coefficient.

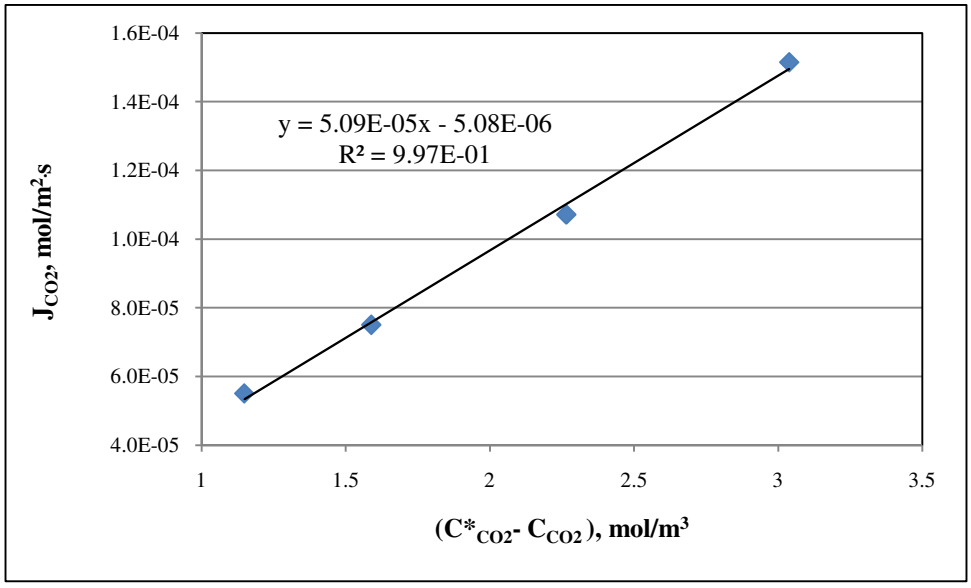

Figure 4-1 Pure CO_2 absorption into water, stirring rate = 400 rpm, T=25°C

The value of k_L was also measured at 25°C and stirring rates of 200, 300, and 400 rpm. The mass transfer resistance decreased with increasing stirring rate (Figure 4-2) without a leveling-off in its value over the range of mixing conditions tested here. All absorption experiments

occurred at the 400 rpm stirring rate to assure that the physical mass transfer resistance is comparable from one experiment to another.

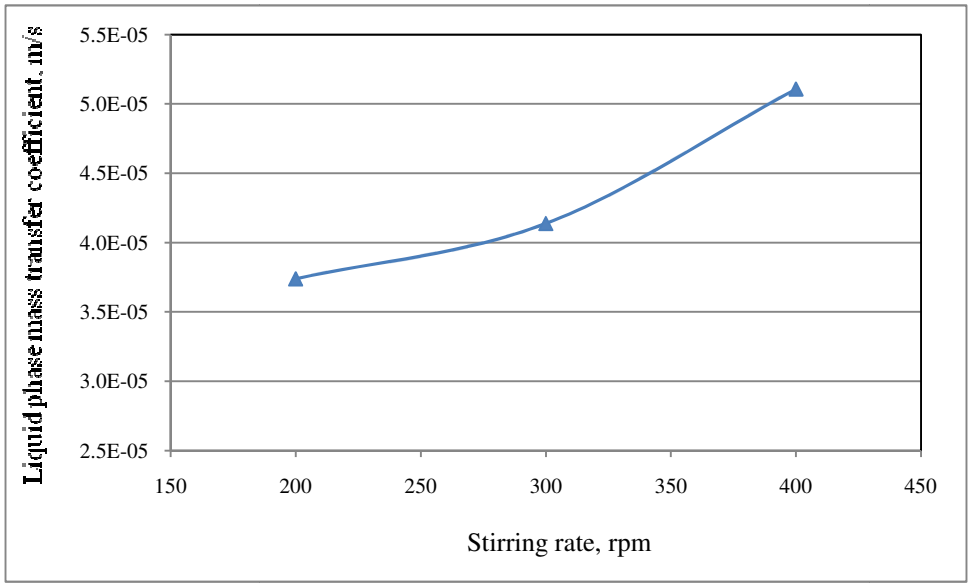

Figure 4-2 Liquid phase mass transfer coefficient dependence on liquid stirring rate for pure CO_2 absorbing into water at 25°C

As previously discussed in Chapter 3, corresponding values for k_L describing CO_2 absorption into aqueous-based PC solutions at select temperatures were estimated based on the change in the viscosity of the solution using equations 3-25 and 3-26.

4.1.2 Absorption of CO_2 into MEA solutions

A few test conditions were selected to evaluate the experimental set-up and procedures. The results of these tests were further used as a reference to evaluate the CO_2 absorption rate into PC-CA as compared to the MEA solution.

The effects of the level of initial MEA conversion in solution to carbamate at the beginning of each test and temperature on CO_2 absorption flux in this system are provided as follows.

4.1.2.1 Effect of MEA conversion on CO_2 absorption rate

Figure 4-3 shows CO_2 absorption flux as a function of MEA conversion, obtained from a semi-continuous test at 25°C and CO_2 partial pressure of 20kPa. It can be seen that the absorption flux decreases with increasing amount of initial MEA conversion. This was expected

and can be explained by the fact that at higher initial conversion, the concentration of MEA is lower. Therefore, as the conversion or loading (mol CO_2 absorbed/ mol amine in the solution) increases, less reactive species are available to react with CO_2.

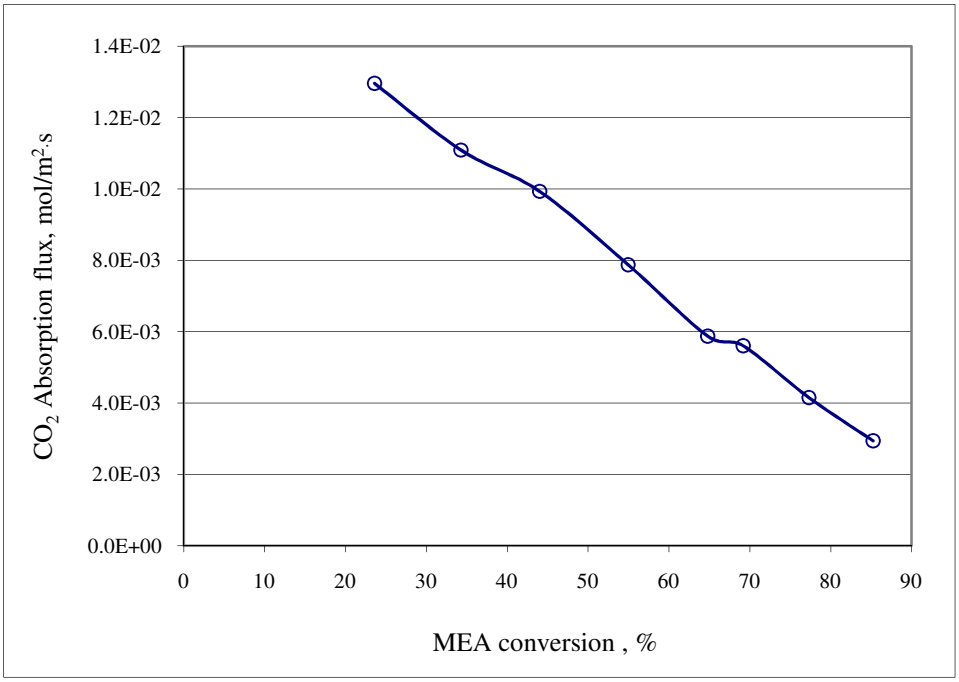

Figure 4-3 Impact of initial MEA conversion on CO_2 absorption rate in 3M MEA at 25 °C and CO_2 partial pressure of 20kPa

4.1.2.2 Effect of temperature on CO_2 absorption rate

Absorption flux as a function of CO_2 partial pressure for two different initial MEA conversions at 25°C and 50°C was obtained by using the batch experimental setup and results are provided in Figure 4-4. The difference between data in Figure 4-4 and Figure 4-3 is due to the difference of experimental setup (batch vs. continuous). It can be seen that temperature increases the CO_2 absorption flux into the 3M MEA solution at 40% and 80% initial conversion. Absorption flux at 50°C is 1.5-4 times higher than that at 25°C. It can be concluded that the impact of the increase in the reaction rate and liquid diffusivity of CO_2 as the temperature increases is larger than the impact of the decrease in the solubility of CO_2 into the solution. It can also be seen that absorption flux increases faster with pressure at higher temperature. This behavior can again be explained by the faster kinetics and diffusion at higher temperature which overcome the decrease in the solubility of CO_2 as temperature increases:

$$J_{CO_2} = k_L E H_{CO_2} P_{CO_2}\ ;\ \frac{\partial J_{CO_2}}{\partial P_{CO_2}} \approx k_L E H_{CO_2} \qquad \text{Eq 4-1}$$

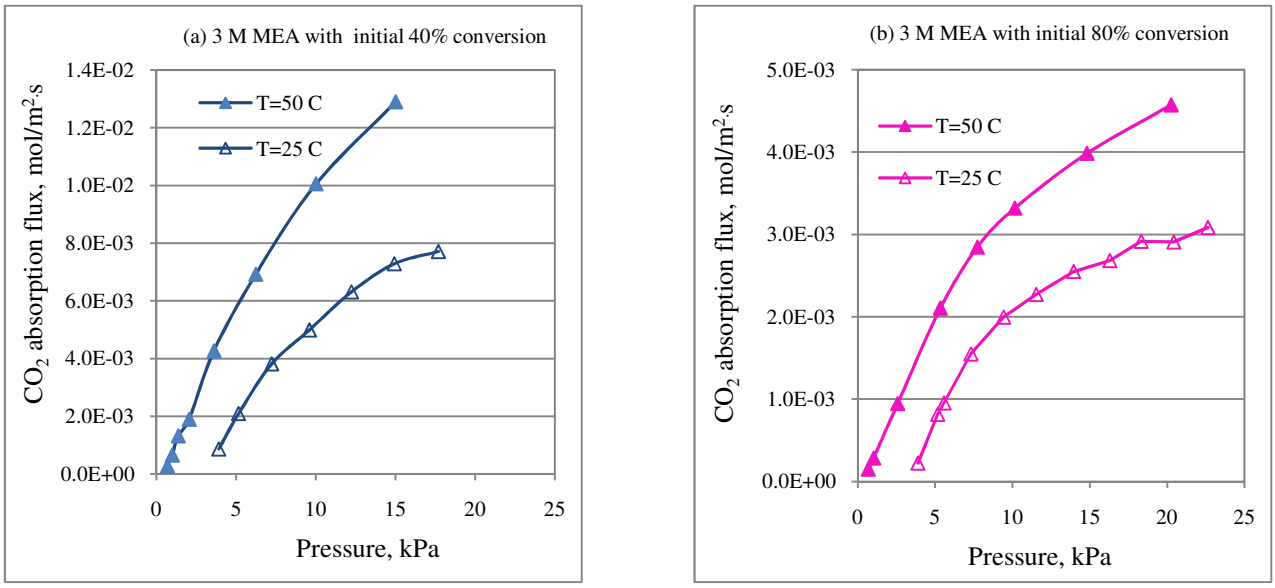

Figure 4-4 Impact of temperature and initial conversion of MEA on CO_2 absorption rate in MEA solution

4.1.2.3 Comparison of experimental results for the reaction rate constant with the literature data

The experimental set-up and procedure to complete 36 experiments were evaluated by determining the reaction rate constants from the experimental data and then comparing them with corresponding values in the literature. An example of the absorption rate profile is provided in Figure 4-5. The CO_2 absorption rate increased with the increase in CO_2 partial pressure, and this trend started to level off with increasing partial pressure up to 19kPa. Absorption flux is zero at CO_2 partial pressure of 2.8kPa, where the gas and liquid are in equilibrium. At the low pressure end, the rate of absorption varied linearly with partial pressure. Therefore, pseudo first order behavior can be assumed for this region. Hence, the reaction rate constant can be calculated using the slope of a linear line and Equation 2-10. Then, the calculated reaction rate constants can be compared with the literature data to evaluate the experimental set-up and procedures.

An example of the absorption rate profile is provided in Figure 4-5 and the pseudo first order region is indicated in the figure.

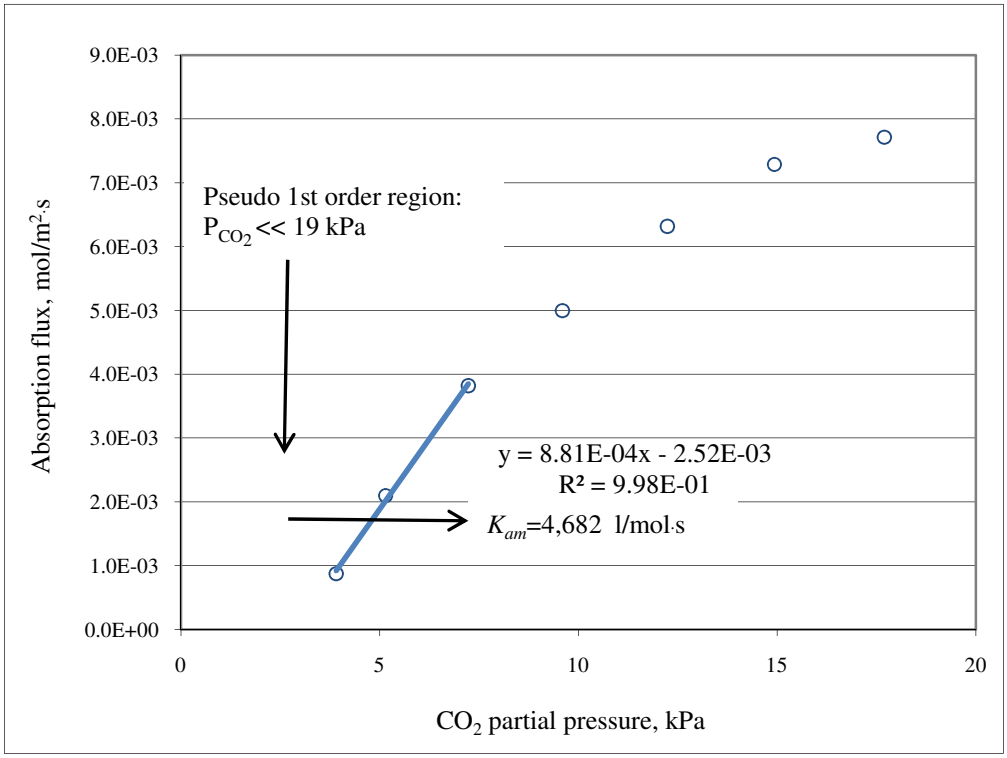

Figure 4-5 CO_2 absorption into 3M MEA with initial 40% conversion at 25°C

Results for the absorption of CO_2 into 3M MEA with initial conversion of 0%, 40% (equivalent to 1.8M MEA) and 80% (equivalent to 0.6M MEA) at 25°C and 50°C were used to determine the rate constants for the reaction of CO_2 with a 3M MEA solution. The estimated rate constants for the absorption reaction from this study are summarized in Table 4-1. In addition, employing results at two different temperatures, the activation energy for the CO_2 reaction with MEA was also determined according to the following Arrhenius equation:

$$\frac{k(T_1)}{k(T_2)} = \exp\left[-\frac{E_a}{R}\left(\frac{1}{T_1}-\frac{1}{T_2}\right)\right] \qquad \text{Eq 4-2}$$

Kinetic data from literature are also included in Table 4-1 to compare the results. These results show that the rate constant increased with increasing initial MEA concentration and increasing temperature. The values of the rate constant obtained in this study are in good agreement with those values reported in the literature, indicating the current experimental setup

is suitable for the absorption measurements. For instance, the value of the rate constant at 25°C for 3M MEA, obtained from this study is 8,066 (l/mol·s), which is in good agreement (agreement within 8%) with the reported value of 7,500 (l/mol·s) by Clarke et al. (1964). The value of E_a for the 1M MEA, as reported by Danckwerts and Sharma (1966) is 41.8 kJ/mol which is between 39.0 kJ/mol and 48.8 kJ/mol measured in this study for initial MEA concentrations of 0.6 M and 1.8 M, respectively.

Table 4-1 Comparison of kinetic data between this study and literature

Source	Temp. (°C)	MEA (M)	Rate constant (l/mol·s)	Ea (kJ/mol)	Experimental technique
This study	25	3	8,066	NA[a]	Stirred cell, semi-continuous
This study	25	1.8	4,682	48.8	Stirred cell, batch
This study	25	0.6	2,404	39.0	Stirred cell, batch
This study	50	1.8	21,532	48.8	Stirred cell, batch
This study	50	0.6	8,137	39.0	Stirred cell, batch
Clarke et al. (1964)	25	1.6,3.2,4.8	7,500	NA[a]	Laminar jet

Table 4-1 Continued from page 53

Laddha and Danckwerts (1981)	25	0.49-1.71	5,720	NA[a]	Stirred cell, batch
Alvarez-Fuster et al. (1980)	20	0.2-2.02	4,300	NA[a]	Wetted wall column
Danckwerts and Sharma (1966)	18	0.0152-0.177	Log k = 10.99-2152/T	41.8	Laminar jet
Danckwerts and Sharma (1966)	35	1.0	9,700-13,000	41.8	Laminar jet
Leder et al. (1971)	80	NA[a]	94,000	39.7	Stirred cell, semi-continuous

[a] NA = not available

4.1.3 Absorption of CO_2 into PC solutions

As previously mentioned, the absorption tests in the CO_2-PC system were performed to provide a reference value to evaluate the enhancement of the CO_2 absorption rate in the presence of CA.

The main reaction contributing to the CO_2 absorption in the PC solution is [Astarita et al., 1981]:

$$CO_2 + OH^- \underset{k_{12}}{\overset{k_{11}}{\Leftrightarrow}} HCO_3^- \qquad \text{Eq 4-3}$$

Reaction (1) (Eq 4-3) is the neutralization reaction between OH^- and dissolved CO_2. This reaction is significant at pH > 10 [Astarita et al., 1981]. The effects of PC conversion, PC concentration and temperature on CO_2 absorption in this system were investigated using the batch experimental set-up and methodology which was described in the chapter 2. Partial pressure of water vapor was obtained by subtracting the initial equilibrium pressure of CO_2 from initial total pressure. Initial equilibrium pressure of CO_2 was estimated from Henry's law using concentration of CO_2 in the solution which was calculated as described in the section 3.4.2.2. Results are provided in the Table 4-2.

Table 4-2 Calculated equilibrium pressure of CO_2 for 20% wt PC solutions at different conversions

Conversion (%)	Equilibrium partial pressure of CO_2 (kPa)	
	25°C	50°C
0	0	0
20	0.3312	0.589
40	1.766	3.125
60	5.964	10.491

4.1.3.1 Effect of initial PC conversion on CO_2 absorption rate

Absorption flux as a function of CO_2 partial pressure for four different PC conversions at 25°C and 50°C is shown in Figures 4-6a and 4-6b, respectively. It can be seen that the CO_2 absorption rate increases with increasing alkalinity (decreasing initial carbonate-to-bicarbonate conversion) of the PC solution. Since, reaction (1) is the dominant reaction in the liquid phase, OH^- concentration is the key factor affecting the absorption rate. Therefore, when the PC solution has a higher OH^- concentration (lower carbonate-to-bicarbonate conversion), the absorption rate is higher.

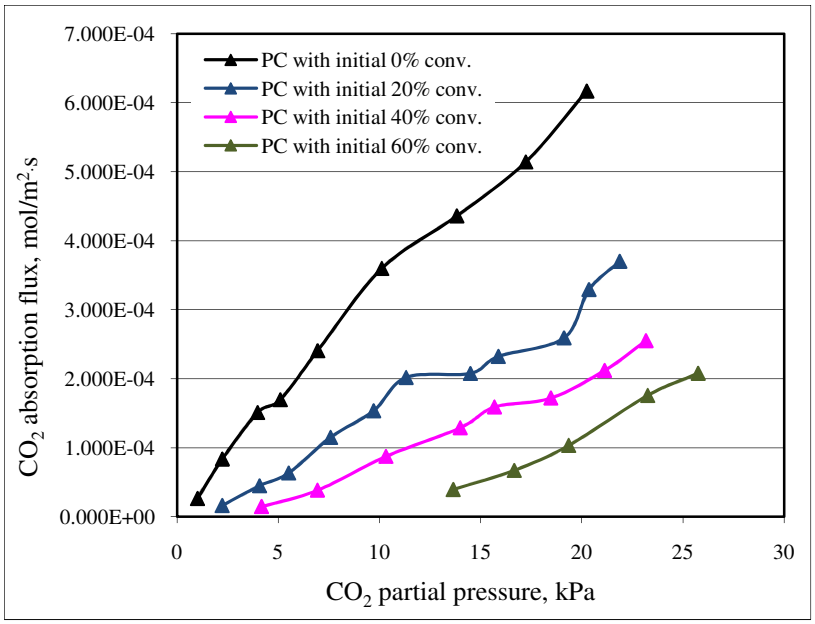

(a) 25°C

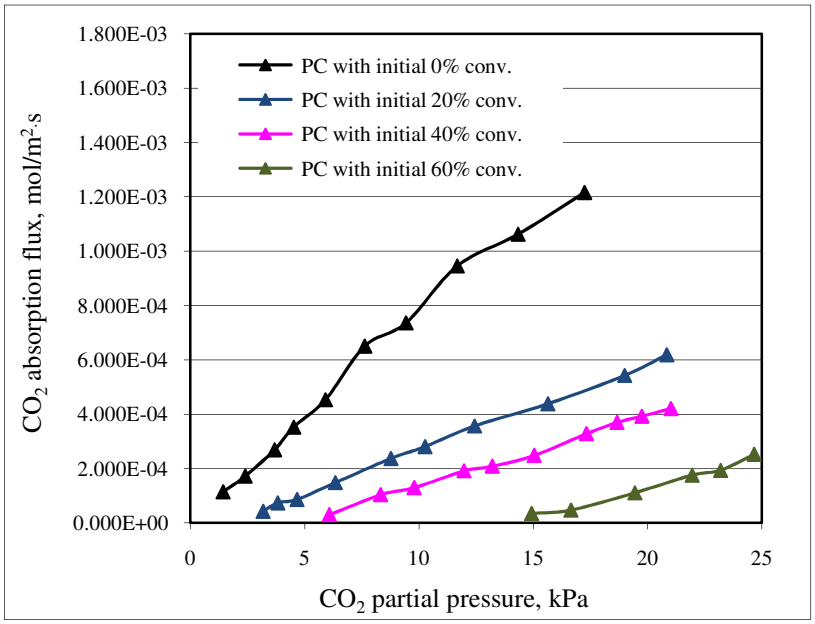

(b) 50°C

Figure 4-6 CO_2 absorption flux varying with temperature and initial carbonate-to-bicarbonate conversion in an aqueous 20% wt PC solution

4.1.3.2 *Effect of temperature on CO_2 absorption rate*

Absorption flux as a function of CO_2 partial pressure at 25°C and 50°C for the PC solutions with initial carbonate-to-bicarbonate conversions of 0%, 20%, 40%, and 60% that were provided in Figures 4-6a and 4-6b were reformatted as Figures 4-7a to 4-7d, respectively. As it can be seen, as temperature increases the absorption rate of CO_2 in the PC solutions also increases with all of the initial conversions tested here. The PC solution at 50 °C presents an absorption rate 20-100% higher than that at 25°C. It can be concluded that the increase in CO_2 flux with increasing temperature was due to the increased reaction rate between CO_2 and OH^-, despite the decrease of physical solubility of CO_2 which is described by Henry's constant.

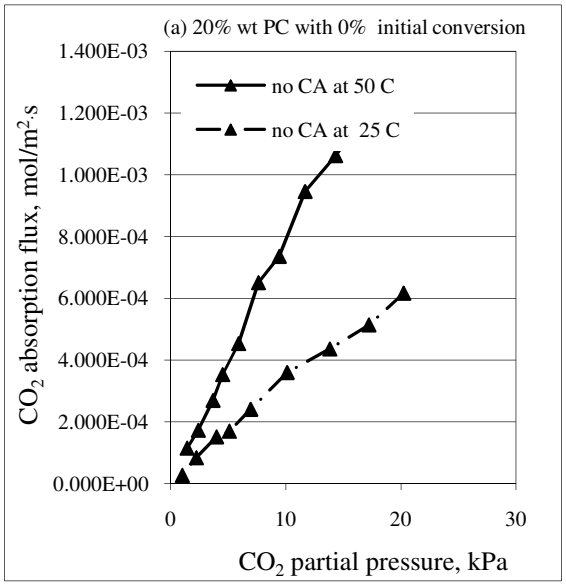

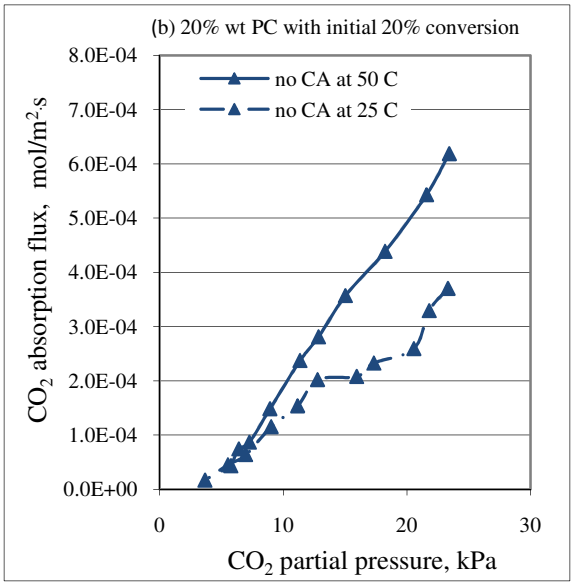

Figure 4-7 continued on page 58

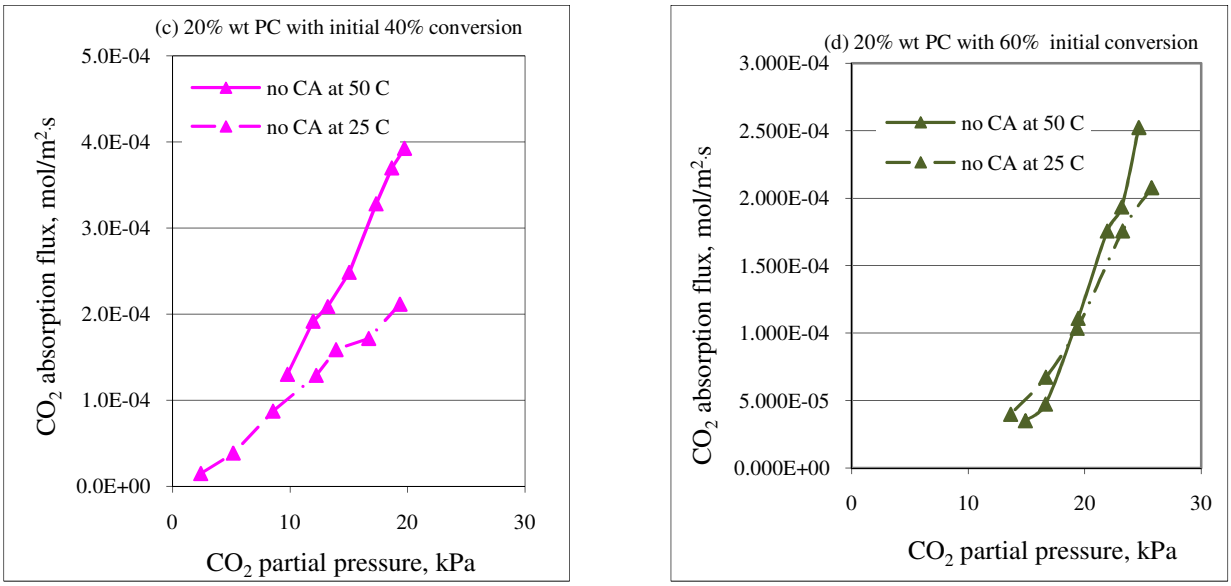

Figure 4-7 Dependence of CO_2 absorption rate into a PC solution on temperature and initial carbonate-to-bicarbonate conversion of PC

4.1.3.3 Effect of PC concentration (20% wt vs. 30% wt) on CO_2 absorption rate

The effect of the PC concentration (20% wt vs. 30% wt) on the CO_2 absorption rate into PC solution with 40% initial carbonate-to-bicarbonate conversion was tested at 50°C (Figure 4-8). The CO_2 absorption rate into 30% wt PC solution is up to 38% lower than that into 20% wt PC solution. This observation can be explained by considering the influence of Henry's constant and reaction kinetics with changes in concentration of PC. By increasing the PC concentration from 20% wt to 30% wt, Henry's constant decreases by 38% while the rate constant for reaction (1) increases by 80%, and concentration of OH^- doesn't change. Since CO_2 absorption rate into the PC solution decreased with increasing PC concentration, it can be concluded that the reduction in the flux caused by the decrease in Henry's constant had more of an impact then the increase in the flux caused by the increase in the reaction rate constant, under the experimental conditions that were tested here.

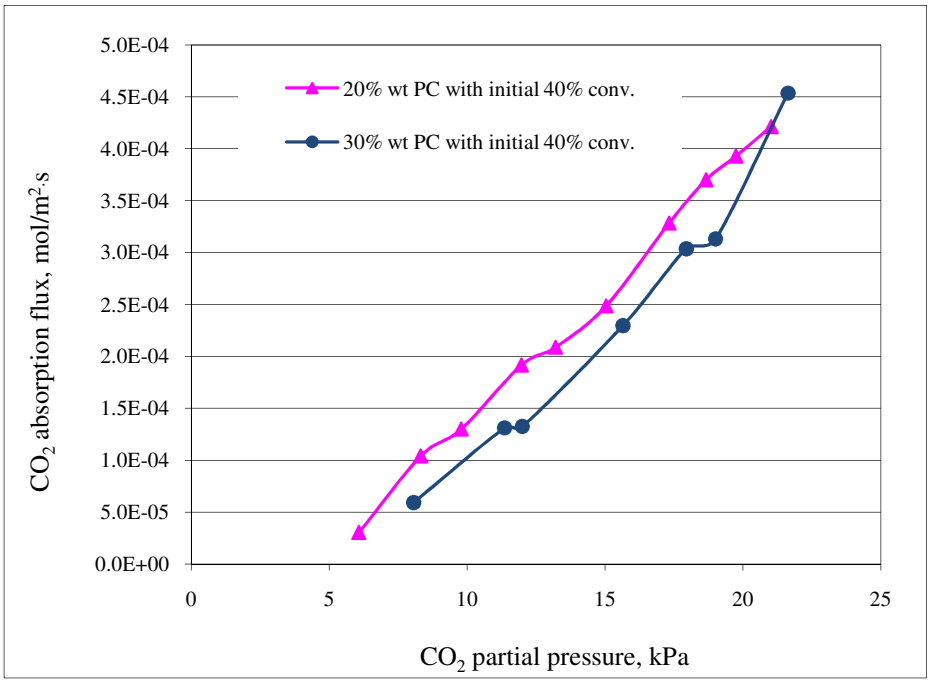

Figure 4-8 Dependence of CO_2 absorption rate on PC concentration at 40% initial carbonate-to-bicarbonate conversion at 50°C

4.1.4 Absorption of CO_2 into PC-CA solutions

There are two reactions contributing to the CO_2 absorption into the PC-CA solution.

$$CO_2 + H_2O + CA \underset{k_{62}}{\overset{k_{61}}{\Leftrightarrow}} HCO_3^- + H^+ + CA \qquad \text{Eq 4-4}$$

Reaction (6) (Equation 4-4) is the CO_2 hydration reaction which is catalyzed by CA enzyme. Reaction (1) (Equation 4-3) is the neutralization reaction which is already discussed in section 4.1.3.

4.1.4.1 Effect of initial PC conversion on CO_2 absorption flux

The dependence of CO_2 flux on four different initial carbonate-to-bicarbonate conversions in the 20% wt PC solution and two different CA concentrations, at 25°C and 50°C, is shown in Figures 4-9a and 4-9b, respectively. These results show that the absorption rate of CO_2 into the PC solution with 0% initial carbonate-to-bicarbonate conversation is higher than that into the less alkaline PC solution (lower OH^- concentration and higher HCO_3^- concentration) such as the one with 40% initial conversion. This can be explained based on the fact that at higher OH^- and lower

HCO_3^- concentrations, the rate of forward reaction (1) is higher and the rate of backward reactions (1) and (6) are lower, as compared to that in a less alkaline PC solution.

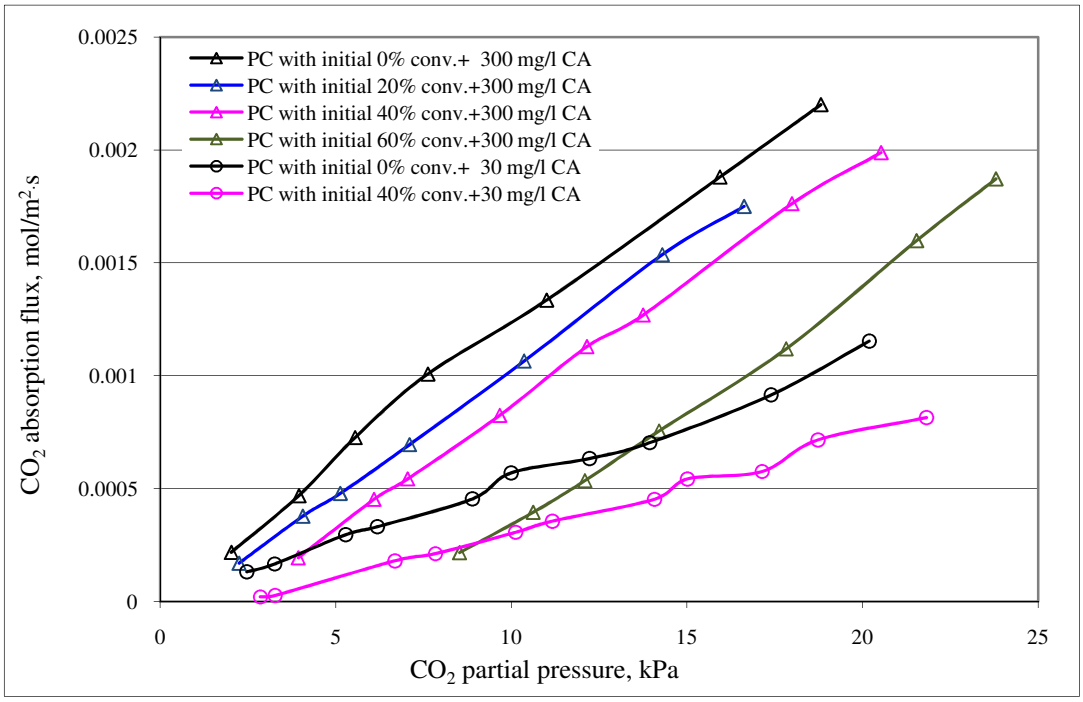

(a) 25°C

Figure 4-9 continued on page 61

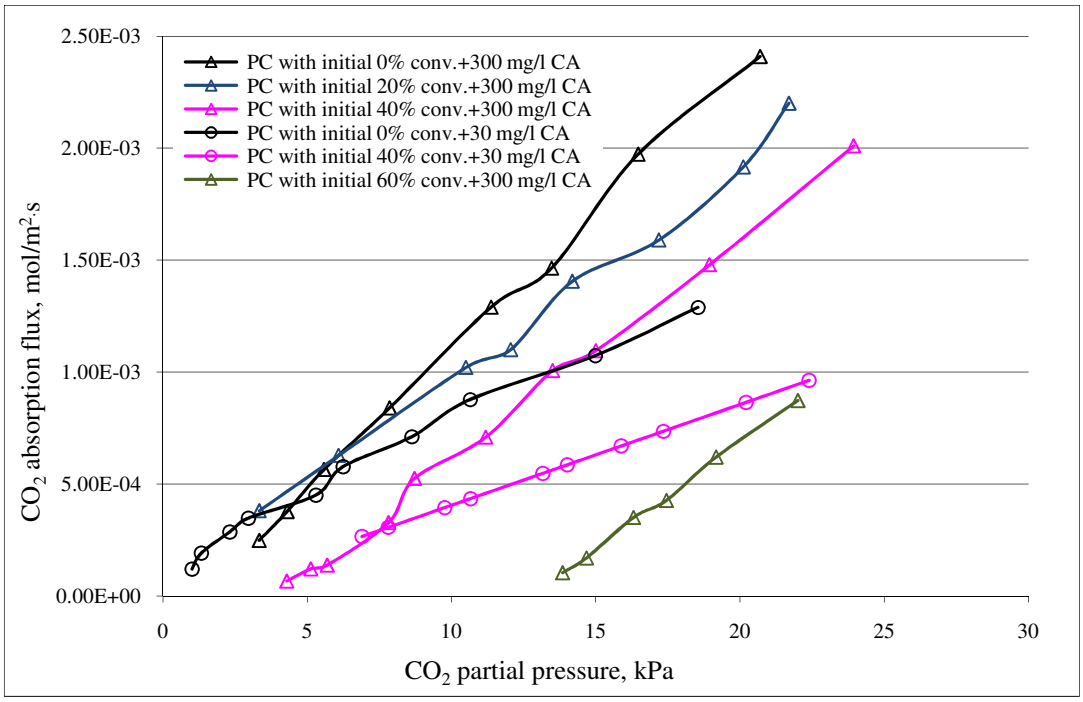

(b) 50°C

Figure 4-9 CO_2 absorption flux in PC-CA solution

4.1.4.2 Effect of temperature on CO_2 absorption flux

The values of k_{cat}/K_M (= k_{61}/C_{CA}) at 25°C and 50°C were determined experimentally using absorption flux-pressure data for 20% wt PC with 40% initial conversion and CA concentration of 300 mg/ l using the same procedure that was described in the section 4.1.2.3 for MEA. The values are 9.56×10^4 and $1.25\times10^5\ m^3/mol\cdot s$ at 25°C and 50°C, respectively. The dependencies of CO_2 flux on CO_2 partial pressure at two different temperatures (25°C and 50°C), two different CA concentrations (30 mg/l and 300 mg/l), and four different initial carbonate-to-bicarbonate conversions (0%, 20%, 40%, and 60%) are described in Figures 4-10a to 4-10d. It can be seen that at the 30 mg/l CA, the rate of absorption increases by up to 40% when increasing the temperature from 25°C to 50°C (Figures 4-10a). However, at 300 mg/l CA, the adsorption rate is decreased by 45% when increasing temperature from 25°C to 50°C (Figure 4-10d) indicating that increasing temperature has a negative impact on the absorption rate at higher CA dosage.

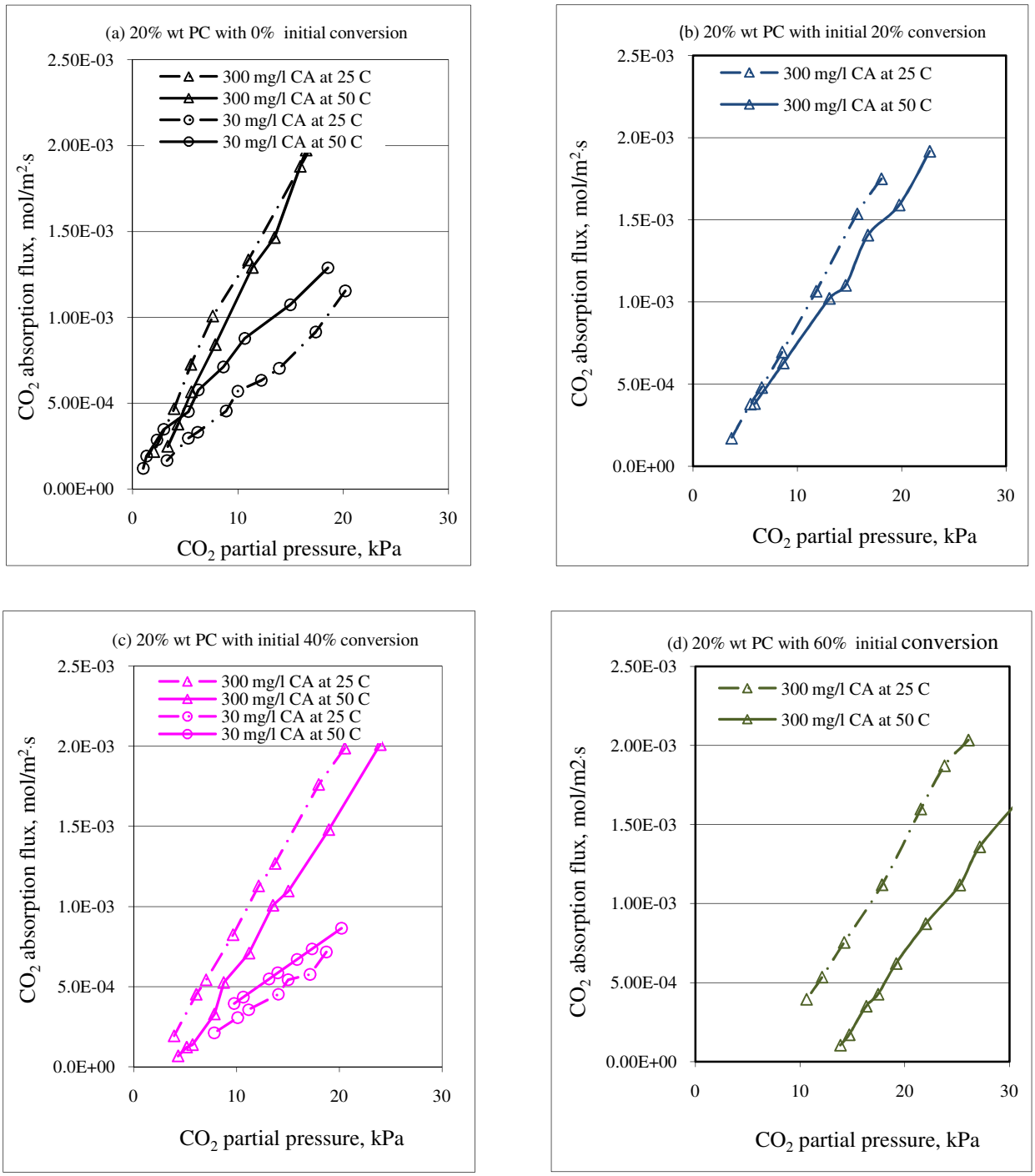

Figure 4-10 Impact of temperature on CO_2 absorption rate in PC-CA solution

This observation can be explained by considering two factors that are influenced by temperature:

1) Henry's constant, which decreases with increasing temperature, and results in a decrease in

absorption flux, and 2) reaction rate constant, which increases with increasing temperature and results in an increase in absorption flux. As temperature increases from 25°C to 50°C, the reaction rate constant for reaction (1) (Equations 3-39 and 3-40) and (6) (experimentally measured) increases by 310% and 31%, respectively. Thus, for reaction (6), the dependency of the rate constant on temperature is less pronounced than that of reaction (1). At higher dosages of CA enzyme, the contribution of reaction (6) to the overall absorption rate dominates over (1). Hence, the impact of the decrease in Henry's constant on the absorption rate is larger than the impact of the increase in the rate constant of reaction (6). As a result, the CO_2 absorption rate into the PC with a high dosage of CA could decrease with increasing temperature. This was verified quantitatively by simulation. It was observed that at a CO_2 partial pressure of 10kPa, the impact of decrease in Henry's constant on the absorption flux is -30%, while the impact of increase in rate constant (k_{61}) on the absorption flux is only +6%.

4.1.4.3 Effect of PC concentration (20% wt vs. 30% wt) on CO_2 absorption flux

The effect of PC concentration on CO_2 absorption rate was experimentally tested at 50°C in the presence of the CA enzyme (Figure 4-11). It is apparent that the absorption rate into the 30% wt solution is less than the rate for the 20% wt PC for the PC-CA solution with 40% initial conversion and 300 mg/l CA. This could be due to the solubility of CO_2 into 30% wt PC is 38% lower than that into 20% wt PC due to higher ionic strength, while their rate constants for the reaction (6) are comparable. In addition, since the 30% wt PC solution was prepared at 50°C before adding the enzyme, because PC becomes supersaturated at 30% wt, 40% conversion, and 25°C, it is possible that the activity of the enzyme was reduced due to thermal shock. Moreover, there is a possibility that the 300 mg/l CA dosage was not completely dissolved in the 30% wt PC which has higher ionic strength.

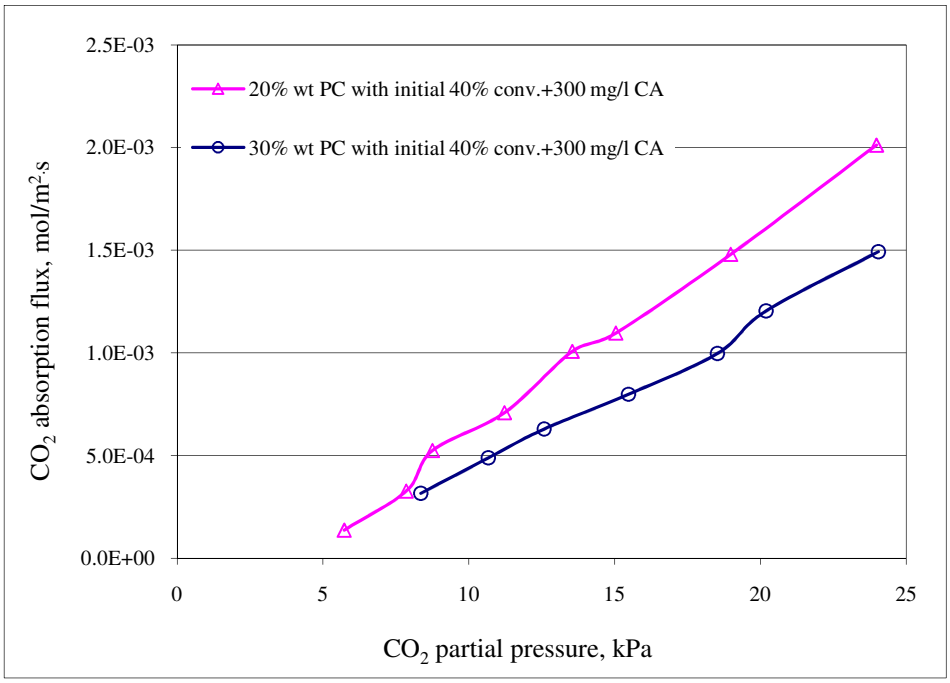

Figure 4-11 Impact of PC concentration on CO_2 absorption rate in PC-CA solution at 50 ºC

4.1.5 Comparison between absorption rate of CO_2 into PC and PC-CA solutions

The previously described enhancement factor (E_{enzyme}) was used to quantitatively evaluate the role of CA to promote the absorption rate of CO_2 into the PC solution at select initial carbonate-to-bicarbonate conversion levels and at 25°C and 50°C (Figures 4-12a and 4-12b, respectively). For example, for the PC solution with 0% initial conversion mixed with 30 mg/l CA, the enhancement factor is 1.5 at 25°C and 1 (no enhancement) at 50°C. These results show that at 30 mg/l CA, there was only up to a 5 times observed increase in absorption rate compared to the reference PC solution of 0% initial conversion with no added enzyme at both 25°C and 50°C. However, at 300 mg/l CA, the absorption rate was promoted by 6-20 times at 25°C and 2-8 times at 50°C. In general, the CA promotes the rate of absorption more effectively when the temperature is low and the PC has a high (e.g., 60%) carbonate-to-bicarbonate conversion (i.e., higher CO_2 loading) as studied here.

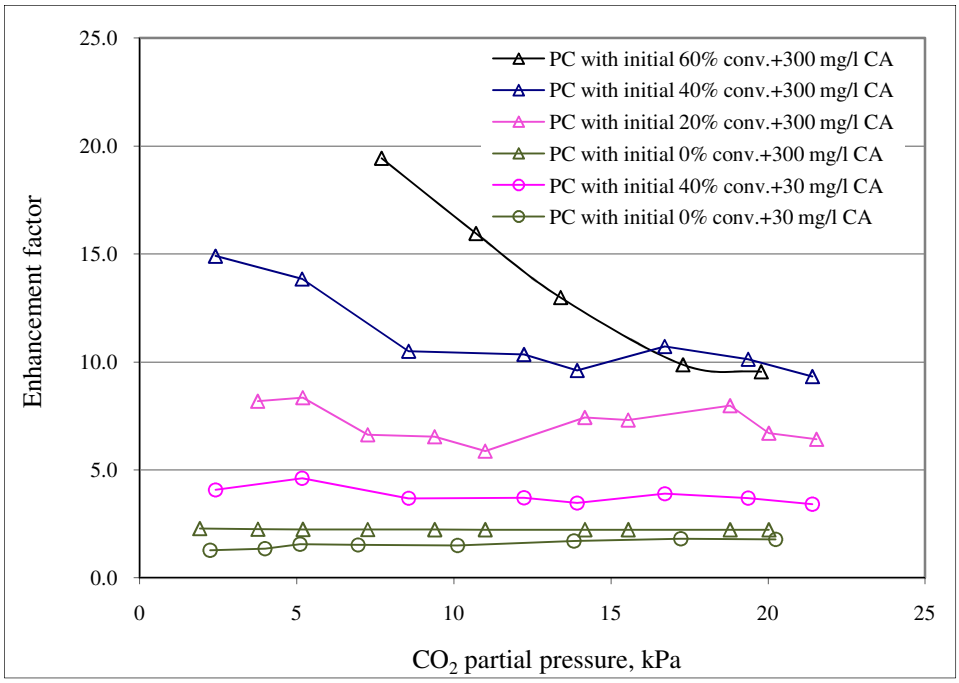

(a) 25°C

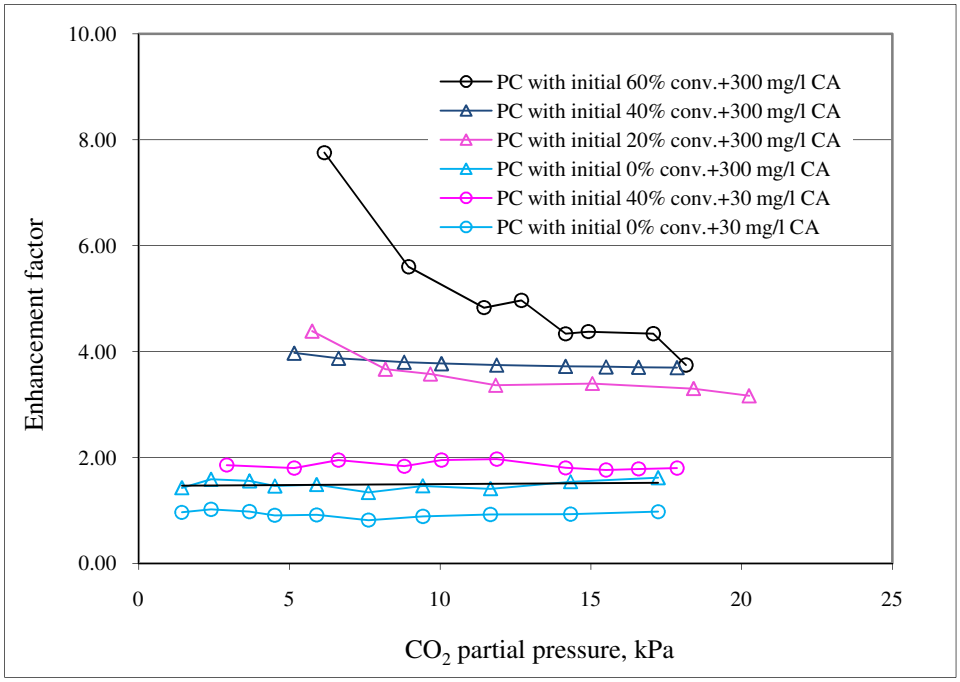

(b) 50°C

Figure 4-12 Dependence of enhancement factor of CO_2 absorption on temperature, CA concentration, and initial carbonate-to-bicarbonate conversion for PC-CA solutions

4.1.6 Comparison between absorption rate of CO_2 into PC-CA and MEA solution

A comparison of experimental CO_2 absorption flux results for PC-CA and MEA solutions is displayed in Figure 4-13. The CO_2 absorption flux into the PC-CA solution is 7-16 times and 5-11 times lower than that of the MEA system at 50°C and 25°C, respectively. The relative differences are higher when the CO_2 partial pressure is lower and the initial carbonate-to-bicarbonate conversion of the PC is lower (lower CO_2 loading) for the conditions tested here. However, this comparison is based on the absence of the gas-phase mass transfer in the current STR experimental setup. In a countercurrent MEA absorption column, however, the gas-phase resistance can be significant. Consequently, the absorption rates in the MEA and PC-CA solutions could be less different. This will be demonstrated quantitatively in the section 4.2.4.

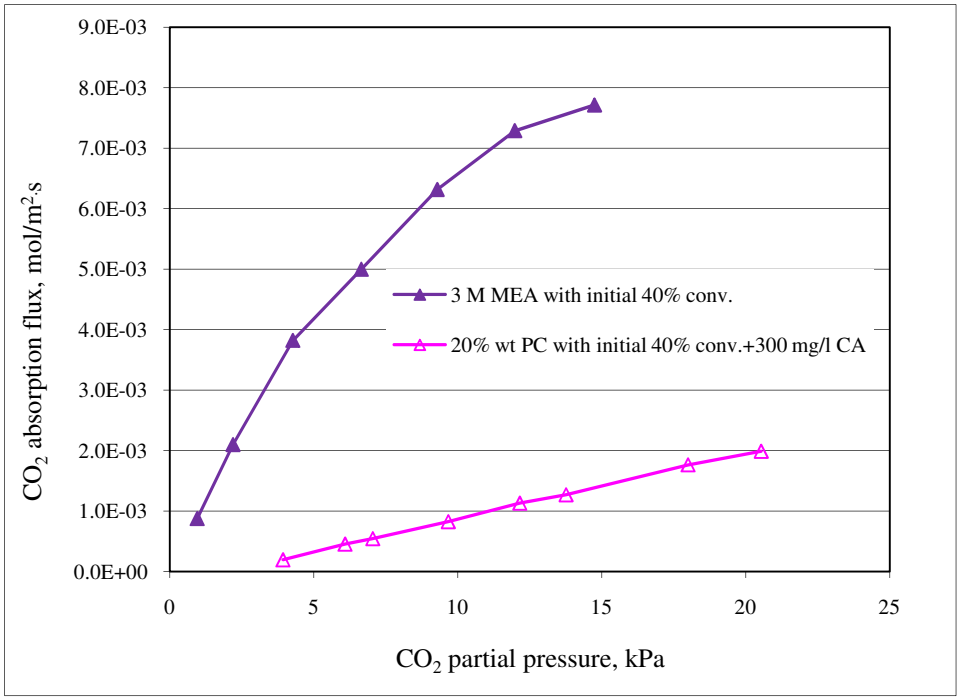

(a) 25 °C

Figure 4-13 continued on page 67

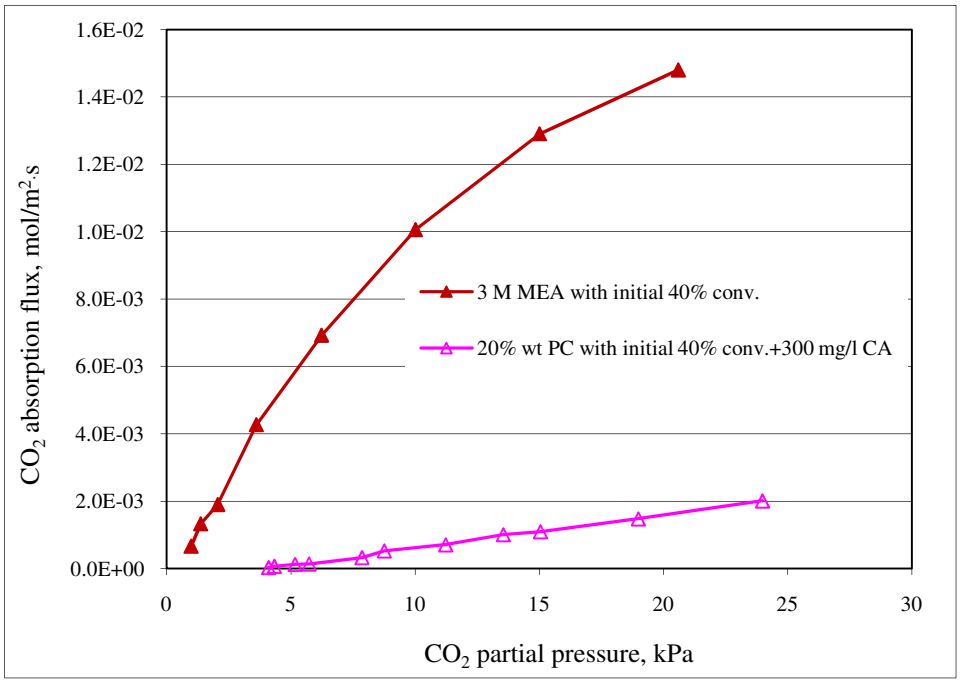

(b) 50 ºC

Figure 4-13 absorption rates into PC-CA and MEA solution

4.2 Modeling results

4.2.1 Comparison between experimental and modeled results describing CO_2 absorption fluxes in PC and PC-CA solutions

A comparison between the experimental results and model predictions describing CO_2 absorption flux into the PC solution (20% wt with 40% initial conversion) at 25°C and 50°C in presence and absence of CA is provided in Figure 4-15.

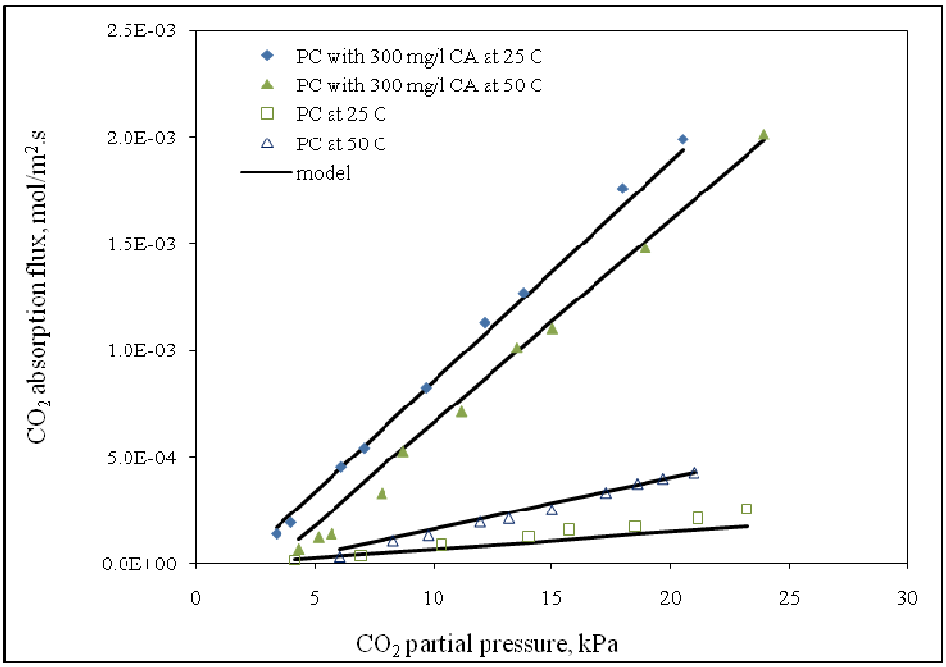

Figure 4-14 Impact of temperature and CA enzyme dosage on CO_2 absorption flux into 20% wt PC solution with 40% initial carbonate-to-bicarbonate conversion

Average absolute error between modeled and experimental results describing CO_2 absorption flux into the PC solution (20% wt with 40% initial conversion) at 25°C and 50°C is less than 30% as provided in Table 4-3. The good agreement between the experimental results and model predictions indicates that the developed model can be used to simulate the studied absorption system.

Table 4-3 Average absolute error* between modeled and experimental results

CA concentration (mg/l)	Temperature (^{o}C)	Average absolute error (%)
0	25	23.8
	50	28.5
300	25	4.6
	50	28.9

Table 4-3 continued on page 69

*Average absolute error is defined as: $\frac{1}{n}\sum_{i=1}^{n}\left|\frac{data_{experimental} - data_{modeled}}{data_{experimental}}\right| \times 100$

4.2.2 Absorption flux of CO_2 into PC solution as a function of temperature

Figure 4-15 describes the modeled absorption fluxes of CO_2 as a function of temperature at three CO_2 partial pressures. Absorption fluxes at CO_2 partial pressure of 14kPa and 21kPa increase with increasing temperature from 20°C to 80°C, while at 7kPa it increases first as temperature rises from 20°C to 70°C, then starts to decrease. This is because at high temperatures (>70°C) and low partial pressures (7kPa), the solubility of CO_2 into the solution is very low (Table 4-4) and its impact on the flux-temperature trend is more important than the impact of reaction rate constant and diffusivity. CO_2 solubility in the Table 4-4 was calculated from Henry's constant (section 3.4.2.2), and bulk concentration of CO_2 was determined assuming equilibrium in the bulk of liquid as described in the section 3.4.2.2. At certain temperatures and pressures, the concentration of dissolved CO_2 on the gas-liquid interface would reach the CO_2 concentration in the bulk of the liquid and there would be no absorption (e.g. 5.6kPa and 80°C). It can also be seen that steepness of the flux-temperature curves increases with increasing the pressure. That is because at higher pressure, absorption flux has a bigger value, and as a result of that, the change in the flux is higher for the same temperature difference.

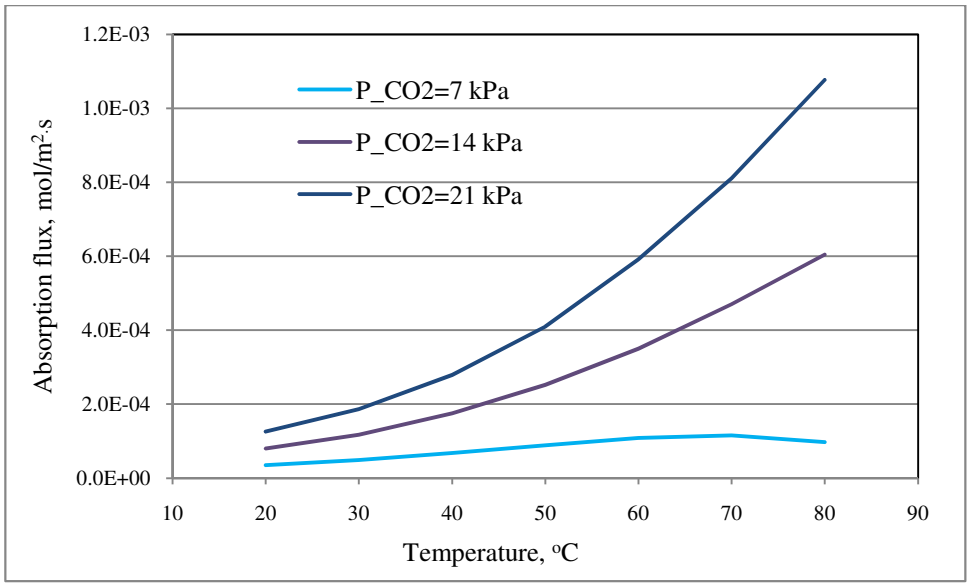

Figure 4-15 Impact of temperature and initial concentration of CO_2 on CO_2 absorption flux into 20% wt PC solution with 40% initial conversion

Table 4-4 CO_2 solubility, bulk concentration, reaction rate constant, and diffusivity in PC solution (20% wt, 40% conversion)

Temperature (^oC)	CO_2 partial pressure (kPa)	CO_2 solubility (mol/m^3)	CO_2 concentration in the bulk of the liquid (mol/m^3)	Reaction rate constant, $k_{61}=k_{cat}/K_M*C_{CA}$ (1/s)	CO_2 diffusivity in the solution (m^2/s)
20	7	0.8457	0.1888	900.9[a]	9.54e-10
	14	1.6915			
	21	2.5372			
80	7	0.3458	0.2749	1643.1[a]	2.28e-9
	14	0.6916			
	21	1.0374			

[a]Calculated from fitted k_{cat}/K_M at 25 ^oC and 50^oC to Arrhenius equation.

4.2.3 Sensitivity analysis: effect of enzyme concentration

Figure 4-16 presents the model predictions describing the impact of the CA enzyme concentration and CO_2 partial pressure on the CO_2 absorption rate into the 20% wt PC solution with 40% initial conversion at 25°C.

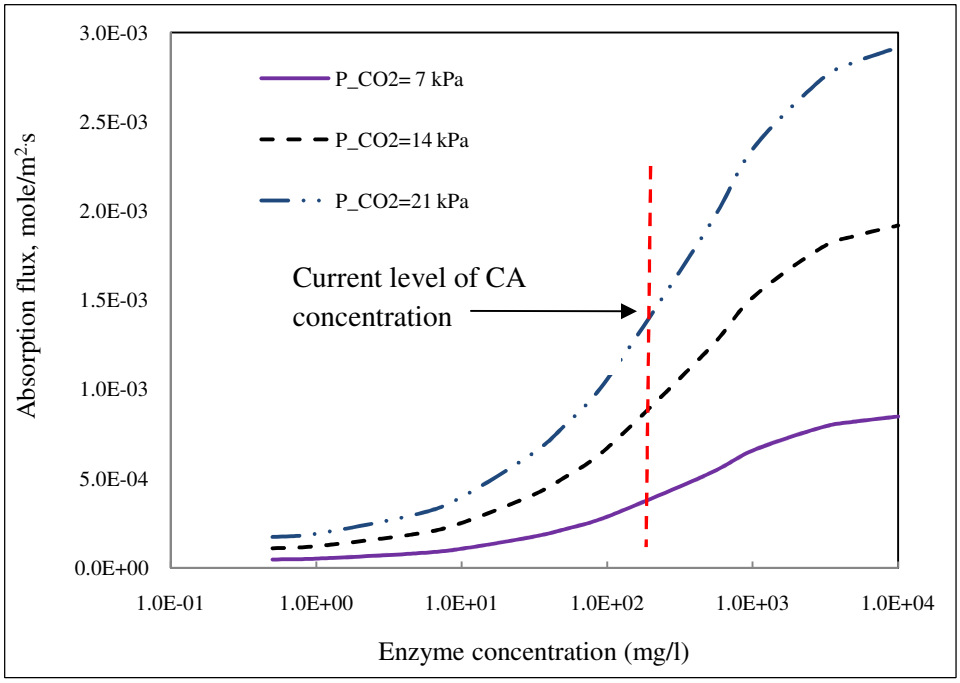

Figure 4-16 Predicted impact of CA enzyme concentration on CO_2 absorption into 20% wt PC solution with 40% initial carbonate to bicarbonate conversion at 25°C

The same trend of the CO_2 absorption rate varying with the addition of CA enzyme can be observed for all three examined partial pressures. Initially the CO_2 absorption rate doesn't increase with the increase of the enzyme concentration. Then, .it starts increasing at CA concentration of 1 mg/l. It is because at lower CA dosage level (e.g. < 1 mg/l), the contribution of reaction (1) is more than that of reaction (6) (at 1 mg/l of CA, overall rate of reaction 1 is 50% more than that of reaction 6). At higher dosage levels of enzyme (e.g. more than 10 mg/l), reaction (6) is much faster and contributes more to the absorption rate of CO_2 (at 10 mg/l of CA, overall rate of reaction 6 is 580% more than that of reaction 1). Therefore, the absorption rate increases linearly with the enzyme concentration. However, at very high enzyme dosage levels, such as > 3,000 mg/l, the absorption rate levels off and a further increase of the enzyme dosage

doesn't impact the adsorption rate. The reason for the leveling-off is that as concentration of enzyme increases, rates of forward and backward reactions (6) increase, and consequently reaction (6) approaches pseudo-equilibrium. At this state, as the product of the reaction leaves the reaction zone, reactants have to diffuse to this zone to retain pseudo-equilibrium. Hence, the overall rate of absorption becomes less dependent on the enzyme concentration and more dependent on diffusion of reactants and products through the liquid.

The modeling results revealed that at CA < 3,000 mg/l the absorption rate of CO_2 increases with increasing CA concentration. Compared to the enzyme concentration (300 mg/l) currently used in this study, further increase of enzyme concentration could further increase the absorption rate of CO_2.

5 SUMMARY, CONCLUSIONS AND RECOMMENDATIONS

5.1 Summary and conclusions

A lab-scale experimental setup was designed and fabricated to perform CO_2 absorption experiments. Liquid-phase physical mass transfer coefficients were measured using CO_2 absorption into deionized (DI) water.

CO_2 absorption tests into aqueous MEA and PC solutions were initially performed to validate the experimental set-up. The CO_2 absorption kinetics, both in terms of the magnitudes and the trends, into these solutions are consistent with those reported in literature. Such results indicate that this new experimental set-up and procedure are applicable to measure CO_2 absorption rates. Results from these tests also provided a baseline for the comparison with the *carbonic anhydrase* (CA) enzyme-promoted PC solution.

Absorption experiments were then performed for aqueous PC solutions without CA at select initial CO_2 partial pressures, temperatures, PC concentrations, and initial conversions of K_2CO_3 to $KHCO_3$. The kinetic measurements of this reference solution are necessary considering that the conditions of PC solution employed in this study were different than previously reported studies. The CO_2 absorption rates into the aqueous PC solutions were then used as a baseline to evaluate the enhancement of CO_2 absorption kinetics into the aqueous PC-CA solutions.

The activity of CA enzyme to promote CO_2 absorption kinetics into the PC solutions was evaluated at select temperatures and CA concentrations. Two parallel reactions, namely CO_2 hydration and neutralization, occur during absorption of CO_2 into the PC-CA solution. The relative importance of these two reactions, which depends on both the temperature and CA concentration, was evaluated using a stirred tank reactor (STR) system. It was observed that the absorption rate of CO_2 into the PC solution mixed with 300 mg/l CA was improved by 6-20 times at 25^{o}C and 2-8 times at 50^{o}C compared to those with no addition of CA. It was observed that, at the CA enzyme concentration of 30 mg/l, the CO_2 absorption rates into the aqueous PC solutions increases by up to 40% when increasing the temperature from 25°C to 50°C. However,

at the 300 mg/l CA dosage, increasing the temperature from 25°C to 50°C decreased the rate of CO_2 absorption by up to 45%.

A mathematical model based on the Higbie's penetration theory was developed for simulation of CO_2 absorption into the PC solution without and with the CA enzyme. These results were validated using experimental results and then further used to predict the maximum achievable CO_2 absorption rate into PC-CA solution in the STR system. The modeling results showed that initially the CO_2 absorption rate increases with the increase of the enzyme concentration. However, at higher CA concentrations, such as > 3,000 mg/l, the CO_2 absorption rate levels off and a further increase of the enzyme concentration doesn't impact the adsorption rate. The modeling results also indicate that an increase of enzyme concentration beyond the maximum enzyme concentration tested here (300 mg/l) could further increase the absorption rate of CO_2 by up to two times.

Experimental results revealed that the CO_2 absorption rate into the PC-CA solution (300 mg/l CA, 20% wt PC solution, 40% initial conversion, 50 °C) in the STR system is 16 times lower than that into a 3M MEA. The STR experiments are performed under conditions such that the absorption rate of CO_2 into the solvent is not limited by the gas-phase mass transfer resistance. However, in a packed-bed absorption system, the gas-phase mass transfer resistance could be important. Consequently, the overall CO_2 absorption rates in the MEA and the PC-CA solutions are expected to be less different.

5.2 Recommendations for future work

The CO_2 absorption rate into PC-CA can be further enhanced by improving other parameters such as the activity of CA enzyme, design optimization of the absorption column, including the type of packing material. Further work is required to investigate the stability of the CA enzyme at longer test duration and use of immobilized CA enzyme. Effectiveness of the regeneration cycle also needs to be investigated. Further work should also include the test of an integrated absorption/ regeneration system for CO_2 capture at a real flue gas condition.

The mathematical model developed in this work is applicable to STR systems. This work should be extended to include the simulation of CO_2 absorption in the packed bed absorption columns.

6 REFERENCES

Astarita G., Savage D.W. and Longo J.M., Promotion of CO_2 mass transfer in carbonate solutions. Chemical Engineering Science, 1981, 36, 581-588.

Aaron D., Tsouris C., Separation of CO_2 from flue gas: a review, Separation Science and Technology, 2005, 40, 321–348.

Aaron D., Tsouris C., Separation of CO_2 from flue gas: a review, Separation Science and Technology, 2005, 40, 321–348.

Abanades J. C., Rubin E. S. and Anthony E. J., Sorbent cost and performance in CO_2 capture systems, Industrial and Engineering Chemistry Research, 2004, 43(13), 3462–3466.

Alper E. and Deckwer W.D., Kinetics of absorption of CO_2 into buffer solutions containing carbonic anhydrase, Chemical Engineering Science, 1980, 35, 549–557.

Alvarez-Fuster C., Midoux N., Laurent A. and Charpentier J. C., Chemical kinetics of the reaction of carbon dioxide with amines in pseudo m-nth order conditions in aqueous and Organic solutions. Chemical Engineering Science, 1980, 35, 1717-1723.

Augugliaro V. and Rizzuti L., Kinetics of carbon dioxide absorption into catalyzed potassium carbonate solutions, Chemical Engineering Science, 1987, 42(10), 2339-2343.

Bailey D. W. and Feron P. H. M., Post-combustion decarbonisation process, Oil & Gas Science and Technology, Rev. IFP, 2005, 60, 3, 461-474.

Bao L. and Trachtenberg M.C., Facilitated transport of CO_2 across a liquid membrane: Comparing enzyme, Amine and Alkaline, Journal of Membrane Science, 2006, 280, 330-334.

Bao L. and Trachtenberg M.C., Modeling CO_2 facilitated transport across a diethanolamine liquid membrane, Chemical Engineering Science, 2005, 60, 6868-6875.

Bao L.H., Goldman S.L. and Trachtenberg M.C., CO_2 transfer across a liquid membrane facilitated by carbonic anhydrase, Paper presented to American Institute of Chemical Engineers Annual Meeting, Austin, TX, 2004.

Billet R. and Schultes M., Prediction of mass transfer columns with dumped and arranged packing, Updated summary of the calculation method of Billet and Schultes, Transactions of the Institution of Chemical Engineers, 1999, 77, Part A, 498 – 504.

Bravo J. L., Rocha J. A. and Fair J. R., Mass transfer in Gauze packings, Hydrocarbon Processing, 1985, 64, 91-95.

Cents A., Brilman D. and Versteeg G., CO_2 absorption in carbonate/bicarbonate solutions: the Danckwerts-criterion revisited, Chemical Engineering Science, 2005, 60, 5830–5835.

Chang H. and Shih C. M., Simulation and optimization for power plant flue gas CO_2 absorption-stripping systems, Separation Science and Technology, 2005, 40, 4, 877 – 909.

Chen S., Lu Y. and Rostam-Abadi M., Integrated vacuum absorption steam cycle gas separation, Patent Application No. 60/798, 489, 2007.

Chen S.S., Rostam-Abadi M., Lu Y., Nyman D. J. and Dracos J. S., Varagani R., Carbon dioxide capture and transportation options in the Illinois Basin, DOE Technical Report, DE-FC26-03NT41994, 2004.

Clarke J. K. A., Kinetics of absorption of carbon dioxide in monoethanolamine solutions at short contact times, Industrial Engineering Chemistry Fundamentals, 1964, 3, 239-245.

CO_2 Solution Inc., http://www.CO_2solution.com/., accessed online 7/14/2009.

Cullinane T. J. and Rochelle G. T., Carbon dioxide absorption with aqueous potassium carbonate promoted by piperazine, Chemical Engineering Science 2004, 59, 3619 - 3630.

Cullinane, T. J. and Rochelle G. T., Kinetics of carbon dioxide absorption into aqueous potassium carbonate and piperazine, Industrial and Engineering Chemistry Research, 2006, 45, 2531-2545.

Danckwerts P. V. and Sharma M. M. ,The absorption of carbon dioxide into aqueous amine solutions of alkalis and amines (with some notes on hydrogen sulphide and carbonyl sulphide), The Chemical Engineer, 1966, 10, CE244–CE280.

Danckwerts P.V. and Gillham A.J., The design of gas absorbers, I—methods for predicting rates of absorption with chemical reaction in packed columns, and tests with 11/2 in. Raschig rings, Transactions of the Institution of Chemical Engineers, 1966, 42, 42–54.

Danckwerts P.V., Gas absorption accompanied by chemical reaction, American Institute of Chemical Engineers, 1955, 4, 456–463.

Davy R., Development of catalysts for fast, energy efficient post combustion capture of CO_2 into water; an alternative to monoethanolamine (MEA) solvents, Energy Procedia, 2009, 1, 885-592.

Derks P.W.J., Carbon dioxide absorption in piperazine activated n-Methyldiethanolamine, PhD thesis, University of Twente, The Netherlands, 2006, ISBN: 90-365-2439-32.

Derks P.W.J. and Versteeg G.F., Kinetics of absorption of carbon dioxide in aqueous ammonia solutions, Energy Procedia, 2009, 1, 1139–1146.

Dilmore R., Griffith C., Liu Z., Soong Y., Hedges S. W., Koepsel R. and Ataai M., Carbonic anhydrase-facilitated CO_2 absorption with polyacrylamide buffering bead capture, International Journal of Greenhouse Gas Control, 2009, 3, 401-410.

Dindore V.Y., Brilman D.W.F. and Versteeg G.F., Modeling of cross-flow membrane

contactors: mass transfer with chemical reactions, Membrane Science, 2005, 255, 275–289.

Dodgson S. J., Tashian R. E., Gros G. and Carter N. D. (eds.), The carbonic anhydrases: Cellular physiology and molecular genetics, Plenum, New York, 1991.

DOE, 2008, 2009http://www.fossil.energy.gov/programs/powersystems/pollutioncontrols/Retrofitting_Existing_Plants.html, accessed online 10/04/2008.
DOE/EIA-038, 2009, http://www.eia.doe.gov/oiaf/aeo/pdf/0383(2009).pdf, accessed online 7/14/2009.
Dugas R., Rochelle G., Absorption and desorption rates of carbon dioxide with monoethanolamine and piperazine, Energy Procedia, 2009, 1, 1163–1169.

Dutta S. and Goodsell D., 2004, http://www.pdb.org/pdb/static.do?p=education_discussion/molecule_of_the_month/pdb49_1.html accessed online 6/11/2009.
Edwards T.J., Maurer G., Newman J. and Prausnitz J.M., Vapor-liquid equilibria in multi-component aqueous solution of volatile weak electrolytes, American Institute of Chemical Engineers, 1978, 24, 966–976.

Eigen M., Protonenübertagung, säure-base-katalyse und enzymatische hydrolyse. teil I: Elementarvorgänge, Angewandte Chemie, 1963, 75, 489–508.

Freeman S. and Rochelle G.T., Carbon dioxide capture with concentrated aqueous piperazine, Proceedings of GHGT-9, October 2008.

Ghannam A. F., Tsen W. and Rowlett R. S., Activation parameters for the carbonic anhydrase IL-catalyzed hydration of CO_2, Biological Chemistry,1986, 261, 1164-1169.

Goff G. S. and Rochelle G. T., Oxidation inhibitors for copper and iron catalyzed degradation of monoethanolamine in CO_2 capture processes, Industrial and Engineering Chemistry Research, 2006, 45, 8, 2513–2521.

Gottlicher G., The energetic of carbon dioxide capture in power plants: National Energy Technology Laboratory, US DOE, 2004.

Greer T., Modeling and simulation of post combustion CO_2 capturing, Master thesis, Telemark University College, Norway, 2008.

Herzog, H.J., The economics of CO_2 capture, in Greenhouse Gas Control Technologies (ed. by Eliasson B., Riemer P. and A. Wokaun), Proceedings of the 4th International Conference on Greenhouse Gas Control Technologies, 30 August – 2 September 1998, Interlaken, Switzerland, Elsevier Science Ltd., 1999, 101-106.

Higbie R., The rate of absorption of a pure gas into a still liquid during short periods of exposure, Transactions of the American Institute of Chemical Engineers, 1935, 31, 364-389.

Hikita H., Asai S. and Takatsuka T., Absorption of carbon dioxide into aqueous sodium hydroxide and sodium bicarbonate solutions, Chemical Engineering, 1976, 11, 131–141.

http://www.rcsb.org/pdb/education_discussion/molecule_of_the_month/download/CarbonicAnhydrase.pdf., accessed online 4/24/2010.

Huang H. P., Shi Y., Li W. and Chang S. G., Dual alkali approaches for the capture and separation of CO_2, Energy & Fuels, 2001, 15, 263-268.
Idem R., Wilson M., Tontiwachwuthikul P., Chakma A., Veawab A., Aroonwilas A. and Gelowitz D., Pilot plant studies of the CO_2 capture performance of aqueous MEA and mixed MEA/MDEA solvents at the university of Regina CO_2 capture technology development plant and the boundary CO_2 capture demonstration plant, Industrial and Engineering Chemistry Research, 2006, 45(8), 2414–2420.

IPCC, First Assessment Report, Climate change, The IPCC scientific assessment, Cambridge University Press, Cambridge, 1990.

IPCC, Fourth Assessment Report, Climate change: Synthesis Report, 2007.

IPCC, Third Assessment Report, Climate change, Impacts, adaptation and vulnerability, 2001.

Joosten G.E.H. and Danckwerts P.V., Solubility and diffusivity of nitrous oxide in equimolar potassium carbonate, Potassium bicarbonate solutions at 25^{o}C and 1 atm, Chemical Engineering Data, 1972, 17, 452.

Kernohan J.C., The pH-activity curve of bovine carbonic anhydrase and its relationship to the inhibition of the enzyme by anions, Biochimica et Biophysica Acta, 1965, 96, 304–317.

Khalifah R.G., The Carbon dioxide hydration activity of carbonic anhydrase I. stop-flow kinetic studies on the native human isoenzymes B and C, The Journal of Biological Chemistry, 1971, 246(8), 2561-2573.

Kohl A.L. and Riesenfeld F. C., Gas Purification (fourth edition), Gulf Publishing Company, Houston Texas, 1985.

Laddha S. S. and Danckwerts P. V., Reaction of CO_2 with ethanolamines: Kinetics from gas absorption, Chemical Engineering Science, 1981, 36, 479.

Leder F., The absorption of CO_2 into chemically reactive solutions at high temperatures, Chemical Engineering Science, 1971, 26, 1381.

Lindskog S., Structure and mechanism of carbonic anhydrase, Pharmacology and Therapeutics, 1997, 74, 1–20.

Liu N., Bond G.M., Abel A., McPherson B.J. and Stringer J., Biomimetic sequestration of CO_2 in carbonate form: Role of produced waters and other brines. Fuel Processing Technology, 2005,

86, 1615–1625.

Nsakala N., Marion J., Bozzuto C., Liljedahl G. and Palkes, M. Engineering feasibility of CO_2 capture on an existing US coal-fired power plant, Presented at first national conference on carbon sequestration, Washington DC, 2001, May 15-17.

Park S.W., Heo N.H., Kim J.S. and Suh D.S., Facilitated transport of carbon dioxide through an immobilized liquid membrane of $K_2CO_3/KHCO_3$ aqueous solution. Korea Journal of Chemical Engineering, 1997, 14, 5, 312–320.

Pohorecki R. and Moniuk W., Kinetics of reaction between carbon dioxide and hydroxylions ion aqueous electrolyte solutions, Chemical Engineering Science, 1988,43, 1677-1684.

Pohorecki R., The Absorption of CO_2 in carbonate-bicarbonate buffer solutions containing hypochlorite catalyst on a sieve plate, Chemical Engineering Science, 1968, 23, 1447-1451.

Rao A.B., Rubin E.S. and Berkenpas M.B., An integrated modeling framework for carbon management technologies, DOE Technical Report, volume 1, 2004.

Riebesell U., Photosynthesis: carbon fix for a diatom, Nature 40, 2000, 959–960.

Schumpe A., The estimation of gas solubilities in salt solutions, Chemical Engineering Science, 1993, 48, 153–158.

Se´vigny P.A., Hour Online Magazine ‘‘Clearing the air: Scientist Sylvie Fradette tackles global warming with a cool new invention’’, November 24, 2005.
http://www.hour.ca/news/news.aspx?iIDArticle=7752, accessed online 9/1/2009.
Sharma M. M. and Danckwerts P. V., Fast reactions of CO_2 in alkaline solutions-(A) carbonate buffers with arsenite, formaldehyde and hypochlorite as catalysts, (B) aqueous monoisopropanolamine (1-Amino-2-Propanol) solutions, Chemical Engineering Science, 1963, 18, 729-735.

Smith K. S., Cosper N. J., Stalhandske C., Scott R. A. and Ferry J. G., Structural and kinetic characterization of an archaeal beta-class carbonic anhydrase, Bacteriology, 2000, 182, 6605–6613.

Stewart C. and Hessami M., A study of methods of carbon dioxide sequestration–the sustainability of a photosynthetic bioreactor approach, Energy Conversion and Management, 2005, 46, 403–420.

Trachtenberg M.C., Biomimetic membrane for CO_2 capture from flue gas, Progressive report from 05/10/06-03/19/07, DE FG26-06NT42824, August 29, 2007.

Tsonopoulos C., Ionization constants of water pollutants, Chemical and Engineering Data, 1976, 21, 190–193.

United States Environmental Protection Agency (USEPA), Draft U.S. greenhouse gas inventory

report, 2010a, http://www.epa.gov/climatechange/emissions/usinventoryreport.htm, accessed online 4/24/2010.
United States Environmental Protection Agency (USEPA), Human-related sources and sinks of carbon dioxide, 2010b, http://www.epa.gov/climatechange/emissions/co2_human.html, accessed online 4/24/2010.
Versteeg G.F., Blauwhoff P.M.M. and van Swaaij W.P.M., The Effect of diffusivity on gas–liquid mass transfer in stirred vessels, Experiments at atmospheric and elevated pressures, Chemical Engineering Science, 1987, 42, 1103–1109.

Versteeg G. F. and van Swaaij W.P.M., Solubility and diffusivity of acid gases (CO_2, N_2O) in aqueous alkanolamine solutions, Chemical Engineering Data, 1988, 33, 1, 29–34.

Voet D. and Voet, J., Biochemistry, John Wiley & Sons, New York, 1990.
Whitman W. G., Preliminary experimental confirmation of the Two-Film Theory of gas absorption, Chemical and Metallurgical Engineering, 1923, 29,146–148.

Yang H., Xu Z., Fan M. and Gupta R., Slimane R.B., Bland A.E. & Wright I., Progress in carbon dioxide separation and capture: a review, Environmental Sciences, 2008, 20, 14–27.

Yeh A.C. and Bai H., Comparison of ammonia and monoethanolamine solvents to reduce CO_2 greenhouse gas emissions, The Science of Total Environment, 1999, 228, 121-133.

Kidnay A. J. and Parrish W.R., Fundamentals of Natural Gas Processing, Boca Raton, Florida: CRC Press, 2006.

Yuwei J., 2008, http://wiki.nus.edu.sg/display/CC/Human+Factors, accessed online 7/15/2009.
Yeh J. T., Resnik K. P., Rygle K. and Pennline H. W., Semi-batch absorption and regeneration studies for CO_2 capture by aqueous ammonia, Fuel Processing Technology, 2005, 86(14- 15), 1533–1546.

7 NOMENCLATURE

A_{gl}	gas liquid interface	[m^2]
C_1	correlation constant in Equation 3-55	[m^3/mol]
C_2	correlation constant in Equation 3-55	[m^3/mol]
C_3	correlation constant in Equation 3-55	[m^3/mol]
C_A	concentration of species A	[mol/m^3]
$C_{A,i}$	concentration of species A at i^{th} numerical point	[mol/m^3]
C_B^b	bulk concentration of component B	[mol/m^3]
C_i^b	bulk concentration of species i	[mol/m^3]
C_{CA}	carbonic anhydrase concentration	[mol/m^3]
C_{CO_2}	CO_2 liquid phase concentration	[mol/m^3]
$C_{CO_2}^*$	CO_2 liquid phase concentration in equilibrium with the bulk gas	[mol/m^3]
C_i^0	initial concentration of species i	[mol/m^3]
C_b	concentration in the bulk of liquid	[mol/m^3]
$C_{CO_3^{2-}}$	carbonate concentration	[mol/m^3]
$C_{G,0}$	gas solubility in the water	[mol/m^3]
C_G	gas solubility in the salt solution	[mol/m^3]
C_G^o	concentration in the gas phase, absorption in water	[mol/m^3]
C_{G^*}	concentration in the gas phase in equilibrium with bulk liquid	[mol/m^3]
C_{T,CO_2}	total concentration of carbonic species in the solution	[mol/m^3]

C_{K^+}	concentration of potassium ion	[mol/m^3]
D_A^0	diffusivity of species A at 25^{o}C	[m^2/s]
D_A	diffusivity of species A	[m^2/s]
E	enhancement factor	[-]
E_a	activation energy	[J/mol]
E_{enzyme}	Enzyme enhancement factor	
E_{inf}	enhancement factor in the infinite diluted solution	[-]
$h_{G,0}$	gas specific parameter in Schumpe's correlation at 25^{o}C	[m^3/mol]
h_G	gas specific parameter in Schumpe's correlation	[m^3/mol]
h_i	specific parameter of species i in Schumpe's correlation	[m^3/mol]
h_T	gas specific temperature parameter in Schumpe's correlation	$[m^3/mol \cdot K]$
H_0	Henry's constant in water	$[mol/m^3 \cdot atm]$
H	Henry's constant in absorption solution	$[mol/m^3 \cdot atm]$
Ha	Hatta number	[-]
$H_{CO_2,0}$	Henry's constant for CO_2 in water	$[mol/m^3 \cdot atm]$
J_{CO_2}	CO_2 flux	$[mol/m^2 \cdot s]$
$J_{CO_2,PC}$	CO_2 flux into PC solution	$[mol/m^2 \cdot s]$
$J_{CO_2,PC-enzyme}$	CO_2 flux into PC solution containing enzyme	$[mol/m^2 \cdot s]$
k_1	rate constant of major reaction	$[m^3/mol \cdot s]$
k_{11}^{∞}	rate constant of forward reaction (1) at infinite dilution	$[m^3/mol \cdot s]$
k_{i1}	rate constant of forward reaction (i)	
k_{i2}	rate constant of backward reaction (i)	
k_{cat}	turnover number	[s^{-1}]

k_G	gas side mass transfer coefficient	$[mol/m^2 \cdot s \cdot atm]$
k_L^0	liquid side mass transfer coefficient at 25°C	[m/s]
k_L	liquid side mass transfer coefficient	[m/s]
K_2	equilibrium constant for reaction (2)	$[m^3/mol]$
K_4	equilibrium constant for reaction (4)	$[mol/m^3]$
K_G	overall mass transfer coefficient based on gas phase	$[mol/m^2 \cdot s \cdot atm]$
K_L	overall mass transfer coefficient based on liquid phase	[m/s]
K_M	Michaelis-Menten constant	$[mol/m^3]$
K_w	dissociation constant of water	$[mole^2/m^6]$
n_1	number of finite difference points in the CO_2 penetration zone	[-]
n	total number of finite difference points	[-]
P_{CO_2}	CO_2 partial pressure	[atm]
$P_{CO_2}^i$	initial partial pressure of CO_2	[atm]
Q_{CO_2}	CO_2 flow rate	$[m^3/s]$
r_A	reaction rate of species A	$[mol/m^3 \cdot s]$
$r_{A,i}$	reaction rate of species A at i^{th} numerical point	$[mol/m^3 \cdot s]$
r_{CO_2}	reaction rate of CO_2	$[mol/m^3 \cdot s]$
R	gas constant	$[J/mol \cdot K]$
R_g	gas constant	$[m^3 \cdot atm/mol \cdot K]$
t	time	[s]
t_e	eddy exposure time	[s]
T	temperature	[K]

V_g	gas volume	$[m^3]$
x	Cartesian coordinate	[m]
δ_l	CO_2 penetration depth	[m]
δ	thickness of the mass transfer zone	[m]
δx_i	i^{th} finite difference interval	[m]
η	mesh growth rate	[-]
μ^0	dynamic viscosity of absorption solution at 25°C	$[kg/m \cdot s]$
$\mu^0_{K_2CO_3}$	dynamic viscosity of potassium carbonate solution at 25°C	$[kg/m \cdot s]$
$\mu^0_{KHCO_3}$	dynamic viscosity of potassium bicarbonate solution at 25°C	$[kg/m \cdot s]$
μ^0_w	dynamic viscosity of water at 25°C	$[kg/m \cdot s]$
μ	dynamic viscosity of absorption solution	$[kg/m \cdot s]$
μ_w	dynamic viscosity of water	$[kg/m \cdot s]$
ρ_w	density of water	$[kg/m^3]$

APPENDIX A: Matlab Code

```
% BSTR_CO2_PC_Enzyme_Initial

tic
clc, clear all, close all
global n1 nt delta1 delta
global K1 K2 Kw C_total_CO3 C_K
global D_A D_B D_C D_D D_E
global K11 K12 K21 K22 K31 K32 K41 K51 K52 K61 K62
global K_H K_g nt delta delx A Vl Tg Vg P_Water
global CA_i CB_i CC_i CD_i CE_i



alpha=0.2;              % Initial mass fraction of Potassium Carbonate in the
solution, -
beta=0.4;               % Initial conversion of Potassium Carbonate to
Potassium Bicarbonate, -

T_l=25.0;               % Liquid temperature, oC
P_CO2_i=1.0/14.696;     % Initial partial pressure of CO2, atm
P_Water=.25/14.696;     % vapor pressure of water, atm
Enzyme=.03;             % Enzyme concentration, g/l

A=.0075;                % Gas-liquid interfacial area, m^2
Vl=.8e-3;               % Volume of liquid in the reactor, m^3
Vg=.555e-3;             % Volume of gas in the reactor, m^3
Tg=25.0;                % Gas temperature, oC
K_g=1.0;                % Gas phase mass transfer coefficient,
mol/m^2.sec.atm

MW_CO2=44;              % Molecular weight of CO2, g/mole
MW_K2CO3=138.2;         % Molecular weight of K2CO3, g/mole
MW_KHCO3=100.1;         % Molecular weight of KHCO3, g/mole
MW_H2O=18.02;           % Molecular weight of H2O, g/mole

D_A_wo=1.88e-009;
D_Bwo=1.18e-9;          % Diffusivity of HCO3- in water(at 24 oC), m^2/sec
D_Cwo=9.2e-10;          % Diffusivity of CO3-- in water(at 24 oC), m^2/sec
D_Dwo=9.21e-9;          % Diffusivity of H+ in water(at 24 oC), m^2/sec
D_Ewo=5.17e-9;          % Diffusivity of OH- in water(at 24 oC), m^2/sec

mu_w0=1.0e-3;           % Viscosity of water(at 20 oC), Pa.s
mu_wo=9.11e-4;          % Viscosity of water(at 24 oC), Pa.s
mu0=1.55e-3;            % Viscosity of solution(at 20 oC),Pa.s

rhoo=1.19*1000.0;       % Density of solution(at 25 oC),kg/m^3

km_l_wo=5.09e-5;         % Liquid phase mass transfer coefficient (for water
at 25 oC), m/sec
```

```
h_K=0.0922;             % specific parameter of K+ ion in Schumpe's
correlation, m^3/kmol
h_H=0.0;                % specific parameter of H+ ion in Schumpe's
correlation, m^3/kmol
h_OH=0.0839;            % specific parameter of OH- ion in Schumpe's
correlation, m^3/kmol
h_HCO3=0.0967;          % specific parameter of HCO3- ion in Schumpe's
correlation, m^3/kmol
h_CO3=0.1423;           % specific parameter of CO3-- ion in Schumpe's
correlation, m^3/kmol
h_G0=-0.0172;           % specific parameter of CO2 in Schumpe's correlation,
m^3/kmol
h_T=-0.338e-3;          % specific parameter of CO2 in Schumpe's correlation,
m^3.K/kmol


K21=6.0e6;              % reaction rate constant for HCO3- + OH- ------->
CO3-- + H2O,  m^3/mol.sec
K31=1.4e8;              % reaction rate constant for OH- + H+ -------> H2O,
m^3/mol.sec
K41=0.24e-1;            % reaction rate constant for CO2 + H2O -------> HCO3-
+ H+, 1/sec
K61=0.45;               % reaction rate constant for HCO3- -------> CO3-- +
H+, 1/sec


%-------------------------------------------------------------------------

t_initial=0.0;          % start time, sec
delta1=2.7e-5;          % penetration depth of CO2 in the eddy, m
delta=1.25e-4;          % thickness of the mass transfer zone in the eddy, m
Xi=2;                   % mesh compression factor, -
m=100;                  % number of time intervals + 1, -
nt=201;                 % number of numerical points in the delta, -

%-------------------------------------------------------------------------
x=zeros(1,nt);                                          % cartesian
coordinate vector, m
delx=zeros(1,nt-1);                                     % finite
difference interval vector, m
n1=round(Xi*delta1/delta*(nt-1))+1;                     % number of
numerical points in the delta1, -
dx1_eta0=[delta/(nt-1) 1.01];                           % [dx1 eta0]
dx1_eta=fsolve('f1_BSTR_CO2_PC_Enzyme_Initial',dx1_eta0);
dx1=dx1_eta(1);                                         % first interval,
m
eta=dx1_eta(2);                                         % mesh growth
rate, -
for i=1:nt-1
    delx(i)=eta^(i-1)*dx1;
end
x(1)=dx1;
for i=2:nt
    x(i)=x(i-1)+delx(i-1);
```

```
end

%-------------------------------------------------------------------------

rho_w= -1.4823E-11*T_l^6 + 5.7958E-09*T_l^5 - 9.7900E-07*T_l^4 + 1.0040E-
04*T_l^3 - 9.5565E-03*T_l^2 + 8.1622E-02*T_l + 9.9982E+02;             %
density of water at T_l, kg/m^3
mu_w= 4.5012E-15*T_l^6 - 1.7286E-12*T_l^5 + 2.7890E-10*T_l^4 - 2.5213E-
08*T_l^3 + 1.4660E-06*T_l^2 - 6.0593E-05*T_l + 1.7899E-03;               %
viscosity of water at T_l, Pa.s
rho_wo= -1.4823E-11*25.0^6 + 5.7958E-09*25.0^5 - 9.7900E-07*25.0^4 + 1.0040E-
04*25.0^3 - 9.5565E-03*25.0^2 + 8.1622E-02*25.0 + 9.9982E+02;      % density
of water at 25oC, kg/m^3
rho=rhoo*rho_w/rho_wo;
% density of solution at T_l, kg/m^3

v=(alpha*(1.0-beta)+2.0*alpha*beta*MW_KHCO3/MW_K2CO3+(1.0-alpha-
alpha*beta*MW_H2O/MW_K2CO3))/rho;
% volume of solution containg alpha kg equivalent PC, m^3
C_K2CO3=alpha*(1.0-beta)/MW_K2CO3/v*1000.0;
% concentration of K2CO3, mole/m^3
C_KHCO3=2.0*alpha*beta/MW_K2CO3/v*1000.0;
% concentration of KHCO3, mole/m^3
C_total_CO3=C_K2CO3+C_KHCO3;
% total concentration of CO3--, mole/m^3
C_K=2.0*C_K2CO3+C_KHCO3;
% concentration of K+, mole/m^3

Kw=10.0^(-5839.5/(T_l+273.15)-22.4773*log10(T_l+273.15)+61.2062)*rho_w^2;
% equilibrium constant for H2O <------> OH- + H+, mole^2/m^6
K1=exp(-12092.1/(T_l+273.15)-36.786*log(T_l+273.15)+235.482)*rho_w;
% equilibrium constant for CO2 + H2O <------> HCO3- + H+, mole/m^3
K2=10.0^(1568.9/(T_l+273.15)-2.5866-6.737e-3*(T_l+273.15));
% equilibrium constant for HCO3- + OH- <------> CO3-- + H2O, m^3/mole

Ci0(1)=K2*Kw/K1*(C_KHCO3)^2.0/C_K2CO3;  % initial guess for initial
concentration of dissolved CO2, mole/m^3
Ci0(2)=C_KHCO3;                         % initial guess for initial
concentration of HCO3-, mole/m^3
Ci0(3)=C_K2CO3;                         % initial guess for initial
concentration of CO3--, mole/m^3
Ci0(4)=2*Kw*C_KHCO3/C_K2CO3;            % initial guess for initial
concentration of H+, mole/m^3
Ci=fsolve('f2_BSTR_CO2_PC_Enzyme_Initial',Ci0);
CA_i=Ci(1);             % initial concentration of dissolved CO2, mole/m^3
CB_i=Ci(2);             % initial concentration of HCO3-, mole/m^3
CC_i=Ci(3);             % initial concentration of CO3--, mole/m^3
CD_i=Ci(4);             % initial concentration of H+, mole/m^3
CE_i=Kw/CD_i;           % initial concentration of OH-, mole/m^3

K11_inf=10.0^(8.916-2383.0/(T_l+273.15));
K11=K11_inf*10.0^(0.11e-3*C_K + 0.17e-3*CC_i); % reaction rate constant for
CO2 + OH- -------> HCO3-, m^3/mol.sec
```

```
K12=K11*Kw/K1;                                  % reaction rate constant for
HCO3- -------->  CO2 + OH-, 1/sec
K22=K21/K2;                                      % reaction rate constant for
CO3-- + H2O -------> HCO3- + OH-, 1/sec
K32=K31*Kw;                                      % reaction rate constant for
H2O -------> OH- + H+ , mol/m^3.sec
%K42=K41/K1;
K51=K41+Enzyme/30000.0*3.097e9*exp(-1.037e3/(T_l+273.15)); % reaction rate
constant for CO2 + H2O + CA -------> HCO3- + H+, 1/sec
K52=K51/K1;                                                % reaction rate
constant for HCO3- + H+ + CA -------> CO2 + H2O, m^3/mol.sec
K62=K61/(K2*Kw);                                           % reaction rate
constant for CO3-- + H+ -------> HCO3-, m^3/mol.sec

h_G=h_G0+h_T*(T_l-25.0);
K_H_w=1000.0*101.325*(2.8249e6*exp(-2044.0/(T_l+273.15)))^(-1);
% CO2-water Henry's constant, mole/m^3.atm
sum=((h_K+h_G)*C_K + (h_H+h_G)*CD_i + (h_OH+h_G)*CE_i + (h_HCO3+h_G)*CB_i +
(h_CO3+h_G)*CC_i)/1000.0;
K_H=K_H_w/10^(sum);          % CO2-solution Henry's constant, mole/m^3.atm

mu=mu0*(mu_w/mu_w0);         % viscosity of solution at T_l, Pa.s
D_Ao=(1-(0.261*CC_i+0.14*CB_i+0.129*CE_i)/1000.0)*D_A_wo; % diffusion
coefficient of CO2 into the solution at 24oC, m^2/sec
D_A_w=2.35e-6*exp(-2119.0/(T_l+273.15));  % diffusion coefficient of CO2 into
water at T_l, m^2/sec
D_A=D_Ao*(mu_wo/mu_w)^0.818;                % diffusion coefficient of CO2
into solution at T_l, m^2/sec
D_B=D_Bwo*(mu_wo/mu)^.818;                  % diffusion coefficient of HCO3-
into solution at T_l, m^2/sec
D_C=D_Cwo*(mu_wo/mu)^.818;                  % diffusion coefficient of CO3--
into solution at T_l, m^2/sec
D_D=D_Dwo*(mu_wo/mu)^.818;                  % diffusion coefficient of H+
into solution at T_l, m^2/sec
D_E=D_Ewo*(mu_wo/mu)^.818;                  % diffusion coefficient of OH-
into solution at T_l, m^2/se

km_l=km_l_wo*(D_A/D_A_wo)^0.6;               % liquid phase mass transfer
coefficient (for solutionr at T_l), m/sec

t_final=4.0*D_A/3.1416/km_l^2.0;               % eddies exposure time, sec

omega0=zeros(1,5*nt-9);
abs_rate=zeros(m,1);
time=zeros(m,1);
CA=zeros(m,nt);
CB=zeros(m,nt);
CC=zeros(m,nt);
CD=zeros(m,nt);
CE=zeros(m,nt);

P_CO2=zeros(m,1);
```

```
for i=1:nt;
CA(1,i)=CA_i;
CB(1,i)=CB_i;
CC(1,i)=CC_i;
CD(1,i)=CD_i;
CE(1,i)=CE_i;
end

CAb=CA_i;
CBb=CB_i;
CCb=CC_i;
CDb=CD_i;
CEb=CE_i;
P_CO2(1)=P_CO2_i;

omega0(1:nt-2)=CA(1,2:nt-1);
omega0(nt-1:2*nt-4)=CB(1,2:nt-1);
omega0(2*nt-3:3*nt-6)=CC(1,2:nt-1);
omega0(3*nt-5:4*nt-8)=CD(1,2:nt-1);
omega0(4*nt-7:5*nt-10)=CE(1,2:nt-1);
omega0(5*nt-9)=P_CO2(1);


delt=(t_final-t_initial)/(m-1);
t1=t_initial;
t2=t1+delt;
time(1)=t1;


options          = odeset('Reltol',1e-6,'Abstol',1e-10,'bdf','off');

for j=2:m
j
time(j)=t2;
[tout,omega]     = ode15s('f3_BSTR_CO2_PC_Enzyme_Initial',[t1
t2],omega0,options);

nrow     = length(tout);

CA(j,2:nt-1)=omega(nrow,1:nt-2);
CB(j,2:nt-1)=omega(nrow,nt-1:2*nt-4);
CC(j,2:nt-1)=omega(nrow,2*nt-3:3*nt-6);
CD(j,2:nt-1)=omega(nrow,3*nt-5:4*nt-8);
CE(j,2:nt-1)=omega(nrow,4*nt-7:5*nt-10);
P_CO2(j)=omega(nrow,5*nt-9);



CB(j,1)=CB(j,2);
CC(j,1)=CC(j,2);
CD(j,1)=CD(j,2);
CE(j,1)=CE(j,2);
```

```
CA(j,1)=(K_g*P_CO2(j)+D_A*CA(j,2)/delx(1))/(K_g/K_H+D_A/delx(1));



CA(j,nt)=CAb;
CB(j,nt)=CBb;
CC(j,nt)=CCb;
CD(j,nt)=CDb;
CE(j,nt)=CEb;


abs_rate(j)=-1.0*D_A*A*(CA(j,2)-CA(j,1))/delx(1);

omega0=omega(nrow,:);
t1=t2;
t2=t1+delt;
end

sum=0.0;
for j=2:m
    sum=sum+(CA(j,2)-CA(j,1))+ (CA(j-1,2)-CA(j-1,1));
end
flux_average=-.5*D_A*sum/delx(1)*delt/t_final;
toc




 figure(1)
 plot(x,CA(m,:)/CA(m,1),'r');
 xlabel('penetration depth(m)', 'FontSize', 16)
 ylabel('normalized concentration (-)','FontSize', 16);

 hold on
 plot(x,CB(m,:)/CB(m,nt),'b');

 hold on
 plot(x,CC(m,:)/CC(m,nt),'green');

 hold on
 plot(x,CE(m,:)/CE(m,nt), 'k');


% This function provides the algebraic equations to calculate dx1 and eta.

function F = f1_BSTR_CO2_PC_Enzyme_Initial(dx1_eta)

global n1 nt delta1 delta

dx1=dx1_eta(1);
eta=dx1_eta(2);
sum1=1.0;
```

```
sum2=1.0;

for i=1:n1-1
    sum1=sum1+eta^i;
end

for i=1:nt-1
    sum2=sum2+eta^i;
end

F(1)=sum1-delta1/dx1;
F(2)=sum2-delta/dx1;


% This function provides the algebraic equations to calculate initial
concentrations.


function F = f2_BSTR_CO2_PC_Enzyme_Initial(Ci)

global K1 K2 Kw C_total_CO3 C_K

CA_i=Ci(1);
CB_i=Ci(2);
CC_i=Ci(3);
CD_i=Ci(4);
CE_i=Kw/CD_i;

F(1)=1.0-CB_i*CD_i/CA_i/K1;
F(2)=1.0-CC_i/CB_i/CE_i/K2;
F(3)=1.0-(CA_i+CB_i+CC_i)/C_total_CO3;
F(4)=1.0-(CE_i+CB_i+2.0*CC_i)/(C_K+CD_i);



% This function provides the time derivatives.


function yprime = f3_BSTR_CO2_PC_Enzyme_Initial(tau,omega)

global D_A D_B D_C D_D D_E
global K11 K12 K21 K22 K31 K32 K51 K52 K61 K62
global K_H K_g nt delx A Tg Vg
global CA_i CB_i CC_i CD_i CE_i


C_A=zeros(1,nt);
C_B=zeros(1,nt);
C_C=zeros(1,nt);
C_D=zeros(1,nt);
C_E=zeros(1,nt);

C_A_dot=zeros(1,nt);
```

```
C_B_dot=zeros(1,nt);
C_C_dot=zeros(1,nt);
C_D_dot=zeros(1,nt);
C_E_dot=zeros(1,nt);

C_A(2:nt-1)=omega(1:nt-2);
C_B(2:nt-1)=omega(nt-1:2*nt-4);
C_C(2:nt-1)=omega(2*nt-3:3*nt-6);
C_D(2:nt-1)=omega(3*nt-5:4*nt-8);
C_E(2:nt-1)=omega(4*nt-7:5*nt-10);

C_Ab=CA_i;
C_Bb=CB_i;
C_Cb=CC_i;
C_Db=CD_i;
C_Eb=CE_i;
P_CO2=omega(5*nt-9);




C_A(1)=(K_g*P_CO2+D_A*C_A(2)/delx(1))/(K_g/K_H+D_A/delx(1));

C_B(1)=C_B(2);
C_C(1)=C_C(2);
C_D(1)=C_D(2);
C_E(1)=C_E(2);
C_A(nt)=C_Ab;
C_B(nt)=C_Bb;
C_C(nt)=C_Cb;
C_D(nt)=C_Db;
C_E(nt)=C_Eb;

for i=2:nt-1
    C_A_xx=2.0*((C_A(i+1)-C_A(i))/delx(i)-(C_A(i)-C_A(i-1))/delx(i-
1))/(delx(i)+delx(i-1));
    C_B_xx=2.0*((C_B(i+1)-C_B(i))/delx(i)-(C_B(i)-C_B(i-1))/delx(i-
1))/(delx(i)+delx(i-1));
    C_C_xx=2.0*((C_C(i+1)-C_C(i))/delx(i)-(C_C(i)-C_C(i-1))/delx(i-
1))/(delx(i)+delx(i-1));
    C_D_xx=2.0*((C_D(i+1)-C_D(i))/delx(i)-(C_D(i)-C_D(i-1))/delx(i-
1))/(delx(i)+delx(i-1));
    C_E_xx=2.0*((C_E(i+1)-C_E(i))/delx(i)-(C_E(i)-C_E(i-1))/delx(i-
1))/(delx(i)+delx(i-1));

    C_A_dot(i)=D_A*C_A_xx+K12*C_B(i)-K11*C_A(i)*C_E(i)-
K51*C_A(i)+K52*C_B(i)*C_D(i);
    C_B_dot(i)=D_B*C_B_xx + K11*C_A(i)*C_E(i)-K12*C_B(i)+K22*C_C(i)-
K21*C_B(i)*C_E(i)+K51*C_A(i)-K52*C_B(i)*C_D(i)- K61*C_B(i)+K62*C_D(i)*C_C(i);
    C_C_dot(i)=D_C*C_C_xx+ K21*C_B(i)*C_E(i)-K22*C_C(i)+ K61*C_B(i)-
K62*C_D(i)*C_C(i);
    C_D_dot(i)=D_D*C_D_xx+ K32-K31*C_E(i)*C_D(i)+K51*C_A(i)-
K52*C_B(i)*C_D(i)+ K61*C_B(i)-K62*C_D(i)*C_C(i);
```

```
    C_E_dot(i)=D_E*C_E_xx + K12*C_B(i)-K11*C_A(i)*C_E(i)+K22*C_C(i)-
K21*C_B(i)*C_E(i)+K32-K31*C_E(i)*C_D(i);
end



P_CO2_dot=-D_A*A*(C_A(1)-C_A(2))/delx(1)*0.0821*(Tg+273.15)/Vg/1000;


yprime(1:nt-2)=C_A_dot(2:nt-1);
yprime(nt-1:2*nt-4)=C_B_dot(2:nt-1);
yprime(2*nt-3:3*nt-6)=C_C_dot(2:nt-1);
yprime(3*nt-5:4*nt-8)=C_D_dot(2:nt-1);
yprime(4*nt-7:5*nt-10)=C_E_dot(2:nt-1);

yprime(5*nt-9)=P_CO2_dot;

yprime=yprime';
```